Current-induced Domain Wall Motion in Nanoscale Ferromagnetic Elements

O. Boulle[1], G. Malinowski[2], and M. Kläui[3*]

[1] *SPINTEC, CEA/CNRS/UJF/GINP, INAC, 38054 Grenoble Cedex 9, France*

[2] *Laboratoire de Physique des Solides, CNRS, Université Paris-sud 11, 91405 Orsay Cedex, France.*

[3] *Laboratory of Nanomagnetism and Spin Dynamics, Ecole Polytechnique Fédérale de Lausanne (EPFL), 1015 Lausanne, Switzerland; SwissFEL, Paul Scherrer Institut, 5232 Villigen PSI, Switzerland*

*Also at Fachbereich Physik, Universität Konstanz, Universitätsstr. 10, D-78457 Konstanz, Germany, Electronic mail: mathias.klaeui@magnetism.ch

Preprint submitted to Materials Science and Engineering: R: Reports September 24, 2010

Current-induced Domain Wall Motion in Nanoscale Ferromagnetic Elements

O. Boulle[1], G. Malinowski[2], and M. Kläui[3*]

[1] *SPINTEC, CEA/CNRS/UJF/GINP, INAC, 38054 Grenoble Cedex 9, France*

[2] *Laboratoire de Physique des Solides, CNRS, Université Paris-sud 11, 91405 Orsay Cedex, France.*

[3] *Laboratory of Nanomagnetism and Spin Dynamics, Ecole Polytechnique Fédérale de Lausanne (EPFL), 1015 Lausanne, Switzerland; SwissFEL, Paul Scherrer Institut, 5232 Villigen PSI, Switzerland*

Abstract

The manipulation of a magnetic domain wall (DW) by a spin polarized current in ferromagnetic nanowires has attracted tremendous interest during the last years due to the fundamental questions it raises in the fields of spin dependent transport phenomena and magnetization dynamics but also due to promising applications, such as DW based magnetic memory concepts and logic devices. We comprehensively review recent developments in the field of geometrically confined domain walls and in particular current induced DW dynamics. We focus on the influence of the magnetic and electronic transport properties of the materials that have been shown to play a key role on the spin transfer effect in DWs. After considering the different DW structures in ferromagnetic nanowires, the theory of magnetization dynamics induced by a spin polarized current is presented. We first discuss the different current induced torques and their origin in the light of recent theories based on simple s-d exchange model and beyond. This leads to a modified Landau-Lifshitz-Gilbert equation of motion where the different spin transfer torques are included and we discuss their influence on the DW dynamics on the basis of simple 1D models and recent micromagnetic

*Also at Fachbereich Physik, Universität Konstanz, Universitätsstr. 10, D-78457 Konstanz, Germany, Electronic mail: mathias.klaeui@magnetism.ch

simulations studies. Experimental results illustrating the effects of spin transfer in different ferromagnetic materials and geometries constitute the body of the review. The case of soft in-plane magnetizted nanowires is described first, as it is the most widely studied class of ferromagnetic materials in this field. By direct imaging we show how confined domain walls in nanowires can be displaced using currents in in-plane soft magnetic materials and that using short pulses, fast velocities can be attained. While a spin polarized current can trigger DW depinning or displacement, it can also lead to a modification of the DW structure, which is described in detail as it allows one to deduce information on they underlying spin torque terms. High perpendicular anisotropymaterials characterized by narrow wide domain walls have raised considerable interest. These materials characterized by only nm wide DWs combined several key advantages over soft magnetic materials such as higher non-adiabatic effects leading to lower critical current densities and high domain wall velocity. We review recent experimental results obtained in this class of materials and discuss the important implications they entail on the nature of the spin torque in DWs.

1. Introduction

The physics of surfaces, interfaces and nanostructures has become one of the main areas of research, due to the trend in science and technology towards miniaturisation of physical systems into the nano-scale. From the scientific viewpoint, such systems pose a whole new set of problems, both theoretical and experimental. Fundamentally, novel properties emerge in magnetic elements as the lateral structure dimensions become comparable to or smaller than certain characteristic length scales, such as spin diffusion length, carrier mean free path, magnetic exchange length, domain wall width, etc. The effects of the governing energy terms determine the interplay between the relevant physical length scales and the sizes of the structured materials.

But not only from a basic physics point of view, have magnetic nanostructures moved into the research focus, but they have also been at the heart of a

multitude of devices ranging from sensing applications to data storage. Probably the best known storage device is the magnetic disc drive [1], which was pioneered in the 1950s by IBM with the RAMAC and since then the storage density has seen a gigantic exponential increase. While hard drives continue to excel in the high capacity market, they entail nonetheless disadvantages, which have led to other memory concepts replacing them for applications, such as lower density mobile storage. A well-known example are MRAMs where the information is stored in the magnetization direction of a magnetic nanoelement. Novel storage class memory devices have also been put forward such as the magnetic shift register [2–5], based on nanoscale magnetic wires with domains delineated by domain walls representing the bits.

While the existence of domains in bulk materials and in continuous films could often be attributed to defects (at least for soft magnetic materials), the situation is radically different when structures are patterned into nanoscale elements. Here a magnetization configuration that constitutes the lowest energy state is often a multidomain state with domain walls, since the dipolar interaction (stray field) leads to the magnetization being parallel to the element edges, which then results in a spatially inhomogeneous magnetization distribution (domains). These domains and domain walls occur, when the geometry changes from the bulk to the nanoscale, since then the magnetic properties of ferromagnetic elements start to be governed by the element geometry and not only by the intrinsic materials properties. Such behaviour and in particular the magnetization configurations and reversal in small magnetic elements have been reviewed in detail for instance in Refs. [6, 7]. Such a strong dependence on the geometry allows one then to tailor the magnetization configuration and spin switching by appropriately engineering the geometry. The magnetization configuration that constitutes the lowest energy state in a small magnetic structure can for instance be set to a multidomain state with domain walls, since the dipolar interaction (stray field) leads to the magnetization being parallel to the element edges. This results in a very reproducible and controllable spatially inhomogeneous magnetization distribution (domain configuration) [7].

The presence of useful spin structures is though not sufficient, since one needs to manipulate these. Conventionally this is done by applying magnetic fields and different reversal modes can be triggered [7]. Field-induced switching though exhibits poor scaling as the necessary current densities to generate the switching fields increase with decreasing design rule of the structure size. An alternative approach that has recently become available is to employ spin-polarized currents to manipulate the magnetization. This approach is not only exciting from the point of view of applications, but entails significant novel physics, which has only recently started to be explored. Its principle is based on the spin transfer effect which occurs when the direction of the current spin polarisation traversing a media is not aligned with the local magnetization. The exchange interaction then leads to a transfer of the current spin angular momentum to the magnetization which thus feels a torque. This torque can generate dynamical states of magnetization and in particular reverse its direction. The spin transfer effect was thus shown to be able to reverse the soft layer of a giant-magnetoresistive multi-layer structure [8] or excite steady precession state [9]. As recently demonstrated, spin-transfer effects can also be used to displace a magnetic domain wall by injecting current, which is at the heart of this review. This effect shows potential for novel memory and logic devices based on domain-wall propagation as it could simplify designs by eliminating magnetic field-generating circuits. While field-induced domain-wall motion is well established, current-induced domain-wall motion is now starting to be more and more understood and the field is now sufficiently mature to warrant a review from an experimental point of view. An excellent review on the theory has been provided by Tatara et al. [10]. We have structured the review as follows. In section 2 we explain and discuss the domain wall spin structures present in soft magnetic materials with in-plane magnetization (2.1) and high anisotropy materials with out-of-plane magnetized layers (2.2). In section 3 the theory of the spin transfer torque effect leading to domain wall motion is presented. Section 4 deals with experimental observations starting with a brief description of the techniques employed. Then the main results for experimental observations of current-induced

domain wall motion are summarized for both in-plane and out-of-plane magnetized materials. Particular emphasis is given to the determination of the spin torque terms from these measurements. The review is concluded by a summary.

2. Magnetic domain walls in nanowires

Domain walls, which constitute the boundary between domains, have been intensively researched in the past, though with a focus on the domain wall types that occur in the bulk or in continuous films. The most prominent examples are the Bloch and the Néel wall types, which occur in continuous thin films [11–13]. A thorough overview of such domain walls is given in Ref. [6]. While previously relatively low resolution imaging has been used to image the wall position, the advent of high resolution imaging techniques has opened up the possibility to image the actual domain wall spin structure on the nanoscale. In addition to imaging the relaxed spin structure, the dynamics on the picosecond timescale can be imaged. In this section the domain walls and related spin structures are reviewed firstly for the case of soft magnetic materials then in out-of-plane magnetized materials with a strong perpendicular anisotropy.

2.1. Domain Wall Spin Structures in Soft Magnetic Materials

In this section, the domain walls spin structures in soft magnetic materials are reviewed. After a brief summary of the techniques employed for the fabrication of the nanostructures, the actual wall spin structures are discussed and their dependence on the geometry is explained.

2.1.1. Techniques

For all these investigations, high quality magnetic nanostructures have to be fabricated. The prevailing geometries to study head-to-head domain walls are straight and zig-zag wires, U-shaped, L-shaped and half-ring elements as well as full rings. Ring elements have proven to be a useful geometry for the investigation of domain walls since due to the high element symmetry, walls can be easily created and positioned by applying an external uniform magnetic field [14, 15]. Ferromagnetic rings can be in the flux closure vortex state or in

the onion state, where they exhibit 180° head-to-head and tail-to-tail domain walls [14, 16]. In order to make sure that the domain walls exhibit the same behaviour in straight parts of the structure as in the curved parts, the radius of the curvature should be much larger than the width, since otherwise the wall can be pinned by the variation in the geometry [17].

In order to make the structures, a range of fabrication methods is available and details as well as reviews can be found in [16, 18–20]. In particular for techniques based on x-ray transmission, the structures have to be defined on membranes, which entails certain complications as discussed in [19]. With the advent of advanced nano-lithography [21], which allows one to fabricate well-defined nanoscale magnetic wires, such nanostructures have become readily available. The samples are often prepared using electron beam lithography including deposition of materials combinations, such as permalloy/Au by molecular beam epitaxy, Pt/Co/Pt multilayers by sputtering, etc. using a naturally oxidized Si wafer as the substrate and a double lift-off process [21] or post-deposition etching for the pattern transfer (for details of different processes, see various articles in Ref. [22]).

To study domain walls and their dynamics, different methods are employed as detailed later in 4.1. Direct imaging of spin structures can be carried out using scanning probe techniques (magnetic force microscopy (MFM), spin-polarized scanning tunneling microscopy, scanning hall microscopy, etc.), magneto-optical techniques (MOKE), electron microscopy and in particular synchrotron - based microscopy techniques. Introductory overviews and more detailed descriptions of the techniques can be found in various articles in [22].

2.1.2. Domain Wall Types and Wall Phase Diagrams

Theory of head-to-head domain wall spin structures. To understand theoretically the domain wall types and their spin structures in nanostructured soft magnetic materials, we need to briefly consider the energy terms that lead to the wall formation. The wall spin structure is a result of the energy minimization (to be more precise the minimization of the appropriate thermodynamic

potential, which is usually the Landau Free Energy (though often entropy effects are neglected and only the internal energy is considered) [7, 23]). Without any externally applied fields and since we neglect anisotropies, the two governing energy terms are the exchange energy, which is at the heart of ferromagnetism, and the stray field energy due to the dipolar interaction of the spins. Qualitatively this means that if the exchange dominates, the wall should be very wide, so that there is only a small angle between adjacent spins resulting in a small exchange energy. If the stray field energy dominates, the spins try to stay parallel to the structure edge as much as possible, resulting in a narrower wall.

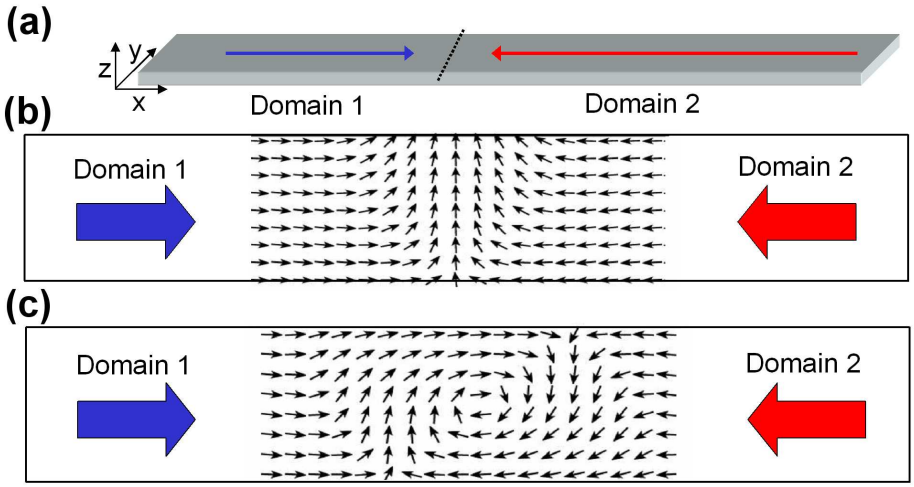

Figure 1: (Color online) (a) Schematic depiction of a magnetic wire with two domains pointing in opposite directions (red and blue arrows) and a domain wall (dotted line) separating the domains. The length of the wire is along the x-direction, the width W along the y-direction and the thickness t along the z-direction. Top view (x-y plane) of the spin structure of a transverse head-to-head domain wall (b) and a vortex head-to-head domain wall (c).

To go beyond such qualitative considerations, numerical calculations are necessary to ascertain the spin structures that constitute local energy minima (stable wall structures). For the case of domain walls in wires, such micromagnetic simulations [24–26] were carried out by McMichael and Donahue in 1997 [27]. Two wall spin structures were predicted to occur: transverse walls (TW, see Fig. 1 (b)) and vortex walls (VW, see Fig. 1 (c)). In the case of the transverse wall, the spins rotate in the plane of the structure (Fig. 1 (b)). The vortex wall

exhibits a very different spin structure. Here the spins curl around the vortex core, where the magnetization is pointing out of the plane (Fig. 1 (c)) [28–30]. This yields a fourfold energetically degenerate state where the in-plane magnetization can crul clockwise or counter-clockwise and the out-of-plane vortex core points up or down. The energies of the two wall types vary with geometry and material and can be calculated from the simulations. More instructive though is an analytical calculation of the energies of the two wall types as a function of geometry, as carried out by McMichael and Donahue [27]. They assumed that as a first approximation, the difference in stray field energies between the two wall types is effectively the stray field of the transverse component in the TW, which is less present in the VW. They calculate this stray field energy difference to be

$$\Delta E_{strayfield} \approx -\frac{1}{8}\mu_0 M_s^2 t^2 W, \tag{1}$$

with M_s the saturation magnetization, t the thickness and W the width of the structure [27]. For the difference in exchange energies they assume that it is given by the vortex in the VW, which yields

$$\Delta E_{ex} =\approx 2\pi t A \ln \frac{r_{max}}{r_{min}}, \tag{2}$$

with A the exchange constant, t the thickness, r_{max} the outer radius of the vortex, which is assumed to be half the strip width and r_{min} the inner radius of the vortex, which is given by the vortex core radius δ. From this we can now deduce a "phase diagram" where the energetically favourable wall type is determined as a function of the geometry (width, thickness). In particular to obtain the phase boundary, which delineates the region where one wall is favoured or the other, the sum of the energy differences is set to zero (both wall types have the same energy). Neglecting the weak logarithmic dependence this yields $Wt \approx const$, with the constant depending on the material. This means that in a width vs. thickness diagram the phase boundary is a hyperbola.

These calculations were later refined by Nakatani and Thiaville [31] and they found, in addition to symmetric transverse walls, tilted transverse walls

that constitute the energy minimum in a small range of geometries and such tilted transverse walls were actually observed experimentally [32].

These micromagnetic simulations were carried out in the 0K limit, but the influence of thermal excitations on the wall spin structure has also been investigated theoretically [33, 34].

Experimental determination of head-to-head domain wall spin structures.

Spin structures in $Ni_{80}Fe_{20}$ (Permalloy) Here the main properties of head-to-head domain walls are presented, while a more extensive discussion can be found in [17]. To study the domain wall types experimentally [35, 36], arrays of 5×5 polycrystalline Co and Permalloy ($Ni_{80}Fe_{20}$) rings with different thicknesses and widths were fabricated as described in [20, 37]. For the investigation of the phase diagram, the edge-to-edge spacing between adjacent rings was more than twice the diameter to prevent dipolar interactions which might otherwise influence the domain wall type (see [17, 38] for a study of interacting domain walls). To determine the spin structure of the domain walls as a function of the ring geometry, the samples were first saturated with an external field and then after the field is reduced to zero, the resulting domain wall spin structure is imaged.

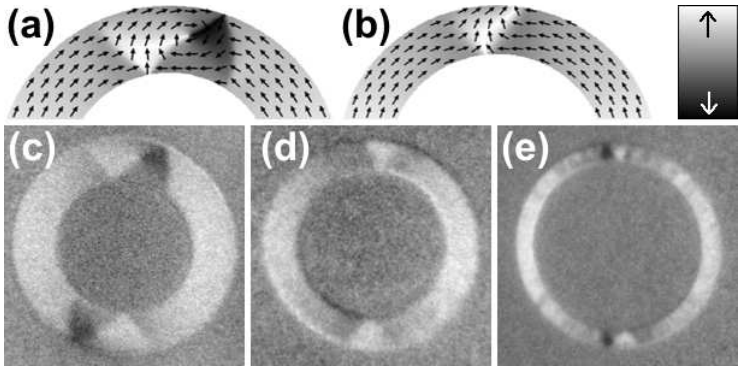

Figure 2: (from [36]) Spin structure of (a) a vortex and (b) a transverse wall simulated using OOMMF. PEEM images of (c) 30 nm thick and 530 nm wide (outer diameter $D = 2.7\,\mu$m), (d) 10 nm thick and 260 nm wide ($D = 1.64\,\mu$m), and (e) 3 nm thick and 730 nm wide ($D = 10\,\mu$m) Permalloy rings in the onion state. The gray scale indicates the direction of the magnetic contrast.

In Fig. 2, we present PEEM images of (c) a thick and wide Permalloy ring, (d) a thin and narrow ring, and (e) an ultrathin ring measured at room temperature. The contrast of the images is explained in (a) and (b). The domain wall type was systematically determined from PEEM images for more than 50 combinations of ring thickness and width for both Permalloy and Co and the quantitative phase diagrams shown in Figs. 3 (a) and (c) were extracted (a similar phase diagram was also obtained in Ref. [39]). The phase diagrams exhibit two phase boundaries indicated by solid lines between vortex walls (thick and wide rings, squares), transverse walls (thin and narrow rings, discs), and again vortex walls for ultrathin rings.

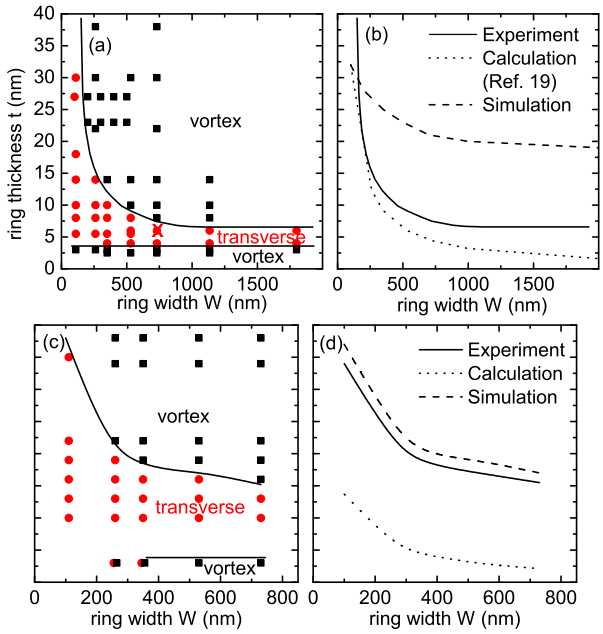

Figure 3: (Color online) (partly from [35, 36]) Experimental phase diagrams for head-to-head domain walls in (a) Permalloy and (c) Co rings at room temperature. Black squares indicate vortex walls and red discs transverse walls. The phase boundaries are shown as solid lines. (b, d) Comparison of the upper experimental phase boundary (solid lines) with results from calculations (dotted lines) and micromagnetic simulations (dashed lines).

We discuss first the upper boundary shown in Figs. 3 (a, c). This phase boundary was investigated theoretically by McMichael and Donahue as described above [27]. The theoretical phase boundary (dotted lines) is shifted

to lower thickness and smaller width compared to the experimental boundary (solid lines in Figs. 3 (b, d)). This discrepancy can be understood by taking into account the following: The calculations [27] compare total energies and therefore determine the wall type with the absolute minimum energy as being favorable. In the experiment, the wall type was investigated after saturation of the ring in a magnetic field and relaxing the field to zero. During relaxation, first a transverse wall is formed reversibly [40]. For the formation of a vortex wall, an energy barrier has to be overcome to nucleate the vortex core, which leads to a hysteretic behaviour of the wall formation. So the observed spin structure does not necessarily constitute the absolute minimum energy, but transverse walls can be observed for combinations of thickness and width where they constitute local energy minima even if a vortex wall has a lower energy for this geometry. Next we have simulated the experiment by calculating the domain wall spin structure after reducing an externally applied field stepwise using the OOMMF code [41] (for Permalloy: $M_\mathrm{s} = 800 \times 10^3\,\mathrm{A/m}$, $A = 1.3 \times 10^{-11}\,\mathrm{J/m}$; for Co: $M_\mathrm{s} = 1424 \times 10^3\,\mathrm{A/m}$, $A = 3.3 \times 10^{-11}\,\mathrm{J/m}$; for both: damping constant $\alpha = 0.01$, cell size 2–5 nm). The simulated boundary (dashed line) is shifted to higher thickness and larger width compared to the experiment. This can be attributed to the fact that thermal excitations help to overcome the energy barrier between transverse and vortex walls in the case of the room temperature experiment, while they are not taken into account in the 0 K simulation. Thus we can expect that for temperatures above room temperature the upper experimental phase boundary is shifted to lower thickness and approaches the theoretical phase boundary. In other words, transverse walls formed at room temperature change to vortex walls with rising temperature.

In addition to studying domain wall spin structures in Permalloy and Co, we have also used XMCD-PEEM to image domain walls in amorphous CoFeB [42]. Here we find that due to the reduced saturation magnetization, transverse walls prevail for all the geometries studied (up to 1500 nm width and 20 nm thickness) [42].

Transverse and vortex walls have also been imaged using TXM [43] and

vortex cores have been imaged by STXM [44, 45] and electron holography [29] in 3d metal structures with similar geometries to those we discussed here.

Further head-to-head domain wall types. The description in the context of the phase diagrams presented here is limited to a certain geometry regime and to soft materials with no or low magnetocrystalline anisotropy. In structures with material specific anisotropies and in elements that are significantly wider than $\approx 1\,\mu$m, we observe more complicated domain wall spin structures such as distorted transverse walls and these are discussed in detail in [17, 46, 47].

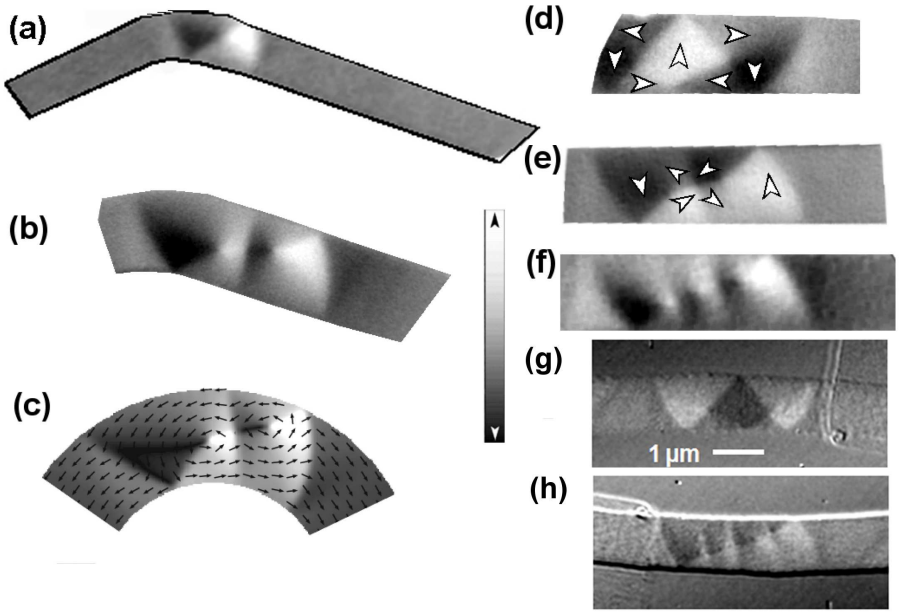

Figure 4: ((a-f) from [48], (g,h) courtesy of G. Meier taken at the XM-1 microscope at the Advanced Light Source in Berkeley) Further domain wall types in a 1 μm wide and 28 nm thick Permalloy wire. The magnetization direction is given by the grey scale bar: (a) Single vortex wall (VW type) located next to a kink in the wire; (b) Double vortex wall with two parallel vortices and an antivortex in between (2P type); (c) Micromagnetic simulation of such a 2P wall, visualizing the spin structure; (d) Double vortex wall with two anti-parallel vortices (2AP type); (e) Extended vortex wall; (f) Triple vortex wall with three parallel vortices and 2 anti-vortices (3P). In (g) and (h) TXM images of domain walls in 960 nm wide and 80 nm thick permalloy wires are shown. The spin structure of the 2P type in (g) agrees well with the PEEM image in (d) while (h) shows a more complicated multi-vortex wall type.

Complex wall types in permalloy In general, in wider structures, the influence of shape anisotropy is reduced and thus more complicated spin structures can constitute local energy minima and become observable. To classify these wall types, the notion explained in Fig. 4 was suggested [48, 49] and will be used here. Apart from the simple single vortex wall (Fig. 4 (a)), more complicated wall spin structures including several vortices with the same sense of rotation (parallel P) or opposite sense of rotation (antiparallel AP) are found (Fig. 4 (b–f)). One of the reasons that such spin structures are stable in very thick structures is the magnetic stray field that is present for single transverse or vortex walls due to magnetic (pseudo-)charges at the edge of the structure as discussed in detail in [49]. Observation of the double vortex wall with antiparallel vortices (2AP) was also reported using magnetic force microscopy [50] and transmission electron microscopy techniques [51]. In Fig. 4 (g), a transmission x-ray microscopy image of a 2AP wall is shown, and comparison to the XMCD-PEEM image in (d) shows nice agreement (the wall exhibits inverted contrast to that in (d)) [43]. To show that even more complicated spin structures can be stable in thick wires, we present in (h) a domain wall spin structure with an even higher number of (anti-)vortices.

Domain wall spin structures in Fe_3O_4 (Magnetite) The performance of devices based on current-induced domain wall dynamics depends on the spin polarization of the current. This means that it can be enhanced using ferromagnetic materials exhibiting a high degree of spin polarization. Of particular interest are so-called half-metallic ferromagnets, compounds that are metallic for one spin component while insulating for the other spin component, thus leading to 100% spin polarization at the Fermi energy. In this context magnetite is a promising material combining a high Curie temperature T_C =851K with a high spin polarization of up to -80% at room temperature [52].

Another key difference between the soft magnetic permalloy and the magnetite is the fact that magnetite exhibits an intrinsic cubic magnetocrystalline anisotropy [53, 54], while permalloy has no significant magnetocrystalline anisotropy.

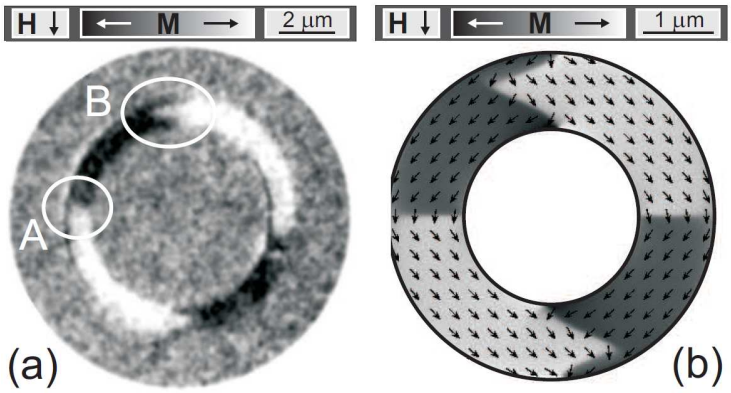

Figure 5: (from [53]) (a) High resolution XMCD-PEEM image of a Fe_3O_4 ring (D=10 μm, nominal width W=1135 nm) at zero-field. 90^o DWs are visible in the image (marked with A). A tail-to-tail zig-zag DW (marked with B) as well as a head-to-head zig-zag DW at the opposite side of the ring are also present. Black and white contrasts correspond to the magnetization pointing to the left and right, respectively. (b) Simulated magnetization orientation obtained from the micromagnetic calculation for the Fe_3O_4 ring (D=5 μm, W=1135 nm) in the remanent state after saturation.

Furthermore previously polycrystalline permalloy has been used, where all magnetocrystalline anisotropies are averaged out anyway.

After lithographically defining various ring and wire structures in magnetite films (the details of the fabrication process are given in [53]), the spin structure is imaged using XMCD-PEEM. The image in Fig. 5 shows (a) a Fe_3O_4 ring structure (D=10 μm, nominal width W=1135 nm) initially magnetized along one of the magnetocrystalline hard axes (the [001] direction) is compared with a simulated magnetization configuration obtained from micromagnetic calculations (b). The black (white) contrast in the XMCD-PEEM image (Fig. 5 (a)) reflects the horizontal component of the in-plane magnetization direction pointing to the left (right). The main difference to the magnetization configurations of polycrystalline 3d metal rings is that here the in-plane magnetization deviates from the direction given by the shape of the structure. Instead of following the ring perimeter, the magnetization is divided into four domains. Within each of the domains, the magnetization points along one of the in-plane magnetocrystalline easy axes. In the neighboring segments of the ring, the magnetization vectors are perpendicular to each other, causing two 90^o DWs at the right and

the left side of the ring (marked with A). The configuration resembles the onion state magnetic configuration observed in 3d metal rings [17]. In this state the Fe_3O_4 ring structure contains characteristic head-to-head and tail-to-tail DWs, indicated by the change from black to white (and vice versa) at the top and bottom of the ring (the position of the tail-to-tail DW at the top is marked with B). In contrast to the transverse or vortex DWs observed in permalloy, the head-to-head (tail-to-tail) DWs in Fe_3O_4 exhibit a zig-zag shape (see e.g. the tail-to-tail DW marked with B). In order to understand the remanent magnetic states observed in Fe_3O_4 rings, micromagnetic simulations of the equilibrium state at remanence are performed as shown in (b). The gray scale for the magnetization directions is chosen to be identical with the XMCD-PEEM image contrast in (a). The micromagnetic simulation reproduces the four domain structure measured by XMCD-PEEM extremely well, exhibiting two 90^o DWs and two zig-zag DWs. The four domain structure is a consequence of the strong fourfold in-plane magnetocrystalline anisotropy of $Fe_3O_4(100)$ films as further detailed in Ref. [53].

2.2. Domain Wall Spin Structures in out-of-plane magnetized nanowires

2.2.1. Materials

Whereas most of CIDM experiments in in-plane magnetized materials were carried out in permalloy nanowires, a large variety of out-of-plane magnetized materials have been investigated these last years. A first family of materials are ultrathin film with a strong *surface* uniaxial perpendicular anisotropy, such as $(Pt/Co)_n$ [55–58], $(CoFeB/Pt)_n$ [59], Pt/Co/AlOx [60], $(CoFe/Pt)_n$ [61] or $(Co/Ni)_n$ multilayers [62, 63]. A second family of materials are thicker magnetic film with a volume out-of-plane magnetocrystalline anisotropy. Such films are sputtered alloys such as $Co_{63}Cr_{11}Pt_{26}$ (8 nm) [64] and $Tb_{30}Fe_{58}Co_{12}$ (30-60 nm) [65] or epitaxial thin films of $SrRuO_3$ (37,5 nm) grown by electron beam evaporation [66] or high chemically ordered L10 FePt grown by molecular beam epitaxy [67]. Magnetic spin valves composed of one magnetically free layer separated from a magnetically fixed layer by a non-magnetic spacer have also been considered [67–70]. In most materials, the uniaxial anisotropy easy axis

is perpendicular to the film plane and the anisotropy K is larger than the demagnetizing energy density $K_0 = \mu_0 M_S^2/2$ so that the magnetization is oriented perpendicularly to the film plane. For ultra-thin magnetic films, the thicknesses are generally smaller than the exchange length or the DW width so that the magnetization can be considered as being uniform across the film [71, 72] and DWs exhibit a nearly perfect Bloch or Néel spin structure (see Fig. 6(a-b)). In ultra-thin films with surface anisotropy, the effective anisotropy $K_{eff} = K - K_0$ is typically of the order of several 10^5 J/m^3 resulting in a DW width Δ of of the order of 5 nm. However, epitaxial layer, such as $SrRuO_3$ and FePt films have a much stronger uniaxial magnetocrystalline anisotropy with Δ of the order of 1 nm. Finally, except for $SrRuO_3$ with a Curie temperature of 150 K, these materials are metallic and ferromagnetic with out-of-plane magnetization at room temperatures. CIDM has also been investigated in the diluted magnetic semiconductor (Ga,Mn)As with a perpendicular magnetization and a typical Curie temperature around 100 K [73–76].

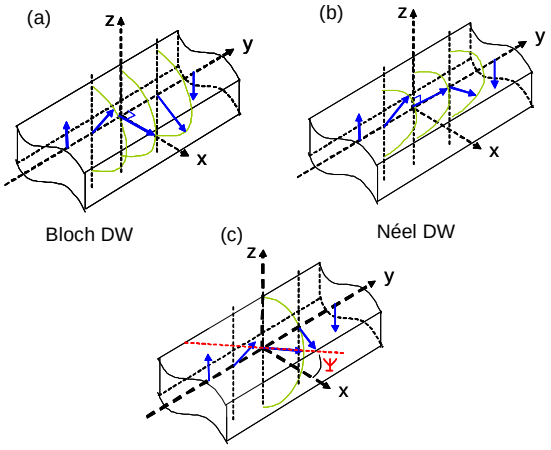

Figure 6: (a-b) Schematic representation of a Bloch ($\psi = 0$) (a) and a Néel ($\psi = \pi/2$) DW (b). (c) DW with a non zero internal angle ψ.

2.2.2. Domain wall spin structure

The equilibrium DW configuration (Bloch or Néel) depends on the demagnetizing energy in the DW. One can define an effective out-of-plane anisotropy $K_{eff} = K - N_z \mu_0 M_s^2/2$ and a DW demagnetizing energy density $K_d = \mu_0 M_s^2 (N_y - N_x)/2$, where N_x, N_y and N_z are the demagnetizing factors in the DW. K_d represents the magnetostatic energy difference between a Bloch and a Néel DW. The DW energy σ and the DW width parameter Δ depends on the internal in-plane angle ψ (see Fig. 6(b))) as [77]:

$$\sigma = 4\sqrt{A\kappa(\psi)} \tag{3}$$

$$\Delta = \sqrt{A/\kappa(\psi)} \tag{4}$$

$$\kappa = K_{eff} + K_d \sin^2(\psi) \tag{5}$$

$$\tag{6}$$

For K_d positive (resp. negative), σ is minimum for $\psi = 0$ or $\psi = \pi$ (resp $\psi = \pm\pi/2$) and thus the equilibrium DW configuration is a Bloch DW (resp. Néel DW). In an extended thin film, $N_x \ll 1$, so that a Bloch DW is expected and $\Delta = \sqrt{A/(K - N_z \mu_0 M_s^2/2)}$. In a nanowire geometry, K_d depends on the dimensions of the nanowire and is expected to decrease as its width and the thickness decreases [78]. For a thin nanowire of thickness t and width w, the DW volume can be modeled as an ellipse and the demagnetizing factors can be approximated as $N_y \sim t/(t + \pi\Delta)$ and $N_x \sim t/(t + w)$ [79, 80]. In most experiments, the wire width (typically between 70 nm and 500 nm) is large compared to the DW width so that $N_x > N_y$ and a Bloch DW is generally prevailing.

The simple Bloch DW structure is predicted for single ultra-thin magnetic layers but films composed of several magnetic layers separated by an ultrathin spacer may exhibit more complex DW structure. The strong magnetostatic and/or exchange coupling between the layers favors a composite DW composed of one DW in the respective layers but the exact structure of such a DW has been little investigated so far. Recently, by combining magnetic force and ballistic

electron emission microscopies, Bellec *et al.* identified two superposed Néel walls with opposite polarities in Co(1.6 nm)/Au(5.0 nm)/Co(1.4 nm)/Au(5.0 nm) multilayer instead of a standard Bloch DW structure in the two layers [81]. The DWs structure in magnetic spin valves may also be more complex than expected. It was shown recently that in a Co/Cu/NiFe spin valve with a head-to-head DW in the NiFe layer, a quasi DW appears in the magnetically "fixed" Co layer due to the magnetostatic interaction between the layers [82]. Such quasi-static DW affects the DW profile in the NiFe layer as well as its dynamics. The effect of such coupling in spin valves with out-of-plane magnetized layers remains to be studied.

3. Theory of current-induced Domain Wall Motion (CIDM)

The idea that the transfer of spin from conduction electrons moving across a spin texture of a DW can be used to manipulate the DW was first introduced by Berger at the end of the seventies [83]. When a current, which is naturally polarized in a metallic ferromagnet crosses the DW, the exchange interaction aligns the conduction electron spin polarization direction along the direction of the local magnetization. As the exchange interaction conserves the total spin, this angular momentum has to be transferred to the local magnetization, which is equivalent to a torque acting on the magnetization resulting in a DW displacement in the direction of the electron flow. As this effect is independent of the film thickness, it dominates for thin films over the hydrodynamic drag effect that originates from the Lorentz force [84].

The interaction between a spin polarized current and a magnetic DW strongly depends on the relation between the DW width and the length scale describing the transfer of spin angular momentum, i.e. the Fermi wavelength or the Larmor precession length depending on the model and the assumptions used, which is typically a few nm in 3d metals [85–89]. Two limits can be distinguished. When the DW width is very wide, the conduction electron spins adiabatically follow the local magnetization. In the case of a narrow DW, nonadiabatic effects might

occur. These two limits are discussed in the following.[1]

3.1. Current induced torques

In the absence of spin relaxation, the spin transfer torque density τ_{ST} can be expressed as a function of the spin current density $\vec{J_s}$ [86]. For a 1D system with the spin current flowing along the x-direction this reads:

$$\vec{\tau}_{ST} = -\frac{\partial \vec{J_s}}{\partial x} \tag{7}$$

Eq. 7 is a continuity equation for the spin current that expresses the conservation of the total spin of the conduction electron and of the local magnetization.

Note that here the vector $\vec{J_s}$ denotes the spin direction and the current distribution is assumed to be homogeneous along the x-direction. The adiabatic limit assumes that the spin polarization is aligned along the direction of the local magnetization due to the exchange interaction, so $\vec{J_s} = -J_s \vec{m}$ with $\vec{m}$ the unit magnetization vector and $J_s = |\vec{J_s}|$. J_s can be written as a function of the spin polarization P and current density J as $J_s = JP\hbar/2e$ with e the conduction electron charge. This leads to

$$\vec{\tau}_{ST} = \frac{JP\hbar}{2e}\frac{\partial \vec{m}}{\partial x} \tag{8}$$

As pointed by Xiao *et al.* [86], although the current spin polarization is aligned along the local magnetization, the local out-of-equilibrium spin density $\vec{s}_{ad}$, also called spin accumulation, is on the contrary slightly tilted and has a component transverse to the magnetization. In a simple s-d model where the torque is represented as the effective field due to $\vec{s}$ through the exchange interaction J_{sd}, this transverse component is responsible for the spin transfer torque with $\tau_{ad} = -J_{sd}\,\vec{S} \times \vec{s}_{ad}$ where S is the localized d electron spin. Note that $\vec{s}_{ad}$ is actually perpendicular to $\partial \vec{m}/\partial x$.

[1] For more details, see the extensive review on microscopic theories applied to current-driven DW motion published by Tatara et al. [90].

The torque $\vec{\tau}_{ST}$ can also be converted into a time derivative of the unit magnetization $\vec{m}$ by multiplying Eq. 8 by $-\gamma/M_s = -g\mu_B/(\hbar M_s)$:

$$\left(\frac{\partial \vec{m}}{\partial t}\right)_{ST} = -u\frac{\partial \vec{m}}{\partial x} \tag{9}$$

With $u = JPg\mu_b/2eM_s$, μ_B the Bohr magneton and M_s is the saturation magnetization. u is generally called the spin drift velocity and is actually the maximum velocity that the DW can reach when the conduction electron spin moments are fully converted into DW displacement.

Indeed, in the adiabatic limit, every electron passing through a DW undergoes a change of angular momentum of $\hbar$ and thus adds a magnetic moment of $2\mu_B$ to the DW [91]. Thus the change of magnetic moment in the wire due to an electric current during a time Δt is

$$\delta m_{current} = \frac{2P\mu_B JA\Delta t}{e} \tag{10}$$

where A is the cross-sectional area of the wire.

If angular momentum is fully converted into a DW displacement Δl , this leads to a change of magnetic moment in the wire reading $\delta m = 2M_S\Delta lA$ where M_S is the saturation magnetization. By balancing these two contributions, the velocity of the DW is obtained,

$$v = \frac{\Delta l}{\Delta t} = \frac{P\mu_B}{eM_S}J \equiv u \tag{11}$$

Since theories developed to describe spin transfer torque in the adiabatic limit were not able to reproduce experimental results, it was suggested that the effect of spin transfer was more complicated and that nonadiabatic contributions are present. The corresponding nonadiabatic torque was first introduced by Zhang *et al.* [92] and Thiaville *et al.* [93] and is characterized by a dimensionless parameter β

$$\frac{\partial \vec{m}}{\partial t} = \beta\, \vec{m} \times \left[\left(\vec{u}\cdot\nabla\right)\vec{m}\right] \tag{12}$$

This torque is perpendicular to the adiabatic torque and although its amplitude is expected to be small in typical 3d metals with wide DWs ($\beta_{sr} \approx 0.01$), it significantly alters the dynamics of the DW and in particular can determine the critical current density and the terminal velocity of the DW. Two different contributions have been identified for this torque. The first one is due to the spin relaxation in the DW, (β_{sr}) [85, 89, 90, 92–96]. Such spin relaxation can occur through spin-flip scattering events with impurities, phonon, etc. where the spin is not conserved due to the spin-orbit interaction. This process can be accounted for by an additional term on the right hand side of Eq. 7 describing the spin flip rate, Γ [97], which thus tilts the direction of the spin torque. Note that this torque is present even for a wide DW in the full adiabatic limit.

Several authors have carried out calculations to extract the value of β_{sr}. In a phenomenological approach, Zhang et Li [92] approximated Γ as $-\vec{s}/\tau_{sf}$ where τ_{sf} is the spin relaxation time and $\vec{s}$ the spin accumulation. This leads to an additional transverse spin accumulation along $\partial \vec{m} / \partial x$ which, through the exchange interaction, exerts a torque of the form of Eq. 12 where $\beta = \xi/(1+\xi^2)$ with $\xi = \tau_{ex}/\tau_{sf}$ and $\tau_{ex} = \hbar/J_{sd}$. Using a different approach based on a phenomenological argument, i.e. Galilean invariance implying a DW velocity identical to the carrier drift velocity, it was predicted that $\beta_{sr} = \alpha$ with α the Gilbert damping parameter [98]. Although it could be the case in certain limiting cases, in general, any magnetic disorder or spin-orbit interaction would break the Galilean invariance leading to $\beta_{sr} \neq \alpha$. Fully microscopic calculations of β_{sr} and α in the s-d model were performed by Kohno *et al.* [99] using Green's function formalism in which spin relaxation effects are treated consistently and quantum mechanically indicating that $\beta_{sr} \neq \alpha$ and this was supported by the theory derived by Duine *et al.* using the functional Keldysh formalism [100]. Similarly, Tserkovnyak *et al.* [95, 96] found that $\beta_{sr} \approx \alpha$ but, in general, $\beta_{sr} \neq \alpha$ due to the effect of multiband or deviation from weak ferromagnetism.

Recently, the role of spin orbit coupling on β was studied by several authors [97, 101–104] who considered the effect of spin-orbit coupling due to impurities [97] but also the intrinsic spin-orbit coupling of the lattice [101–103].

In a rough scheme, spin-orbit coupling leads to additional spin relaxation to the lattice and a resulting spin mistracking in the DW which enhances the non-adiabatic torque. Actually, strong non-adiabaticity was predicted in systems with high intrinsic spin-orbit coupling, such as in 2D electron gas with a Rashba spin-orbit interaction or (Ga,Mn)As [101, 102, 104].Garate *et al.* [102] calculated the parameters α and β_{sr} taking into account intrinsic spin-orbit coupling. They underline that the nonadiabatic STT that α can be seen as a correction to the Gilbert damping in the presence of an electric current; the nonadiabatic spin transfer torque are both dissipative due to the fact that both originate from the same microscopic processes.

A second contribution to β is a pure nonadiabatic contribution occurring when the gradient of magnetization is too large for the current spin polarization to follow the local magnetization direction (described by the nonadiabaticity parameter due to nonadiabatic transport β_{na}). The effect of nonadiabatic transport on the DW torque and dynamics was studied by several authors and is expected to occur only for very narrow DWs. Viret *et al.* [89, 105] and Xiao *et al.* [86] showed that nonadiabaticity leads to a non-local oscillatory torque due to the fast precession of conduction electron spins around the exchange field. Ohe *et al.* [106] arrived at similar conclusions from full quantum mechanical calculation as well as Thorwart *et al.* [107]. This non-oscillatory torque was shown to lead to a distortion of the DW spin structure and can modify its dynamics, resulting for example in an oscillatory DW velocity [106], as well as DW depinning. Tatara *et al.* [85, 108] underlined that this oscillating torque on each spin is indeed summed up to a force F_{el} when looked at collectively. F_{el} can be seen as the force exerted by the conduction electrons by momentum transfer when reflected by the fast DW texture. In a ballistic transport assumption, $F_{el} = eN_e\rho_w j$ is expressed as a function of the DW resistivity ρ_w with N_e the total number of electrons in the and $\beta_{na} = \frac{ne^2\rho_w\Delta^2}{P\hbar}$ where n is the electron density and Δ the DW width [94].

Different characteristic lengths λ_{na} for the occurrence of nonadiabatic transport have been proposed depending on the authors and the assumption. Tatara [85]

identified λ_{na} to the Fermi wavelength in the ballistic limit and Xiao *et al.* [86] arrived to a similar conclusion in a different formalism. Viret [89, 105] identified λ_{na} to the Larmor precession length $\lambda_L = v_F\hbar/J_{sd}$ with v_F the Fermi velocity and J_{sd}, the s-d exchange, which is the distance travelled on average by an electron during one precession period. In a diffusive limit, Ban and Tatara [88] arrived to a similar conclusion but with $\lambda_L = \sqrt{\hbar D/J_{sd}}$ with D the diffusion constant.

3.2. Theoretical analysis using a one dimensional model and micromagnetic simulations

3.2.1. The Landau-Lifshitz-Gilbert equation of magnetization dynamics including the effects of spin-polarized currents

The phenomenological LLG equation under current and taking into account both adiabatic and nonadiabatic torques was introduced by Zhang *et al.* [92] and Thiaville *et al.* [93] and reads:

$$\frac{\partial \vec{m}}{\partial t} = \gamma\mu_0 \vec{H} \times \vec{m} + \alpha \vec{m} \times \frac{\partial \vec{m}}{\partial t} - (\vec{u} \cdot \vec{\nabla}) \vec{m} + \beta[\vec{m} \times (\vec{u} \cdot \vec{\nabla}) \vec{m}] \qquad (13)$$

where $\gamma = g|\mu_B|/\hbar$ is the gyromagnetic ratio. The first two terms correspond to the well-known Landau-Lifshitz-Gilbert equation describing the magnetization dynamics in a magnetic field where α is the so-called Gilbert damping parameter [109, 110]. The effect of the current is represented by the last two terms. The third term is the adiabatic spin-transfer torque where u is given by equation (11), the fourth term is the previously introduced nonadiabatic torque described by the parameter β.

3.2.2. One dimensional model

This equation can be written in a simple analytical form by assuming a constant DW profile [111]. The DW dynamics can then be described by two independent variables, the DW position q and its conjugate momentum, the DW magnetization angle ψ as shown in Fig. 7 [111–113]. The 1D model equations of motion read [93, 114–117]:

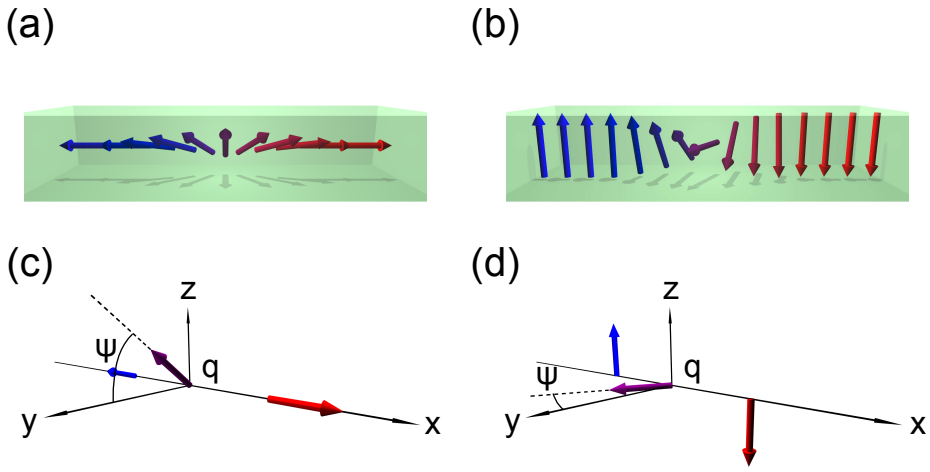

Figure 7: Schematic representation of (a) a wire with in plane easy axis containing a transverse wall and (b) a wire with out-of-plane easy axis containing a Bloch wall. Definition of the variables used in the 1D model for a transverse wall (c) and a Bloch wall (d) where q is the position of the center of mass of the wall and ψ is the tilt angle of the DW's magnetization.

$$\dot{\psi} + \frac{\alpha \dot{q}}{\Delta} = \gamma \mu_0 H + \frac{\beta u}{\Delta} - \frac{\gamma}{2M_s} \frac{\partial V_{pin}}{\partial q} \tag{14}$$

$$\frac{\dot{q}}{\Delta} - \alpha \dot{\psi} = \frac{\gamma \mu_0 H_k}{2} \sin 2\psi + \frac{u}{\Delta} \tag{15}$$

where H_k is the restoring field for the DW transverse orientation, H is the external magnetic field applied along the easy axis, and $\Delta(\psi) = (A/(K_0 + K \sin^2 \psi))^{1/2}$ is the DW width with K_0 being the uniaxial longitudinal anisotropy and $K = \mu_0 M_s H_k/2$ is the transverse anisotropy mainly due to magnetostatic effects [80]. V_{pin} is the pinning potential that may depend on q. As reported by Bruno [118], equation 14 is only valid for slowly varying V_{pin} compared to the DW width. Otherwise, the pinning potential can lead to a modification of the DW width. One can note that the nonadiabatic torque enters the equation 14 with an analytical form similar to an external field H_I with $\mu_0 H_I = \beta u/\Delta\gamma$. Despite its simplicity, the 1D model provides a qualitative understanding of DW motion in a nanowire even for rather complicated spin structures such as vortex

walls [117].

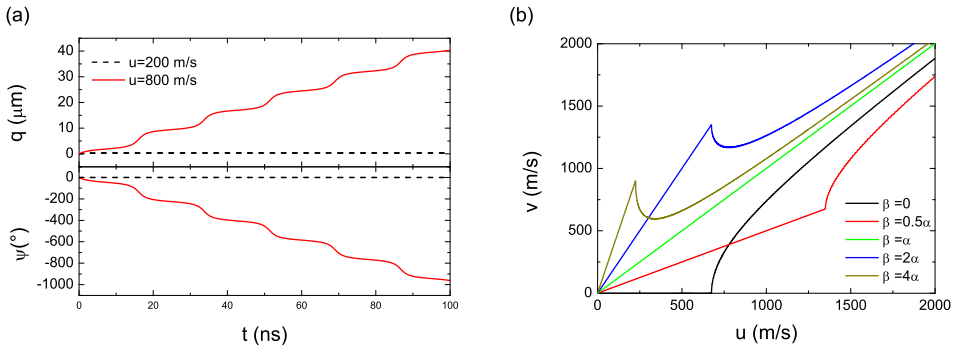

Figure 8: (a) Time evolution of the position q and the angle ψ obtained for the same parameters as described below (β=0) and for two different values of u. (b) Average DW velocity as a function of u calculated using the 1D model for $\beta = 0$, $\alpha = 0.02$, $H_K = 1600$ Oe, $M_S = 800$ emu.cm^{-3}, and $\Delta = 50$ nm.

This simple 1D model can be used to deduce the critical current and the DW velocity when the motion is driven by current (see Fig. 8) in the absence of pinning (perfect wire with no roughness).

For $\beta = 0$, there is a threshold current value below which there is no steady DW motion. Below the threshold current, after a small displacement of the wall during the application of the current, the DW relaxes back to its initial position as soon as the current is suppressed. As noted by Zhang *et al.*, the initial DW velocity is equal to u [92]. In this regime, the angular momentum transferred by the conduction electrons to the DW is completely absorbed by the angle ψ.

Above a critical velocity u_c, the DW starts moving. This threshold can easily be calculated by finding the stationary solutions of equation 14, solving $\dot{\psi} = 0$, $\dot{q} = 0$, and $\sin 2\psi = 1$, resulting in $u_c = \gamma\mu_0 H_k \Delta/2$ [119].

This threshold value corresponds to the onset of a periodic DW transformation associated with an increase of ψ similar to the one observed above the Walker breakdown in the case of field-driven DW motion [120]. For $u > u_c$, the domain wall velocity oscillates periodically with a non-zero average value [119] (Fig. 8(b)) :

$$< v >= \frac{\sqrt{u^2 - u_c^2}}{1 + \alpha^2} \tag{16}$$

The introduction of the β term strongly modifies the dynamics of the DW (Fig. 8(b)). The nonadiabatic torque acts as a magnetic field that can sustain a steady state DW motion resulting in the disappearance of the intrinsic threshold current even for very small values of β, the real threshold current for DW motion being only determined by extrinsic pinning. The DW velocity in the steady state regime increases linearly as $v_{final} = \beta u/\alpha$ up to a critical velocity [92, 94, 119]

$$u_W = u_c \frac{\alpha}{|\beta - \alpha|} \tag{17}$$

Above u_W, the average DW velocity drops ($\beta > \alpha$) or increases ($\beta < \alpha$) because the DW structure undergoes periodic transformations similarly to the field-driven case above the Walker threshold. Since the nonadiabatic torque behaves as a nonuniform magnetic field, it controls the final velocity of the DW. For very large u, the average final DW velocity converges towards:

$$\bar{v} = \frac{u}{1+\alpha^2}(1 + \alpha\beta) \tag{18}$$

Only in the case of $\beta = \alpha$, the DW propagates without distortion, in agreement with the Galilean invariance principle [98].

In the presence of pinning, the determination of the critical current is more complex. Using the 1D model, Tatara *et al.* [94, 121] identifies three different regimes depending on the pinning strength.

- In the weak pinning regime, the critical current density required to depin the DW depends on the magnitude of β. When β is negligible but finite, the depinning is due to the adiabatic torque. In that case, the DW escapes from its pinning site due to an effective kinetic energy supplied by the spin transfer. Note that this holds only for current pulses that are short compared to the relaxation time of the DW in the potential well so that the kinetic energy is not dissipated by Gilbert damping. The critical current density varies as $J_c^{(1)} \propto \sqrt{H_p}$ with H_p the pinning field. For a larger β, the depinning is governed by the nonadiabatic torque and depinning occurs when the force exerted by the nonadiabatic torque exceeds the pinning

force. The critical current is then $J_c^{(2)} \propto H_p/\beta$. Therefore, the larger β, the smaller $J_c^{(2)}$.

- In the intermediate pinning case, $J_c^{(2)}$ can become higher than the intrinsic critical current density associated with the adiabatic torque $J_c^{(3)}$. If pinning is not too strong, depinning occurs for $J_c^{(3)}$ independent on pinning and depends only on the adiabatic torque.

- Finally, for very strong pinning such that $H_p > H_k/\alpha$ with H_k the DW demagnetizing field, the DW stays pinned in the potential well for $J = J_c^{(3)}$ and the DW angle ψ oscillates continuously. Depinning then occurs for a higher value of the current density $J_c^{(4)}$ with $J_c^{(4)} \propto H_p$.

Thiaville *et al.* theoretically investigated the non steady-state displacement of magnetic DW in a nanostrip submitted to a time-dependent spin-polarized current [114]. The authors related the position to the DW magnetization angle. In the framework of purely adiabatic spin transfer, in the absence of applied magnetic field and neglecting pinning, equation 14 can be written as:

$$\dot{\psi} + \frac{\alpha \dot{q}}{\Delta_T} = 0 \tag{19}$$

With Δ_T the Thiele domain wall width.

This equation simply shows that any modification of the angle ψ results in a displacement of the DW. Therefore, for a vortex to transverse wall conversion, this results in a displacement of $dq = P\pi dy_c \Delta_T/(w\alpha)$ with P the vortex core polarity, dy_c the variation of its position along the wire width w. This displacement can be as large as 3.9 μm for $\Delta = 50$ nm and $\alpha = 0.02$. As this transformation can be triggered by a single pulse of 1 ns, care has to be taken when extracting DW velocities for such short current pulses from quasi-static measurements [122].

3.2.3. Micromagnetic simulations

While the 1D model has proven very powerful to qualitatively understand current induced DW experiments, the assumption of a rigid DW can be limiting.

For instance, the details of the transformation between different domain wall types are not described in the 1D model. For instance the Walker breakdown current density necessary for a vortex to transverse domain wall transformation can be different from the one necessary for the reverse transverse to vortex domain wall transformation. Micromagnetic simulations allow one to model such effects as well as the influence of dc [123], ac [124] and pulsed [114] current on realistic DW structure as well as the influence of the shape anisotropy on the threshold current for DW motion [125]. Moreover, roughness [116, 119, 124, 126] and artificial pinning [127, 128] such as notch can easily be implemented. It was also demonstrated that trapped DW can be used as an effective microwave source which can be useful in information storage or telecommunication applications [129–131]. In the following, we review recent developpment in micromagnetic simulation firstly in soft in-plane magnetized nanowires and secondly in out-of-plane magnetized nanowires with narrow Bloch DWs.

Soft in-plane magnetized nanowires. Thiaville *et al.* calculated the DW velocity as a function of the velocity u and for different values of β [93] in the case of a perfect wire and for different edge roughnesses (Fig. 9). For a perfect wire, the results are in good agreement with the results of the 1D model (Fig. 8.b). The steady DW motion gives way to precessional motion above the Walker threshold. The oscillation in the DW velocity is related to a periodic transformation of the DW. In the case of in plane magnetized materials, the precession of the DW occurs through the crossing of the wire width by an antivortex or vortex, similarly to the field-driven case [115, 119, 126]. The addition of edge roughness leads to extrinsic pinning which has to be overcome before the wall can move, thus resulting in a critical velocity u_c^{pin} even for $\beta \neq 0$. Moreover, for a rough wire, the velocity is reduced compared to the perfect-case relation $v = (\beta/\alpha)u$.

Recently, the effects of disorder on DW propagation was studied by micromagnetic simulations [132]. In this study, the authors simulate the displacement of a vortex wall along a magnetic stripe while disorder is modelled as a fluctua-

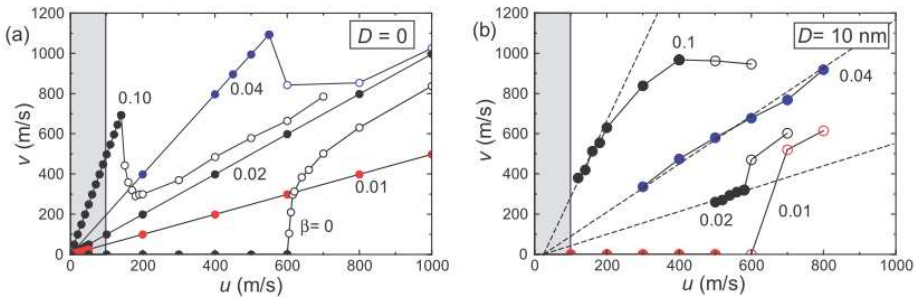

Figure 9: Average velocity of a transverse DW as a function of the velocity u and for different values of β computed by micromagnetics in the case of a wire with a $120 \times 5\text{nm}^2$ cross-section. The used parameters are: $M_s = 8 \times 10^5 A/m$, $A = 10^{-11} J/m$, $K = 0$, and $\alpha = 0.02$ .The shaded area represents the experimentally available range of u. Open circles denote vortices nucleation. (a) Perfect wire and (b) wire with rough edges (mean grain size $D = 10nm$). The dashed line display a fitted relation with an 25 m/s offset. From Ref. [93]

tion in the saturation magnetization of the ferromagnetic layer. The presence of disorder results in an increase of energy dissipated by the vortex core through spin waves emission which are associated with the motion of the core in areas of strong disorder. However, the main contribution to energy dissipation comes from the area around the DW itself pointing towards the increase in the excitement of internal degrees of freedom of the DW. It is shown that the disorder increases or decreases the DW wall velocity depending on the applied field or current compared to the corresponding Walker threshold. The main results indicate that disorder affects DW dynamics in a way that can be interpreted as a modification of the effective damping parameter. Therefore, the extraction of fundamental parameters such as the damping parameter α from DW motion experiments requires precautions.

Out-of-plane magnetized material. The recent interest in out-of-plane magnetized materials has stimulated the modeling and the micromagnetic simulation of the CIDM in these materials.. Although the main dynamical features are generally well described by the 1D model, simulations also reveal important additional features arising from the thin Bloch DW structure and the different magnetic properties of these materials [78, 133–138].

Domain wall propagation In a perfect nanowire, *i.e* no edge roughness or local pinning of the DW due to defects, micromagnetic studies [135, 137–139] show that the main features of the current or field induced propagation of a Bloch DW in an out-of-plane magnetized nanowires, such as the dependence of the DW velocity with the applied field and/or current, is generally well described by the simple 1D model. In the 1D model, the current density J_W for Walker precession can be expressed as:

$$H_W = \alpha H_k/2 \tag{20}$$

$$J_W = \frac{e\mu_0 M_s H_k \Delta}{\hbar P} \frac{\alpha}{|\beta - \alpha|} \tag{21}$$

with $H_k = 2K_d/\mu_0 M_s$ the in-plane transverse DW demagnetizing field (see also section 3). Micromagnetic simulations underline that J_W and H_W depend directly on the wire width and thickness [133–135] which actually results from the dependence of H_k on the wire geometry. Szambolics *et al.* though revealed a small discrepancy (10 %) between the prediction of the 1D model and the micromagnetic simulation for H_W. This can be explained by the small non-invariance of the DW magnetization along the wire width leading to different magnetostatic field in the middle and on the sides of the wires [139].

It is well known that in out-of-plane magnetized materials with narrow DWs, the DW dynamics is strongly sensitive to local defects in the films leading to a local DW pinning. Garcia-Sanchez *et al.* [138] and Szambolics *et al.* [140] studied the effect of the polycristalline nature of the film by introducing a random anisotropy distribution. The authors observe that such a distribution alters the DW shape during its propagation which is no more straight as well as its internal structure by locally twisting the DW internal angle ψ so that it loses its Bloch or Néel nature. This affects the DW dynamics and in particular the periodic DW transformation in the Walker regime where the characteristic periodic velocity disappears. The effect of disorder is particularly important at low current density where the DW propagation is actually a succession of pinning/depinning events separated by a more or less steady DW propagation.

Dependence of J_c on the wire geometry. Several authors [78, 133–138] studied the depinning of a DW induced by a current pulse from a geometrical pinning sites such as a notch in the nanowire or a local change of the anisotropy in the wire.

Using both 1D model and micromagnetic simulation, Jung *et al.* [78] showed that for narrow (typically below 100 nm) and thin (< 10 nm) nanowires, the critical current density J_c does not depend on the pinning strength nor on the nonadiabaticity factor β and reaches a minimal value for a certain geometry (width-thickness) of the wire. For this critical geometry, the demagnetizing energy K_d changes sign and the DW switches from a Bloch to a Néel structure. The intrinsic critical current associated with the adiabatic torque proportional to K_d thus becomes very low ($J_c < 10^{10}$ A/m^2) (in an ideal geometry it would vanish as the anisotropy barrier goes to zero as also for round wires with shape anisotropy [141]) and controls the depinning process. As a consequence, the nonadiabatic spin torque term β and extrinsic pinning effect play a little role on the depinning. The geometry for minimal J_c is obtained for thick enough and very narrow wires: for a 10 nm thick film, Jung *et al.* [78] found the critical current density to be minimal for $w \approx 70$ nm, with the exact dimensions depending critically on the magnetic parameters. In most nanowire geometry considered experimentally so far, theminimal J_c was not attained and J_c is expected to decrease as the wire width and thickness decrease [134–136]. Such scaling law would be of high interest for application to magnetic memories as it means that it is possible to decrease the critical current density while maintening a high DW pinning force (bit stability). One can note however that in these works, the authors generally considered a relatively low value of β (0.02) compared to the one that were measured experimentally in out-of-plane magnetized materials (from 0.1 up to 1) (see next section), so that the effect of nonadiabaticity may actually be underestimated.

Domain wall oscillator The possibility to combine low intrinsic critical current density and high pinning forces can also be exploited to generate new

steady dynamical states. Above the intrinsic current density, the DW enters a precession regime with a periodic change of the internal DW structure from Bloch to Néel associated with an oscillation of the internal angle ψ with time (the so-called Walker regime). If the pinning is not too high, this leads to DW depinning followed by DW propagation with a velocity oscillating in time [142, 143]. However, if the pinning is strong enough, the DW stays pinned in the potential well while its internal structure steadily oscillates [144, 145]. This situation actually corresponds to the high pinning case of Tatara *et al.* [85] (see discussion above), with a pinning field H_p larger than H_k/α, with H_k the DW demagnetizing field. Out-of-plane magnetized nanowires are well suited to obtain small H_k/α as they are generally characterized by high values of α (typically higher than 0.1 in $(Co/Pt)_n$ multilayers [146]) and a very low value of H_k can be obtained by playing on the wire geometry. Bisig *et al.* have demonstrated the validity of this idea by using micromagnetic simulations [145]. The authors considered a Bloch DW pinned in a 16 nm wide notch patterned in a 7 nm thick wire. The magnetic parameters used are those typical of $(Co/Pt)_n$ multilayers and only the effect of the adiabatic torque is taken into account ($\beta = 0$). This geometry corresponds actually to a minimal value of H_k and a critical current density of $J_c = 1.34 \times 10^{11}$ A/m^2. Micromagnetic simulations show that for $J > J_c$, the DW stays pinned in the potential well and periodically oscillates between a Bloch and a Néel structure. The average frequency $< \dot{\psi} >$ scales approximately linearly with the spin current drift velocity $u = JP\mu_B/eM_s$ (see Fig. 10) in agreement with a simple 1D model that predicts $< \dot{\psi} >= -u/\alpha\Delta$. This simple concept of localized DW steady-state oscillator opens an interesting way for current controlled tunable nanoscale microwave oscillators that can work at zero external magnetic field.

3.3. Thermally activated domain wall motion

So far, we have considered the current induced domain wall dynamics at zero Kelvin. However, experiments are carried out at finite temperatures and most often at room temperature. In addition, Joule heating can lead to ad-

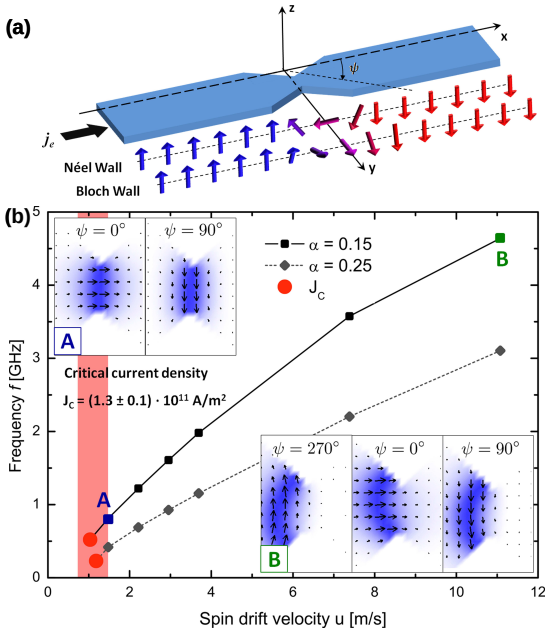

Figure 10: (From Ref. [145]) (a) Schematic illustration of the geometrically confined structure. The arrows represent the magnetization configuration inside the structure, which can be either a Bloch or a Néel domain wall. (b) Domain wall oscillation frequency f as a function of the injected spin current drift velocity u for constant $\alpha = (0.15, 0.25)$. (A) The domain wall profile is symmetric under rotation for low current density $j_e = 1.79 \times 10^{11}$ A/m^2. (B) At a high current density $j_e = 1.34 \times 10^{12}$ A/m^2, the domain wall shows asymmetric oscillations, this leads to a nonharmonic behavior.

ditional significant temperature increase of the nanowire during the current injection [55, 147, 148]. The inclusion of thermal effects is particularly relevant for current/magnetic field values that are smaller than the zero K critical values as the thermal energy helps the DW to overcome the DW pinning potential. They are also expected to play an important role for temperatures close to the Curie temperature [149], which may occur due to the Joule heating effect when injecting a high current density.

The inclusion of thermal effects on the current induced domain wall dynamics was studied by numerous authors [128, 149–159]. Thermal activation is generally included by adding to the Landau-Lifschitz Gilbert equation a stochastic Gaussian distributed magnetic field [160] $\vec{H_T}$ with zero mean value and

correlations

$$< H_{Ti}(t,\vec{r})H_{Tj}(t',\vec{r'}) >= \frac{2\alpha k_B T}{\gamma_0 \mu_0 M_s}\delta_{ij}\delta(\vec{r}-\vec{r'})\delta(t-t') \tag{22}$$

. Duine *et al.* [156] derived from Eq. 22 modified equations of the 1D model where stochastic Gaussian distributed forces η_ψ and η_q are included to account for the effect of the temperature:

$$\dot{\psi} + \frac{\alpha\dot{q}}{\Delta} = -\frac{\gamma}{2M_s}\frac{\partial V_{eff}}{\partial q} + \eta_\psi \tag{23}$$

$$\frac{\dot{q}}{\Delta} - \alpha\dot{\psi} = \frac{\gamma}{2M_s\Delta}\frac{\partial V_{eff}}{\partial \psi} + \eta_q \tag{24}$$

η_i are characterized by the correlation $< \eta_i(t)\eta_j(t') >= (2\alpha k_B T\gamma)/(M_s\Delta)\delta(t-t')\delta_{i,j}$. The effect of the current, external field H and demagnetizing field H_k is included in an effective potential (per surface unit):

$$V_{eff} = \mu_0 H_K M_s \Delta \sin^2\psi + \frac{2M_s}{\gamma}u\psi - 2M_s q(\mu_0 H + \frac{\beta u}{\Delta\gamma}) \tag{25}$$

One can note that the adiabatic torque only changes the potential V_{eff} along the ψ axis whereas the nonadiabatic torque affects the potential along the q axis as does H.

3.3.1. Thermally activated DW depinning

Kim *et al.* [158] and Lucassen *et al.* [155] used these equations to study the effect of the thermal activation on the DW depinning. Kim *et al.* consider a general pinning potential $V_{pin}(q)$ with a width δX. From the Fokker-Planck equation related to the Langevin equation 23, they obtained a mean depinning time that follows an Arrhenius law over a single energy barrier:

$$\frac{1}{\tau} = \frac{1}{\tau_0}\exp\left[\frac{-E_b(J)}{k_b T}\right] \tag{26}$$

with $1/\tau_0$ the attempt frequency. The current dependent energy barrier is

$$E_b(I) = E_{b,0} - \sigma I + \sigma' I^2 \tag{27}$$

where $\sigma = \beta P \frac{\hbar}{e} \frac{\delta X}{\Delta}$ and σ' depends on the local curvature on the top and bottom of the potential barrier. $E_{b,0}$ is the potential barrier height in the absence of current and depends on the external magnetic field H. Importantly, only the nonadiabatic torque modifies the potential barrier. Under usual conditions, the dominant contribution is expected to come from the linear term whereas the quadratic current contribution can become important for small applied fields and for fields close to the switching field. By calculating the energy barrier ΔV associated with V_{eff} for a pinning potential $V_p(q) = aq^2 + bq^4$, Lucassen *et al.* [161] found an Arrhenius law with ΔV scaling as $(\mu_0 H + \beta u/\Delta\gamma)$, so that the nonadiabatic torque acts similarly to an effective field in this case.

Micromagnetic simulations of the thermally activated depinning of a Bloch DW was studied by Garcia-Sanchez *et al.* [138]. The pinning site was composed of a small defect in the wire with lower anisotropy and they included the effect of thermal activation by adding a Gaussian distributed thermal field (T=300 K) (See Eq. 22). The simulation reproduce qualitatively the prediction of Kim *et al.* with a potential barrier for depinning $E_b(H, I)$ decreasing linearly with H and I and σ proportional to β. Current acts thus on the pinning energy barrier similar to an external effective magnetic field $H_{eq} = \epsilon I$ and this is due to the effect of the nonadiabatic torque. The proportionality factor is found relatively close (by about 10%) to the one expected in the 1D model but σ_I is significantly different from the one expected in Kim's theory (a factor 5). This may be explained by the assumption in this theory of a pinning that is homogeneous along the wire width, which does not hold in this case.

3.3.2. Thermally activated DW propagation

Thermal activation also affects the DW propagation. Using micromagnetic simulations, Martinez *et al.* [153] have shown that when the driving force, either field or current, is below the deterministic propagation threshold, thermal activation leads to non-zero velocities. On the contrary, when the driving force is larger than the pinning force, thermal perturbations have a negligible effect on the DW velocity. In the thermally activated regime, the DW velocity is found

to depend exponentially on the external force. Tatara *et al.* [150] and Duine *et al.* [155, 156] also studied the effect of thermal activation using the 1D model. In the pure adiabatic case, DW propagation is obtained at current density smaller than the zero current critical current density due thermally activated jump of the DW angle ψ over the demagnetizing energy barrier. However, this process affects the DW propagation only in systems with a small DW demagnetizing energy such as in the magnetic semi-conductor (Ga,Mn)As and has little effect for metallic systems. Lucassen *et al.* also considered Eq. (23) with $\beta \neq 0$ in the presence of disorder in Ref. [155].

Schieback *et al.* [149] tackled the problem differently. Instead of a modified LLG equation (22), they included thermal effects through a Landau-Lifschitz Bloch (LLB) equation [162] where the magnetization modulus is not assumed to be constant and is temperature dependent. Hence, besides the usual precession and relaxation, the LLB equation contains another term which controls the longitudinal relaxation. Under this assumption, they obtain a strong temperature dependence of the critical current for the Walker breakdown (see Fig. 11(a)), which can strongly modify the current induced domain wall motion (see Fig. 11(b)).

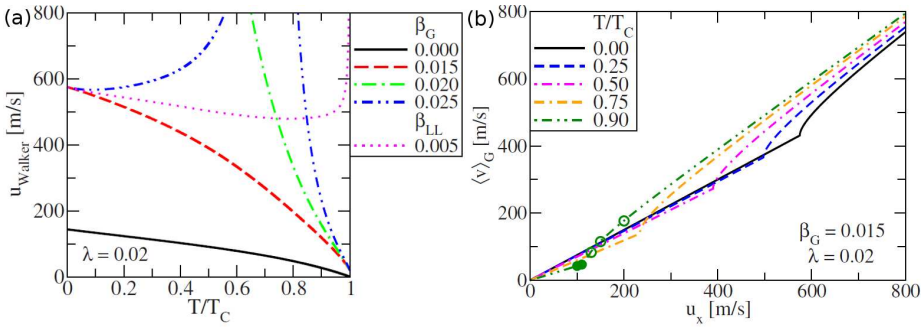

Figure 11: (a) Walker breakdown velocity as a function of T/T_c (T_c is the Curie temperature) for several value of β in the case of Gilbert damping (β_G) or Landau-Lifschitz damping (β_{LL}). The damping parameter is $\alpha = 0.02$ for Gilbert damping. (b) Average domain wall velocity as a function of the spin drift velocity for several value of T/T_c, $\beta_G = 0.025$ and $\alpha = 0.02$. From Ref. [149].

3.3.3. Domain wall creep

At very low field and/or current, the DW internal structure is strongly affected by the local disorder and the simple 1D model does not apply. In this regime, the DW propagation process is similar to an interface in a disordered medium and results from the competition between the elastic energy of the DW that tends to make to keep the domain line straight and the disorder which tends to roughen it. The dynamics of a DW driven by an external magnetic field H in this regime was shown to follow a law of the form [163, 164]:

$$v = v(H_c) \exp\left[-\frac{U_c}{k_B T}\left(\frac{H_c}{H}\right)^{\eta}\right] \tag{28}$$

with $H \ll H_c$ the critical field associated with the pinning force. Here U_c is a constant describing the pinning energy and η a constant characteristic of the disorder and of the dimensionality of the system, equal to 1/4 in ferromagnetic metals.

To describe the DW dynamics in the presence of current in this regime, Duine *et al.* [154, 155] extended Eq .25 to the case of a DW line described by the coordinate $q(y,t)$ and $\psi(y,t)$, which depends on the y coordinate transverse the wire axis. By considering extrinsic pinning, they obtained a velocity scaling as:

$$\ln v \propto -\frac{\epsilon_{el}}{K_b T}\left(\frac{J_c}{J}\right)^{\mu_c} \tag{29}$$

where ϵ_{el} is the elestic energy and μ_c the critical exponent.

The main results of there calculations was that the exponent characterizing the creep regime strongly depends on the presence of a dissipative spin transfer torque. In ferromagnetic metals, μ_c is found equal to 1/4 for $\beta \neq 0$ as is in the case of field driven DW motion, once again underpinning the fact that the β term acts on the DW in the same fashin an applied magnetic field.

4. Experimental observation of current-induced Domain Wall Motion

We now explore CIDM experimentally. Different techniques can be exploited for the measurements including magnetotransport, imaging by magnetic microscopy techniques and others which are briefly presented below. For an overview of techniques see for instance various chapters in Refs. [71, 165, 166]. For the experimental results we separate the systems into in-plane magnetized materials (for instance Permalloy) and out-of-plane magnetized materials (for instance Co/Pt multilayers) that exhibit distinctly different domain wall structures.

4.1. Characterization and measurement methods

In this section, we introduce some of the experimental techniques that are commonly used for detection and characterization of DW motion in magnetic nanowires. The choice of the technique to be used depends on the DWs properties that one wants to study. For instance, anisotropic magnetoresistance measurements (AMR) are more suited to detect the presence of the DWs in a certain section of the wire, while giant magnetoresistance (GMR) or magneto-optical Kerr effect (MOKE) measurements can be used to detect the DW position. Magnetic microscopy techniques allow for the characterization of the DW structure with the possibility to study the DW dynamics by using a stroboscopic approach.

4.1.1. Electrical measurements

Electrical characterization of the interaction between a spin polarized current and a magnetic DWs provides an easy and fast approach to carring out in-depth and systematic studies. The AMR and GMR effects are usually used to probe the magnetic properties of materials with in-plane anisotropy while the use of the extraordinary Hall effect (EHE) is favored for systems with out-of-plane anisotropy. While GMR and EHE measurements can provide information on the DW position, AMR can only probe the presence of the DW.

Anisotropic magnetoresistance. The AMR effect which is generally observed in ferromagnetic metals, arises from the anisotropy of scattering produced by spin-orbit interaction [167, 168]. A stronger scattering applies for electrons flowing parallel to the local magnetization, leading to a larger resistivity $\rho_{\parallel}$ compared to electron flowing perpendicularly to the magnetization resulting in a lower resistivity $\rho_{\perp}$. The material resistivity finally depends on the angle θ between the magnetization and the direction of the current flow in the material and is given by:

$$\rho(\theta) = \rho_{\perp} + (\rho_{\parallel} - \rho_{\perp}) \cos^2(\theta) \tag{30}$$

This effect can reach few percents in some alloys based on Fe, Co, and Ni [169]. In the study of current induced DW motion, AMR measurements have been mostly used to study NiFe nanowires which show an AMR signal of about 1%.

3d ferromagnets exhibit very low intrinsic DW resistance (0.1 to 1% of the resistivity) [170], so that the magnetoresistance of a nanowire is dominated by AMR and its resistance is maximum if the magnetic moments are parallel (or antiparallel) to the current flow. The presence of a DW involves a local variation of the magnetization direction with some magnetic moments having a component perpendicular to the current direction resulting in a lowering of the resistance.

In spite of the rather small magnitude of its signal, AMR measurements have been successfully used, not only to detect a DW [171, 172] but also to discriminate between different DW spin structures [173] since they all possess a different component of the magnetization perpendicular to the current direction. The major limitation of this technique is that the resistance of the magnetic nanowire only depends on the presence or absence of a DW independently on its position between the probing contacts. Therefore, static AMR measurements cannot provide any information about the position and the displacement of the DW. However, time resolved measurements of AMR have been used to study the

dynamics of DW propagation in Py nanowires and the periodic transformation of its internal structure [174, 175]. In order to obtain a reasonable signal to noise ratio in dynamic measurements, this technique requires one to average over a large number of measurements.

Giant magnetoresistance. GMR is usually observed in multilayer structures in which ferromagnetic layers are separated by a thin metallic non magnetic spacer[176, 177]. While the GMR effect was first observed in samples with a large number of repetitions of $(\mathrm{Fe/Cr})_x$ bilayers with $x = 30, 35, 40$, a big steps towards applications was achieved with the development of spin-valves structures [178]. In these structures, one ferromagnetic layer is used as a free layer. Its magnetization is easily reversed by a small magnetic field. The other ferromagnetic layer acts as a reference layer, i.e. its magnetization remains unchanged under a small magnetic field due to a larger coercive field or the use of an induced uniaxial anisotropy. Spin-valves have been used to characterized DW propagation either with a current flowing in the plane of the layer [67–70, 179–187] or perpendicular to the plane of the layer [188, 189].

Typical GMR effects in these experiments are much larger (few %) than the AMR signal coming from the only presence of a DW in a single nanowire. The resistance level in such a system is directly proportional to the amount of reversed magnetization in the free layer. Therefore, the GMR is directly sensitive to the position of the DW along the nanowire making spin-valves structures very attractive for studying DW motion.

The main drawbacks in the use of spin-valves structure for studying current induced DW motion lie in the presence of the additional layers, i.e. the reference and spacer layers. Indeed, the current distribution in such a multilayer is usually not uniform due to the different materials resistivities. This can lead to the creation of Oersted field which might influence the DW dynamics [190, 191]. Moreover, magnetostatic interactions between the free and reference layer can result in local pinning of the DW wall affecting its motion. Finally, Thomas *et al.* have shown that a high critical current density required to depin the DW

from a notch in a spin-valve structure can lead to a large temperature increase resulting in a perturbation of the reference layer magnetization. In such case, the resistance level is no longer a good measurement of the DW position and makes the interpretation difficult.

However, the spin-valve structures can also be an asset for realizing spintronic applications based on CIDM if pinning can be controlled. Indeed, Pizzini *et al.* [187] and Bonne *et al.* [189] have shown that very high DW velocity can be observed in such structures possibly due to the presence of current flowing perpendicularly to the layers and the Oersted field effect[191]. These perpendicular currents also lead to a reduction of the critical current which can be lower than 10^7 A.cm^{-2}.

Hall effect. The extraordinary Hall effect (EHE) is usually used to characterize DW motion in magnetic systems with perpendicular anisotropy [55, 68–70, 164, 192, 193]. Such measurements require the sample to be patterned into a Hall cross geometry. Detection of DW displacements smaller than 1 nm can be achieved due to the large EHE signals [60]. One drawback of this technique lies in the need for lateral contacts which modify the current distribution and the geometrical pinning at the Hall cross restricting its use to depinning or small displacement experiments.

4.1.2. Magnetic microscopy techniques

While magnetoresistance measurements can be used to differentiate between different DW structures, their exact spin configuration can only be obtained from magnetic imaging techniques. The different techniques commonly applied to characterize magnetic DW include Kerr microscopy, magnetic force microscopy (MFM), Lorentz microscopy, scanning electron microscopy with polarization analysis (SEMPA), scanning transmission X-ray microscopy (STXM), and photoemission electron microscopy (PEEM). For magnetic imaging, the last two techniques are used combined with X-ray magnetic circular dichroism (XMCD) which characterizes the dependence of the absorption coefficient of a magnetic material on the helicity of circularly polarized X-rays.

MFM has been widely used to characterize CIDM in magnetic nanowires with in-plane [91, 147] and out-of-plane [194–196] anisotropy. The main asset of the MFM technique lies in its easy and fast implementation together with a high resolution of down to 10 nm depending on the details of the system. The principle of MFM measurement is based on the interaction between the tip magnetization and stray fields coming from a nonuniform distribution of the magnetization in the probed sample. This interaction results in a force which alters the deflection of the magnetic tip as it is scanned over the sample. A large MFM signal is expected when a large gradient of the sample magnetization is present, making this technique especially adapted for DW imaging. However, one of the main drawbacks of MFM is that the electromagnetic force acting on the magnetic tip is reciprocal. Therefore, scanning the magnetic tip can affect a DW resulting in a modification of its spin structure or even a displacement of the wall.

Electron microscopy techniques are particularly well suited for mapping the spin structure of a magnetic nanostructures since they provide high resolution with the advantage of being largely non-invasive. Transmission electron microscope can be used to perform Lorentz microscopy [197] or electron Holography [198]. These two techniques take advantage of the fact that the high energy electrons which are accelerated to energies of few 100 of KeV have both particle and wave like properties. In the Lorentz mode, when the high energy electrons are passing through the magnetic induction in the sample, they are deflected due to the Lorentz force like any charged particles submitted to a magnetic field. Electron holography is based on the interference of coherent electron waves which produces an interference pattern which is then processed to access information of the sample magnetization. Both techniques have been recently used to study the structure and pinning of DWs at constriction [199, 200] and the structure variation of a DW in a NiFe nanowires with different antinotches [201].

The main limitation of these techniques is that they require the nanostructure to be fabricated on a thin membrane to allow the electron to go through the all sample. Besides the complication in the fabrication process, this results

in a reduction of the substrate heat dissipation which can lead to an important temperature rise when injecting current in the nanowire due to the Joule heating effect. For the high current density needed for CIDM, the temperature can easily reach the Curie temperature of the magnetic materials resulting in uncontrolled domain nucleation [202, 203].

On the contrary, SEMPA relies on the fact that secondary electrons emitted from a magnetic sample in a scanning electron microscope have a spin polarization reflecting the net spin density in the material. SEMPA has been successfully used to image DW structure in nanoscale constrictions with a lateral resolution of ≈ 20 nm [204]. Moreover, the DW displacement induced by current as well as transformations of the spin structure precluding any propagation were clearly observed [205, 206]. Like other electron microscopy based technique, SEMPA is very surface sensitive and requires the surface of the magnetic sample to be accessible and clean. It is furthermore not compatible with the presence of large applied magnetic fields, which triggers the precession of secondary electron spins leading to the loss of the signal.

A very powerful set of techniques to study magnetization and in particular confined spin structures such as domain walls is based on synchrotron radiation. Recently synchrotron x-ray sources have become available that provide highly intense and collimated X rays of variable well-defined polarization and energy. In 1987 the X-ray magnetic circular dichroism (XMCD) effect was discovered by Schtz et al. [207] opening a new field to study the magnetic characteristic of solids by various techniques. These effects occur when the x-ray energy is tuned to an energy close to an inner-shell absorption edge and depend on the polarization of the symmetry selected empty density of states (DOS). A quantitative determination of local magnetic spin and orbital moments can even be obtained from the sum rules and using the element-specificity this can be done for the various materials involved. The sensitivity of the XMCD - based approach is very good, since the magnetic contribution to the absorption and scattering cross sections can be up to 50% at the transition metal $L_{2,3}$ edges and the rare-earth (RE) $M_{4,5}$ edges. The contrast mechanism by XMCD has been combined with

a variety of microscopy techniques yielding some of the most powerful magnetic microscopes in the world. The techniques used most extensively for the measurements in this review are x-ray magnetic circular dichroism photoemission electron microscopy (XMCD-PEEM) [208, 209], transmission x-ray microscopy (TXM) [210] and scanning transmission x-ray microscopy (STXM) [211]. PEEM is based on secondary electrons, which are emitted after irradiation with monochromatic X rays from a synchrotron and these electrons are imaged by an electron microscope. The lateral resolution is determined by the electron optics (including aberration correction) and for magnetic applications is currently of the order of 30-100 nm. This method is inherently surface-sensitive and has the advantage that samples on bulk substrates can be studied. Since low-energy electrons are emitted in this technique, the application of external magnetic fields in the PEEM is difficult. Furthermore a high voltage needs to be applied between the sample and the microscope lenses, which complicates the measurements for instance when samples have to be contacted for electrical current injection. To obtain spatial resolution in X-ray microscopy techniques where only photons are involved, Fresnel zone plates [212] are used to focus the x-ray beam. This has the advantage that external fields can be applied as no electrons are involved. Both types of microscopes (TXM and STXM) used for the measurements presented here operate in the transmission mode so that samples have to be fabricated on x-ray transparent membranes. The resolution is given by the width of the outermost ring of the zone plate (15-25 nm). For full-field TXM, the micro zone plate images the sample onto an X-ray-sensitive CCD camera. In STXM, micro zone plates focus the beam onto the sample mounted on a scanning stage and the transmitted intensity is monitored by a photomultiplier tube or an avalanche photodiode and the image is obtained by scanning the sample. Further approaches are such as lensless imaging with coherent X-ray scattering [213] are now being used, as these techniques are compatible with future x-ray sources, such as x-ray free electron lasers. In addition to the element-specificity and the high spatial resolution, one can also use the time-structure of the synchrotron to obtain a temporal resolution [214]. One uses

a pump-probe scheme where a pump pulse (for instance triggering a magnetic field pulse) is followed by n successive X-ray flashes [215]. The time resolution is given by the width of the x-ray pulses, which are usually 50-100 ps and can be as low as a few ps in special operation modes (low-alpha mode at BESSY for instance).

4.1.3. Optical measurement techniques

Magneto-optical Kerr effect (MOKE) is a very well established technique to study magnetism in thin solid film [71, 216] and it has been successfully adapted to investigate DW motion in a magnetic sub-micron sized wires [217]. Many experiments on DW propagation have been reported using MOKE magnetometry [218–226] or microscopy [56, 194, 227]. While the laser spot size on the sample is diffraction limited, MOKE microscopy has allowed for imaging of nanostructures as small as 30 nm [228]. Moreover, time-resolved experiments using a time-of-flight measurement technique have been carried out to characterize DW propagation in NiFe nanostrips [229]. This technique has allowed the Walker field to be measured in NiFe as well as the periodical transformation of the DW [223]. This technique based on a stroboscopic scheme averaging over a large number of measurements does not allow observation of stochastic events. This problem has been circumvented by Möhrke *et al.* who developed a single shot Kerr magnetometer allowing for real-time measurements [226].

With this impressive range of techniques, one can find a technique ideally suited for virtually every measurement envisaged.

4.2. Current-induced Domain Wall Motion in in-plane magnetized soft magnetic wires

We now explore CIDM experimentally. First we focus on soft magnetic materials, where the first experimental observations were reported and where in general the largest number of experiments have been carried out. The material most frequently employed is permalloy ($Ni_{80}Fe_{20}$). It has virtually zero magnetostriction and magnetocrystalline anisotropy making it very soft with low propagation fields for domain walls. Other related materials have also been

used, such as CoFeB, which is amorphous and therefore exhibits no grain boundaries, which could act as pinning sites for Domain Walls. Other 3d metals and alloys, for instance polycrystaline Ni, Fe, Co or CoFe are expected to behave similarly albeit with more pinning.

4.2.1. Quasi-static measurements of current-induced Domain Wall displacement

We will here first treat quasi-static measurements of the displacement of head-to-head or tail-to-tail domain walls in soft magnetic permalloy ($Ni_{80}Fe_{20}$) wires. By quasi-static we mean that the domain wall position is determined before and after the injection of a current pulse in a wire. Due to the static nature of the measurement, one can only determine average domain wall speeds by dividing the displacement by the pulse length. This is the most commonly used measurement scheme, as it is technically less demanding than dynamic measurements and faster than inherently slow imaging techniques, such as magnetic force microscopy.

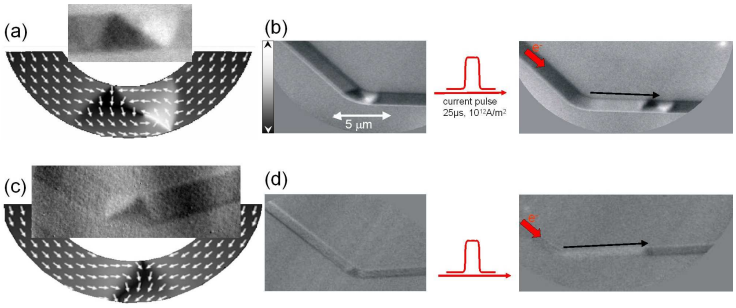

Figure 12: Photoemission electron microscopy images and corresponding micromagnetic simulations of (a) a vortex head-to-head domain wall and (c) a transverse wall. The shades of grey and the arrows indicate the magnetization directions. (b) shows the displacement of a vortex wall by current injection in a 28 nm thick, 1 μm wide permalloy wire. The grey scale bar shows the magnetic contrast direction for all the images. (d) shows the displacement of a transverse wall in a 7 nm thick and 500 nm wide wire. In both cases the wall spin structure stays the same after the displacement.

As discussed in section 2, two domain wall types are generally found in these wires as shown in Fig. 12. In (a), a Photoemission Electron Microscopy [208] image of a vortex head-to-head wall is shown together with a micromagnetic simulation where the spin structure is visualized together with the resulting

contrast of the image. In (c), a transverse wall is shown, which occurs in thinner and narrower structures (for details of the geometry-dependence of the wall spin structure see Ref. [165]). An example of experimentally observed domain wall displacements is shown in Fig. 12 (b), (d). Here we see in (b) that a vortex head-to-head domain wall is displaced by a current pulse with a high current density of 10^{12} A/m^2 in the electron flow direction. In (d) we present the motion of a transverse domain wall.

Using ultra-short pulses with very fast risetimes (< 100 ps) we have recently imaged very fast domain wall motion with velocities > 100 m/s [230]. To create these DWs prior to the current injections, an external magnetic field is applied in a direction perpendicular to the wire. After reducing the field, this results in the domain wall being positioned in the center of the wire. An x-ray magnetic circular dichroism photoemission electron microscopy (XPEEM) image of the initial configuration is presented in Fig. 13 (a) (top wire). To visualize the spin structure, the inset in the lower left shows a micromagnetic simulation of a VW confined in a wire with the same contrast. Once the initial configuration is imaged, single current pulses are injected into the structure. The result of a series of injections is presented in Fig. 13. Current pulses were injected between adjacent images (from top to bottom). After five injections, the DW is displaced by about 2 μm. Fig. 13 (b) presents line scans showing the displacement and the transformation of the DW. We see that the right side of the DW continuously moves in the electrons direction.

After the third current pulse, the left side does not move and it seems to be somehow pinned. The DW is therefore stretched, which results in an increase of the stray field energy. If this energy increase becomes larger than the energy required for a vortex core nucleation, it is energetically more favorable to transform to a double VW by vortex core nucleation. The new DW structure again displaces under current injection similar to the simple VW without changing any more its spin structure. The average displacement per current pulse is 400 nm. With the measured pulse length of 3 ns this results in an average DW velocity of $v = 130$ m/s, which is much larger than for long currents pulses ($> 10\mu$s)

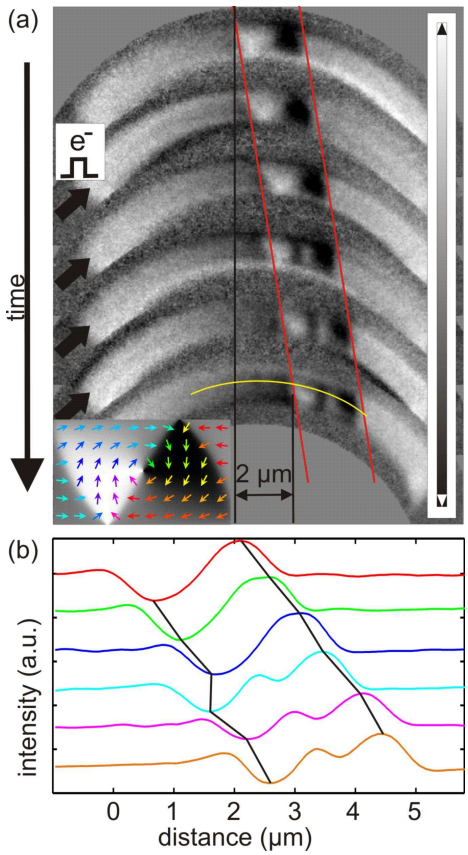

Figure 13: (From [230]) (a) Photoemission electron microscopy image series of a Py wire (1000 nm wide, 40 nm thick with a 2 nm Au capping) containing a VW. The top image shows the configuration after the initialization by a short vertical field pulse. The inset in the lower left shows a micromagnetic simulation of a VW to help visualizing the DW structure. The XPEEM images were taken with vertical contrast (see gray scale bar at the right) and the simulation was adapted to this contrast. Current pulses were injected between adjacent images (from top to bottom). After five injections the DW is displaced by 2 μm, thus about 400 nm on average per current pulse. After the third pulse DW transformed to a double VW that continues moving. (b) Intensity line scans along the yellow curve indicated by the yellow line in (a).

shown in Fig. 12. The fast wall motion as also observed by others for pulses with short risetimes [231] can be explained by the combination of adiabatic and nonadiabatic torque that act initially before the adiabatic torque is balanced by the anisotropy [232]. So by using pulses with fast risetimes, that are shorter than the relaxation (damping) time for the domain walls, a large torque can

develop that aids depinning [232] and can lead to fast wall displacement in the viscous regime.

Experimentally current-induced wall motion of these domain walls has been studied by a large number of groups using various techniques (for an overview see citing papers and references in [91, 117, 165, 170, 175, 183, 206, 231, 233, 234]).

4.2.2. Dynamic measurements of current-induced Domain Wall displacement

Dynamic measurements of the velocity have been carried out by Hayashi et al. for the case of a domain wall which is dynamically generated [234].

4.2.3. Determining the spin torque terms

One of the key pieces of information is the size of the two spin torque terms. While the adiabatic term is reasonably well understood and the parameters entering into the size are reasonably well-known (the diffusive spin polarization P might be the most difficult one), the non-adiabatic term with its parameter β is highly debated and reliable measurements are needed to obtain a theoretical understanding of the origin (spin relaxation, non-adiabatic transport, etc.).

Domain Wall transformations. Starting with a domain wall at rest, wall motion as seen in Fig. 12 [91, 206] has been observed by a number of groups and for sufficiently high current densities, periodic wall transformations have been imaged [206, 233]. From these observations of transformations one could deduce that the nonadiabaticity parameter β does not equal the damping constant α [233]. While this is valuable information, the observation of periodic transformations does not yield the absolute value of β. For this one would need to dynamically measure the distances in between transformations and even then this method would require a good knowledge of the current density and as edge roughness influences the transformation process this might not be extremely accurate.

Depinning Field Measurements. The simplest method to obtain an idea for the value of the non-adiabaticity constant β is to measure the field necessary to depin a domain wall from a pinning site as a function of the applied current. Assuming

that the domain wall can be described by the one dimensional model laid out in the theory chapter (to what extent this holds in wide and complex domain walls in in-plane magnetized materials is debatable, while this is probably more valid in high anisotropy materials as discussed in the next chapter), the efficiency of the depinning is a direct measure for β. An example are the measurements in [235], where an efficiency corresponding to a value of β of 0.1 was found.

Thermally activated Domain Wall motion. A more quantitative measurement of β [236] has recently shown that for wide transverse domain walls where the magnetization gradients are small, β is of the order of α thus pointing to spin relaxation as the dominating contribution to β, which arises from the same impurities that lead to viscous damping. For vortex walls a significantly larger value of β was found and this can be attributed to nonadiabatic transport across the vortex core where particularly high magnetization gradients occur [236]. This means that there is a distinct dependence of the torque terms on the magnetization configuration and thus the torques can be tailored by appropriately engineering the spin structures.

Vortex core displacement. A very robust measurement scheme for β was recently explored in disc structures with a vortex configuration. The direction of the vortex core displacement is a direct measure for β.

4.3. Current-induced Domain Wall Motion in out-of-plane magnetized magnetic wires

Most experimental studies on current induced domain wall motion were carried out in soft-magnetic nanowires made of permalloy. This well known material has the advantage of a domain wall less sensitive to pinning due to the large DW width ($\sim$ 100 nm) and the long exchange length as well as the potentially high spin polarization in these materials. Experiments have however underlined serious limitations concerning the use of this material for the study of CIDM: high critical current densities leading to strong Joule heating, complex domain wall structures with uncontrolled domain wall transformation leading to unreliable and stochastic DW displacements (see for instance Fig. 13 (a)) [206, 237] [238], and domain nucleation induced by current injection [203]. This limits the possibilities for a fundamental understanding of the spin transfer effect in magnetic DWs but is also a serious issue for possible applications based on CIDM. Since 2005, a growing number of experiments were carried out on spin transfer in out-of-plane magnetized materials with a large perpendicular magnetic anisotropy. This class of materials combines several advantages over soft in-plane magnetized materials: narrow domain walls typically below 10 nm with a simpler and more rigid internal Bloch/Néel DW structure; expected higher nonadiabaticity effects due to the higher magnetization gradients and high spin-orbit coupling leading to lower critical current densities and higher velocities; a large variety in the magnetic and transport properties of the available materials that allows one to study the dependence of spin transfer effect on these parameters. For the prospect of high density magnetic memories based on CIDM, these advantages combined with a small DW width, i.e small size of the magnetic bit, makes these materials very attractive. This section is devoted to the review of recent works on CIDM in out-of-plane magnetized magnetic nanowires. After a short introduction on the field induced DW dynamics in these materials, we will review recent experimental works about CIDM in these materials and discuss their implication on the physics of spin transfer in DWs. In the following, we will restrict the discussion to metallic out-of-plane magnetized ferromagnetic materials and

will only address shortly the special case of diluted magnetic semiconductors. The interested reader can find more detailed informations about this last topic in Ref. [239–241].

4.3.1. Magnetic field induced domain wall dynamics in out-of-plane magnetized materials

Understanding the dynamics of a DW under an external magnetic field in out-of-plane magnetized materials is important to study the current induced domain wall dynamics. It allows in particular to introduce some important aspects of the DW dynamics in these materials.

DW propagation. In a perfect magnetic material without pinning, different propagation regimes of the DW are predicted from the Landau-Lifschitz Gilbert equation when applying an external magnetic field H along the anisotropy easy axis. For low magnetic field, the dynamics is characterized by a domain wall velocity v that scales linearly with H: $v = \mu H$ with $\mu = \gamma\Delta/\alpha$, the DW mobility. In this regime, the velocity attains a steady value after a transitional regime. This law holds as long as H is smaller than the Walker field H_W. Above this threshold field, the Walker breakdown occurs and the mean velocity drops sharply. In this regime, the velocity oscillates at a frequency that depends on H. For higher value of H, the mean velocity $< v >$ starts again to increase with H with a reduced mobility $\mu = \gamma\Delta/(\alpha + \alpha^{-1})$. This text book behavior has been clearly identified in permalloy nanowires with a Walker breakdown field around a few Oe [223, 237].

In out-of-plane magnetized materials, the high anisotropy and the small domain wall width make the DW very sensitive to intrinsic local pinning sites that often match the DW width [242]. In a magnetic film, such pinning may arise from nanoscale defects such as atomic step, grain boundaries, surface roughness, local variation of the thickness/composition, variation in stress [243] ... leading to random fluctuations of the anisotropy [244] or of the exchange interaction. Such pinning strongly affects the DW dynamics for small external magnetic field, which is then thermally activated and characterized by discrete jumps be-

tween metastable states that are separated by the typical length scale between pinning sites (a few tens of nanometers).

In a out-of-plane magnetized Pt/Co(0.6 nm)/Pt thin films, three different regimes have been identified depending on the amplitude of the magnetic field H applied along the anisotropy easy axis relative to the critical field H_c [163, 164, 245]. At low magnetic field ($H \ll H_c$), the domain wall velocity is described by a creep law:

$$v = v_0 \exp\left[-\frac{U_c}{k_B T}\left(\frac{H_c}{H}\right)^{1/4}\right] \tag{31}$$

where U_c is a constant describing the pinning energy and v_0. For $0.8H_c < H < H_c$, the dynamics is in the thermally activated regime that can be described by the Arrhenius law :

$$v = v_1 \exp\left(-\frac{2M_s V_B(H_c - H)}{k_B T}\right) \tag{32}$$

where V_B is the activation volume. In both thermally activated regimes, the DW velocity is very low, much smaller than 1 m/s. For $H > H_c$, the viscous regime is recovered with a velocity proportional to H :

$$v = \mu(H - H_c) \tag{33}$$

with μ the mobility of the DW. The amplitude of the critical field depends on the magnetic properties of the material and on the amplitude of the pinning. In high anisotropy Pt/Co/Pt multilayer, H_c usually reaches several tens of mT [163, 246]. Such values can be higher than the Walker field preventing the observation of the steady high mobility viscous regime [246].

The reduction of the lateral dimensions in nanowires affects the DW dynamics in different ways. In the viscous regime, the lateral confinement decreases the in-plane DW demagnetizing field H_k and consequently the Walker field. Micromagnetic simulations carried out by Szambolics *et al.* [139] thus revealed a 60 % decrease of the Walker field in 120 nm wide nanowires with perpendicular anisotropy compared to the extended case.

The edge roughness introduced by the lithographic process will also locally change the energy of the DW and thus lead to additional DW pinning. This

can strongly affect the DW dynamics in sub-micron nanowires in particular in the thermally activated regime. Cayssol *et al.* [164] thus observed a strong decrease of the DW velocity in the creep regime in Pt/Co(1 nm)/Pt multilayer nanowires when the wire width w_0 is decreased. This can be modeled by a renormalized critical field which is simply the sum of the critical field due to the quenched disorder and a topologically induced field due to the modulation of the DW length which scales as $1/w_0$. A similar behavior was observed by Kim *et al.* [247] in Pt/CoFe(0.3 nm)/Pt nanowires but a deviation from the common creep law was revealed at very low field (< 10 Oe) for narrow wires ($w_0 < 500$ nm). This deviation actually occurs when w_0 becomes comparable to the length of a DW segment that thermally jumps over the quenched disorder potential collectively L_{col}. In this regime, the collective DW segment length becomes w_0 instead of L_{col} and the DW can be described as a 1D object.

DW pinning. Being able to pin a DW on a given pinning site in a nanowire is a prerequisite for the study of current induced DW dynamics. Local pinning sites in out-of-plane magnetized materials can be obtained in a nanowire by using lithographically defined geometrical pinning sites [60, 66–68, 192], local change of the layer thickness [64, 248], holes or trenches created using an AFM tip [249], local decrease of the anisotropy using ion irradiation [250, 251] or local exchange bias with an antiferromagnetic layer [136]. Geometrical pinning sites are the most used and obtained by changing locally the width and shape of the nanowire using for example a constriction [67] or a Hall cross [60, 66, 68, 192]. Pinning arises in this site from several contributions. First, the pinning due to the geometry that tends to pin the domain wall on the position where his length is minimal. When applying a magnetic field, the elasticity of the 1D DW line however can lead to a distortion of the DW shape due to the competition between the wall energy (minimum DW length) and the Zeeman energy (maximum reversed area). In a Hall cross geometry, the DW was thus shown to expend in a bubble shape when driven by an external magnetic field [192]. Beyond this defined geometrical pinning field, the DW experiences pinning due

to the natural defects in the films which can be of the same order of magnitude or even dominates [55, 68, 193, 246]as well as pinning due to the edge roughness or lithographic defects. All these contributions make the precise control of the position and shape of the DW in the pinning sites difficult in out-of-plane magnetized materials.

Experimentally, time resolved DW depinning experiments from natural defects [193] or a Hall cross [67, 192] generally show a depinning time distribution following an exponential law consistent with thermally activated process over a single energy barrier [2]. The mean depinning time $\tau(H)$ follows an Arrhenius-Néel [252] law:

$$1/\tau(H) = 1/\tau_0 \exp(-E_b(H)/kT) \tag{34}$$

with $1/\tau_0$ the attempt frequency. The potential barrier for depinning $E_b(H)$ is found to decrease linearly with the applied field [67, 68, 192, 193]. Note that this dependence may however depend on the exact nature of the pinning site.Indeed, other forms have been predicted: for example, Gaunt [253, 254] predicted a linear scaling with H for "weak" DW pinning, where the wall breaks away cooperatively from many pinning sites when depinned. In the "strong"pinning case, where the wall breaks away from an individual pinning site, $E_b(H)$ is expected to scale as $(1 - H/H_0^{1/2})^{3/2}$ with H_0 a constant. A similar scaling law was calculated by Kim *et al.* [158] for a point like defect induced by a local reduction in the uniaxial anisotropy or a local hard axis pinning field.

4.3.2. Experimental considerations

Due to the particular geometry of the wires and the magnetization direction, other effects beyond the spin torque effect can occur when injecting current in out-of-plane magnetized nanowires. This means that particular cares is necessary to separate these effects when interpreting the data.

[2]More complex laws involving linear combination of exponential laws were also found [67, 193] which can be described a Markov process that involved two possible DW configurations possibly due to small deformations of the wall (depinning in two times), or to domain wall chirality (presence of a small in-plane component, presence or absence of a vertical Bloch line,...) [67, 193].

Joule heating. For a given current density, the heating amplitude depends on the material and the geometry of the wire as well as on the metallic contacts and the nature of the substrate where heat is dissipated [255, 256]. In typical CIDM experiment, heating can reach up to several hundreds of K for high current densities ($\sim 10^{11}$-10^{12} A/m^2 depending on experiments) [55, 58, 147, 148, 186, 255–257]. In out-of-plane magnetized materials with strong DW pinning, the DW dynamics is in a thermally activated regime over a large range of current and field where it is controlled by the pinning potential landscape in the nanowire. In this regime, the DW dynamics is particularly sensitive to the temperature increase due to Joule heating that helps the DW to overcome the pinning energy barrier. Joule heating thus strongly affects the DW motion and will tend to decrease the critical current for depinning and enhance the DW velocity in this regime. This is particularly true in the case of current induced DW motion or depinning experiments in the presence of an external magnetic field that lowers the pinning energy barrier [55, 67]. Boulle *et al.* [55] showed that the strong decrease of the DW depinning field observed when injecting current pulses can be mostly attributed to the effect of the Joule heating and a smaller part to spin torque effects. Burrowes *et al.* [67] also observed in time resolved depinning experiment in the presence of an external magnetic field that changes of a few tens of kelvins due to Joule heating can mask the effects of spin-transfer. A possible way to exclude the influence of Joule heating properly is to measure the CIDM at several external temperatures such that the nanowire temperature stays always the same for different amplitudes of the current as was done in Ref. [55, 76, 148, 194]. The effect of the temperature rise can also be accounted for by measuring the current dependence of the wire temperature and using an Arrhenius activation law to normalize the data at a fictive constant temperature [57] or by including a current dependent temperature in the activation law [56].

Another consequence of Joule heating is that the temperature rise can reach the Curie temperature and thus leads to uncontrolled domain nucleation [58, 258]. This is particularly problematic in ultra-thin magnetic film where the

Curie temperature can reach a relatively low value ($T_c \sim 400 - 500$ K) [246] compared to permalloy ($T_c \sim 850$ K) and thus prevents the study of CIDM at high current densities and/or long current pulses. This also makes the search for low DW pinning material difficult as it is often associated with a decrease of the Curie temperature, as is the case for example when irradiating ultra-thin magnetic films with ion [58, 259–261].

Even if Joule heating can not be suppressed, its amplitude can be significantly reduced by using magnetic materials with small resistivity, thin films, and choosing a substrate with high thermal conductivity [255, 256], such as Si or diamond [262]. Another approach is to cover the wire with a high thermal conductivity but electrically insulating layer to play the role of a heat sink, such as an AlN capping [55].

Oersted field effect/Domain wall drag. The concentric Oersted field can play a significant role for the magnetization dynamics in out-of-plane magnetized nanowire. Fig. 14 shows the simulated distribution of the out-of-plane component of the Oersted field in a nanowire [59] characterized by a rapid increase of the field amplitude as one approaches the wire edges. Actually, the maximum Oersted field on the sides H_z depends on the width w and the thickness t of the wire and can be approximated as $H_z = Jt(3 + 2\ln(w/t))/4\pi$ for a thin conductor ($t \ll w$) [194] and is thus larger for wide and thick nanowires. For a typical 200 nm wide 5 nm thick wire, the resulting Oersted field is about 5 mT for $J = 1 \times 10^{12}$ A/m^2. Although the net force on the complete DW is zero, such an Oersted field can bend the DW at the edges and lead to an asymmetric DW motion [194]. Experimentally, the influence of the Oersted field on the DW depinning and propagation can be identified by comparing the DW dynamics for domain configurations with opposite magnetization [263].

In wide nanowires in soft out-of-plane magnetized materials, the Oersted field can also have some unexpected effects on the domain configuration. Figure 15(a) shows a magnetic image of a DW in a 2 μm wide nanowire patterned in out-of-plane magnetized Pt/CoFeB(0.6 nm)/Pt. This comparably soft material is

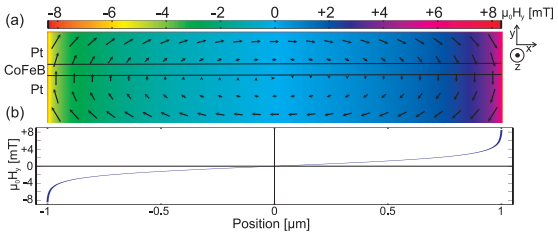

Figure 14: (From Ref. [59]) Cross-section of a wire with the calculated distribution. The current (10^{12} A/m^2 flows homogeneously in the wire in the -z direction. The wire dimensions are 5.6 nm×2μm (x and y are plotted at different scales). The out-of-plane component of the Oersted field H_y is plotted in color. (b) H_y as a function of the lateral position x in the wire.

characterized by a relatively low coercive field ($\sim$ mT). When injecting a high current density in the nanowire ($\sim 10^{12}$ A/m^2), a new domain structure appears with two domains with opposite magnetization separated by a DW aligned along the wire (see Fig. 15(b)). The appearance of this domain structure is attributed to the combined effect of the Oersted field and the reduction of the magnetostatic energy (closure of flux line). Interestingly, when injecting successive current pulses of opposite polarities, the magnetization in the DW can be reversed back and forth by the sole effect of the Oersted field (see Fig. 15(c-d). This underlines the high Oersted field generated in these wide wires, which was estimated to reach 8 mT on the edges for $J = 1 \times 10^{12}$ A/m^2.

A second electromagnetic effect is the domain wall drag [264]. The change of sign of the anomalous Hall voltage around the DW leads to an additional current that circulates around DW and induces a magnetic field B_z that can lead to domain wall motion. For $t \ll w$, Viret *et al.* found $H_z \approx 7J \tan(\theta_h) t \ln(w/t)/2\pi^2$ where θ_h is the Hall angle. In 50 nm thick and a few 100 nm wides Fe wires, Viret *et al.* [265] found this effect to actually dominate over spin transfer. On the contrary, in nm thick multilayer films, such as in $(\mathrm{Pt/Co})_n$, the effective magnetic field is very weak and can generally be neglected [55].

4.3.3. Experiments to determine the spin torque terms in out-of-plane magnetized wires

A large number of experiments on current induced domain wall motion in out-of-plane magnetized structures were devoted to the characterization of the

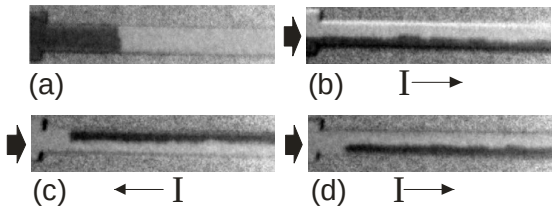

Figure 15: (From Ref. [59]) XPEEM magnetic images of a 2 μm wide Pt/CoFeB/ Pt wire. A white contrast corresponds to the magnetization pointed up and a black contrast to the magnetization pointing down. (a) A DW is shown in the wire. (b) After the injection of a current pulse $J = 1.0 \times 10^{12}$ A/m^2 for 25 μs, direction indicated by the arrows in the wire, the original DW structure disappears and a long DW parallel to the wire is created. When the current direction is reversed, the magnetization in the domain also reverses ((c) and (d)).

highly debated nonadiabatic torque. Most of these experiments were carried out in the presence of an external magnetic field in addition to the injected current. Indeed, the effect of the nonadiabatic torque on the DW dynamics is predicted to be equivalent to an external magnetic field [138, 155, 266] so that the relative changes induced by the current in the field induced DW dynamics allows one to characterize nonadiabatic effects. Most experiments presented in this section considered long time scale (injection of long pulse/DC current) and the current/magnetic field values are lower than the zero temperature critical values associated with pinning so that experiment can generally be described in a thermally activated picture where the dynamics is dominated by pinning. These experiments thus probe how current and field affect the pinning potentials felt by the DW.

Variation of the depinning field with current injection. In most experiments [55, 68, 136, 263, 267], the depinning field H_{dep} strongly decreases as current is injected and for sufficiently high current densities a linear dependence is found. Importantly, the slope $\epsilon = \mu_0 \Delta H_{dep}/\Delta J$ of the curve $H_{dep}(J)$, generally called "efficiency", is much higher compared to what is observed in permalloy [55, 148].

As an example, we have studied the variation of the depinning field when injecting 50 μs current pulses in an out-of-plane magnetized $(\mathrm{Pt/Co(0.6\ nm)})_3$/Pt Hall cross with 540 nm lateral dimensions at several temperatures. At con-

stant cryostat temperature, a strong decrease of the depinning field is observed for both current polarities when injecting current densities higher than 4×10^{11} A/m^2 although the depinning field is always higher for one current polarity compared to the other one (See Fig. 16(a)). From the slope of the curve for $T_{cryo} = 130$ K, one obtains a high efficiency $\epsilon \sim 10^{-13}$ T.m^2/A. However, the weak dependence of the depinning field on the current polarity clearly suggests an important contribution of the temperature rise due to Joule heating, that was measured to be about 200 K for the maximum injected current.

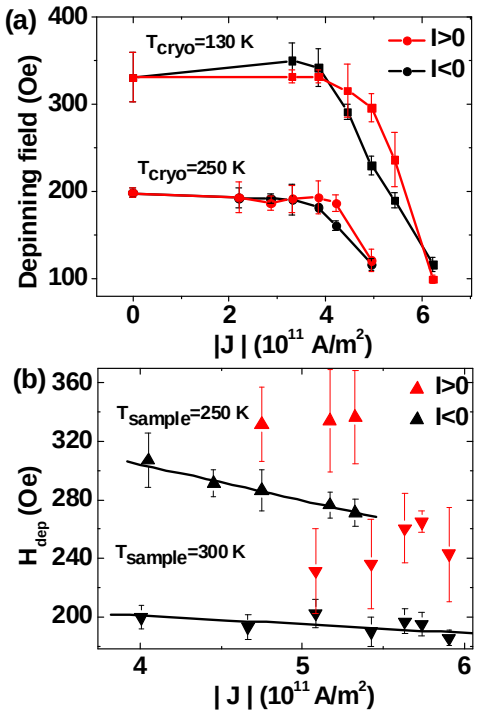

Figure 16: Depinning field as a function of $|J|$ for (a) a constant *cryostat* temperature of $T_{cryo} = 130K$ (squares) and $T_{cryo} = 250$ K (circles) and (b) a constant *sample* temperature of $T_{sample} = 250$ K (up triangles) and $T_{sample} = 300$ K(down triangles).In (b), the black lines are a linear fit of the data.

To extract the spin torque contribution, we carried out the same depinning experiment but at a constant *sample* temperature by playing on the external

temperature and the amplitude of the injected current. Figure 16(b) shows the resulting depinning field vs current density curve for two different *sample* temperatures of $T_{sample} = 250$ K and $T_{sample} = 300$ K. We observe now a clearly different behavior: the depinning field decreases linearly for one current polarity (current helps the DW depinning) whereas it is approximately constant or slightly increases for the other current polarity (current hinders DW depinning). From the slope of the current polarity for negative current that helps the depinning, one can derive a real efficiency $\epsilon = 2.5 \pm 1.15 \times 10^{-14}$ T.m^2/A for $T_{sample} = 250$ K and $\epsilon = 6 \pm 4.5 \times 10^{-15}$ T.m^2/A for $T_{sample} = 300$ K. To analyze the results, we carried out simulations of the DW dynamics using the 1D model with thermal activation (see section 3). We assume a pinning potential $V_{pin}(q)$ such that V_{pin} is quadratic with the position q in the potential well and constant outside. Our simulations show that only the nonadiabatic torque can change the depinning field. Actually, the adiabatic torque tilts the domain wall internal angle ψ but does not change the equilibrium position of the DW in the potential well due to the damping. On the contrary, the nonadiabatic torque modifies the potential profile as well as the DW position and thus acts on the pinning energy barrier. In the 1D model, the nonadiabatic torque acts on the DW as an effective field $\mu_0 H_I = \epsilon I$ with [266]

$$\epsilon = \beta P \hbar / (2 e M_s \Delta) \tag{35}$$

From the experimental efficiency, one obtains $\beta = 1.45 \pm 0.7$ from the T=250 K experiment and $\beta = 0.35 \pm 0.26$ from the T=300 K experiments to be compared to the damping parameter $\alpha \sim 0.15$ in our film. Note that these values are rough estimations as the spin polarization is not known and assumed to be similar to the one in Co ($P = 0.46$). This value is however in the range of the spin polarizations extracted by Cormier *et al.* [58] in Pt/Co(0.5 nm)/Pt from CIP GMR data ($P \approx 0.35$) and by Aziz *et al.* [250] by DW resistance measurement ($P \approx 0.7$). Finally, the model does not explain the difference in the efficiency between both temperatures.

We also carried out complementary experiments at constant *cryostat* tem-

perature ($T = 100$ K) to characterize the contribution of the Oersted field in the DW depinning. This is done by comparing the depinning field for opposite domain configuration around the DW. We find a negligible contribution of the Oersted field much smaller than that of the nonadiabatic torque [263].

Finally, Fukami *et al.* [136] observed in narrow (70-200 nm) $(\mathrm{Co(0.3\,nm)/Ni(0.6\,nm)})_{4,5}$ that the critical current density does not depend on the external magnetic field. This can be explained by a depinning which is driven by the adiabatic torque in these narrow wires. Indeed, as discussed in section 3.2.3 and 4.3.4, the critical current associated with the adiabatic torque can be lower than the one associated with the nonadiabatic torque for narrow wire due to the small demagnetizing field.

Time resolved depinning experiment. Ravelosona *et al.* [67–70, 268] carried out time resolved depinning experiment in the s range under constant current and external magnetic field in spin valve with a (Co/Pt), $(\mathrm{Co/Ni})_4$ or FePt free layer. DW was pinned in a geometrical pinning sites or on natural pinning sites and depinning was monitored on the nm scale using the extraordinary Hall effect (EHE) [68, 69, 268] or 100 nm scale using GMR [67].

All experiments show the mean depinning time $\ln \tau$ scales linearly with the current with τ the mean depinning time. This combined with magnetic field induced depinning experiments suggest an Arrhenius activation law over a single energy barrier E_b:

$$E_b(H, I) = 2\mu_0 M_s V(H_p - H) + \sigma I \tag{36}$$

where V is the activation volume and H_p the depinning field.

These results are consistent with Kim's *et al.* [158] theory of thermally activated current induced DW depinning (see section 3.3) that predicts a linear variation of $\Delta E_b(I) = \sigma I$. Using Eq .(27) for the expression of σ, Burrowes *et al.* deduced $\beta = 0.022 \pm 0.002$ in CoNi and $\beta = 0.06 \pm 0.03$ in FePt, similar to the value of the Gilbert damping constant, $\alpha_{CoNi} = 0.032 \pm 0.006$ and $\alpha_{FePt} \approx 0.1$. As the DW width in FePt (1 nm) is much smaller than in Co/Ni(10 nm), the

authors conclude that $\beta \approx \alpha$ in general, independent of the DW width. A value $\beta \sim 0.015$ can be also be estimated from similar experiments in Co/Pt *et al.* [68, 155].

Importantly, very different values of β are obtained from the efficiency derived from the variation of the depinning field with the injected current. Indeed, from the current/field equivalence obtained in the 1D model, one gets a β value about one order of magnitude higher than the β estimated from the value of σ.

Small DW displacement. Miron *et al.* [60] studied the quasi-static nm scale displacement of a pinned DW induced by the combined effect of a low frequency (10 Hz) current I and field excitation. The DW was placed in the center of a 100 nm wide double Hall cross geometry so that sub-nm scale displacement was detected using the EHE. The authors observed that the application of a small AC field H leads to a shift ΔI of the EHE signal vs I curve with $\Delta I \propto H$ and thus current acts on the DW similarly to an effective magnetic field. From ΔI, an efficiency $\epsilon = 8 \times 10^{-14}$ T.m^2/A is measured in a Pt/Co(0.6 nm)/AlOx multilayer which leads to $\beta \sim 1.9$ using Eq. 35 and $P = 0.6$. The same experiment carried out on Pt/Co/Pt multilayer leads to $\epsilon < 2 \times 10^{-15}$T.m^2/A and $\beta < 0.017$. The authors attribute this difference to the presence of a Rashba spin-orbit coupling (RSO). Actually, RSO is expected in two-dimensional (2D) systems with broken inversion symmetry as in Pt/Co/Al_2O_3. The RSO leads to a strong effective magnetic field on the conduction electron, whose directions depends on their k vector. As conduction electrons have different k vector on the Fermi surface, this leads to additional spin relaxation and thus enhances β. The presence of a Rashba field in this structure was proved later on by domain nucleation experiments [269].

Current-induced DW creep under external magnetic field . Several authors studied the influence of a small DC current on the well characterized thermally activated DW creep driven by an external magnetic field [56, 57, 70]. Alvarez *et al.* and Lee *et al.* thus observed that when injecting a current density of a few 10^{10} A/m^2, the DW moves in the same direction as the one imposed by the

external field and the DW velocity is enhanced or decreased depending on the current polarity, in agreement with a spin transfer effect.

Lee *et al.* [57] studied the DW creep in Pt/Co(0.3 nm)/Pt nanowires over more than 4 orders of magnitude in velocity. The authors observed that the injection of a small current density ($\sim 10^{10}$ A/m^2) in the wire leads to the same dependence of the velocity v with the magnetic field but shifted horizontally by a quantity $\Delta H(J) = \epsilon J + \eta\sqrt{H}J^2$. Current acts thus on the DW in the creep regime similarly to an effective field $\Delta H(J)$. The authors measure an efficiency $\epsilon = 1.6 \pm \times 10^{-14}$ Tm^2/A equivalent to $\beta \sim 0.38$ for $P = 1$. The origin of the term in J^2 still remains to be understood.

Similarly, Alvarez *et al.* [56] studied the DW creep in Pt/[Co(0.5 nm)/Pt(1 nm)]$_2$ 5 μm wide wire in the presence of both an external magnetic field and current. Although the measured velocity range is small (about an order of magnitude), the authors show that the dependence of the velocity with the current and magnetic field is consistent with a standard creep law where the external field H is replaced by an effective field $H_{eff} = H + \epsilon J$ with $\epsilon = 3.6 \pm 0.6 \times 10^{-14}$ Tm^2/A. Using a spin polarization of 0.7 in Co/Pt measured from DW resistance measurement, this leads using Eq. 35 to $\beta = 0.7 \pm 0.1$.

Discussion. Table 1 summarizes the results obtained from current induced domain wall motion in the presence of an external magnetic field. The first column lists the different values of the experimental efficiency. Note that many experiments consider magnetic multilayer with a complicated structure and the authors generally assume that the current flow is homogeneous. However, the actual current density within the different layers depends on their relative resistivity and thickness as well as the spin-dependant resistances at the interface and this may lead to significant deviation compared to the simple homogeneous case [58]. The third column lists the author best estimates of β from their experimental data. β is estimated from a current/ field equivalence using Eq. 35 [55–57, 60, 66] or from the linear variation with current of the pinning barrier energy [67, 158]. Note that β is directly proportional to the current

Material	$\epsilon(10^{-14}$ T.m^2/A)	$\sigma(10^{-17}$ J/A)	β	β_{min}	α	Δ (nm)	Type of exp.	Ref
Cu/Co(0.5)/Pt	17	1.5		7.6		10	I	[68]
Pt/Co(0.6)/Pt	< 0.2		$< 0.017^{(1)}$	0.029		4.2	Di	[60]
Pt/Co(0.3nm)/Pt	1.6 ± 0.1			0.34		$4.5^{(2)}$	Cr	[57]
Pt/[Co(0.6)/Pt]$_3$ $^{(3)}$	0.6±0.45		0.35 ± 0.26	0.16	0.15	6.3	D	[55]
Pt/[Co(0.6)/Pt]$_3$ $^{(4)}$	2.5±1.15		1.45 ± 0.7	0.67	0.15	6.3	D	[55]
Pt/[Co(0.5)/Pt]$_2$	3.6 ± 0.6		0.7 ± 0.1	0.49		$4^{(2)}$	Cr	[56]
Pt/Co/AlOx	8		$1.9^{(1)}$	1.16	0.5	4.2	Di	[60]
(Co/Ni)$_4$/Co/Pd (SV)	1.5	0.94	0.022 ± 0.002	0.21	0.032	10	I, D	[67]
$SrRuO_3$	100			0.48		1	D	[66]
FePt (SV)	30	2.37	0.06 ± 0.03	0.9	0.1	1	I, D	[67]

Table 1: Summary of results from CIDM in the presence of an external magnetic field. Type of experiment : D: Dependence of the depinning magnetic field with the injected current; I : Dependence of the depinning time with the injected current; Di : Displacement of the DW with the injected current and external magnetic field. Cr : Dependence of the DW velocity on current and field in the thermally activated creep regime. (1): This best estimate value was corrected compared to the published one to take into account different definitions of ϵ and β. (2): Rough estimation assuming typical parameter for the material. (3) From Ref. [55], $T_{sample} = 250$ K. (4) From Ref. [55], $T_{sample} = 300$ K.

spin polarization P, which is subject to large uncertainty. Furthermore, the two different methods can lead to very different estimates of β in the same material [67]. In addition, when β is extracted from ϵ and (Eq. 35), the current/external field equivalence is assumed as well as the 1D approximation. In the 1D model, current should act similar to an effective field through the nonadiabatic torque for pinning potential V_{eff} that depends only on the DW position q even in the thermally activated regime [155]. One can note however that this may not hold if V_{eff} depends on ψ (for example for asymmetric notches as was shown in permalloy [270]) as the adiabatic torque may also affect the pinning barrier. Beyond the 1D model, the deformation of the DW line may also affect ϵ and this may depends on the nature of the pinning. To take into account the first two biases, we also computed β from the efficiency ϵ using the current/field equivalence (Eq. 35) and assuming $P = 1$. This value β_{min} corresponds actually to a lower bound for β derived from the current/field equivalence.

Table 1 shows a large dispersion of ϵ and β_{min} for different materials and experiments. A striking example is the large difference for ϵ and β for Pt/Co(0.3 nm)/Pt

in Ref. [57] and Pt/Co(0.6 nm)/Pt for Ref. [60]. Besides the variation in the spin polarization for the different materials, this suggests that β depends also strongly on the exact material composition and structure. Despite this large scattering, one can however identify three groups depending on the efficiency. A first one, composed of $[Co/Pt]_n$ and $[Co/Ni]_n$ where, except for Ref. [68] and Ref. [60] with extreme values, ϵ is of the order of 10^{-14} T.m^2/A. A second one, composed of $SrRuO_3$ and FePt with narrow DW walls and a much higher efficiency. A third group is composed Pt/Co/AlO_x with intermediate value of ϵ and high value of β.

Interestingly, despite large variations in ϵ, β_{min} typically ranges between 0.2 and 1, which is much higher than the values of β estimated from measurements in permalloy. There is currently no consensus to explain such a high nonadiabaticity in these materials and this remains an open question. One can however invoke several different approaches for an explanation. One relies on the high spin orbit coupling in these materials with strong uniaxial anisotropy. Actually, strong nonadiabaticity was predicted in systems with high intrinsic spin-orbit coupling, such as in 2D magnetic gas with a Rashba spin-orbit interaction or (Ga,Mn)As [101, 102, 104]. This scheme seems to support the enhancement of the nonadiabaticity observed in Pt/Co/Al_2O_3 where a strong Rashba spin-orbit coupling was recently identified [269]. Momentum transfer expected for narrow DW is another possibility. However, this mechanism is expected to be relevant for DWs with widths of the order of the Fermi wavelength ($\sim$ 1 nm) or the Larmor precession length (a few nm) [85, 86] which is not completely the case for standard out-of-plane magnetized multilayers with larger DW widths ($\sim 5-10$ nm). The condition seems to hold though in FePt and $SrRuO_3$ with very narrow DW ($\sim$ 1 nm),[3]. Furthermore, there seems to be no clear correlation between the measured β_{min} and α and in general, β_{min}, which is a minimum boundary for β, is higher than α. However, one should consider that except for Ref. [60], the value of α were obtained from FMR or magnetic

[3]although the role of scattering may have to be considered [88].

relaxation experiments on thin film which might differ from the one extracted from DW velocity measurements and effectively felt by the DW. For example, Adam *et al.* [76] in (Ga,Mn)As measured a damping parameter about 1 order of magnitude higher using the dependence of the DW velocity with the magnetic field as compared to the one obtained by ferromagnetic resonance. Actually, recent theories predict an enhancement of the damping parameter in the case of narrow DW [271] or due to the disorder [132].

Finally, several authors mentioned an intrinsic link between DW resistance and nonadiabatic effects [85, 101, 272, 273]. Using experimental value of β for $[Co/Pt]_3$ multilayer (Ref. [55]) and $SrRuO_3$ (Ref. [66]), one can actually deduce a DW resistivity from Tatara's theory of momentum transfer which is comparable to the one that was measured in these materials [250, 274]. This theory holds however for very narrow DWs and in the ballistic limit, but Tserkovnyak *et al.* [273] found a similar correspondence between β and the DW resistance without these restrictions from more generally thermodynamic arguments. Similarly, Nguyen *et al.* [101, 104] proposed a mechanism for high nonadiabaticity in (Ga,Mn)As directly related to carrier scattering at the DW. Indeed, they showed that strong intrinsic spin orbit coupling in this material can cause significant carrier reflection at the domain wall and thus high domain wall resistance even in the adiabatic limit when the wall is much thicker than the Fermi wavelength. When the carriers scatter off the domain wall, their momentum changes, and through the spin-orbit coupling, their spin also changes. The reflected spins thus do not follow the magnetization of the domain wall and thereby cause a large nonadiabatic torque. Similarly, Berger *et al.* [272] associated with the different existing theory of nonadiabatic effect, a theory of DW resistance. A more systematic experimental study of β and the DW resistance in the same sample is needed to clarify this point.

4.3.4. Current induced domain wall motion at zero external field

Several groups reported CIDM at zero external magnetic field in out-of-plane magnetized materials.

Material	$J_c(10^{11}$ A/m$^2)$	$\epsilon^*(10^{-14}$ T.m^2/A)	v_{min} (m/s)	Displa-cement	Pulse length	H_p (mT)	Wire width(nm)	Direction	Ref
$Co/(Ni/Co)_4$	5	3,6	~ 50	2.6 μm	50 ns	18	70-160	-e	[63, 64]
$(Co/Ni)_5/Co$	3-9	5	20	200 nm	100 ns	15	70-200		[136]
$(Co/Ni)_4/Co$	5-11	3	20	200 nm	100 ns	15	70-200		[136]
$(Co/Ni)_4/Co/Pd$ (SV)	8	1,9			quasi DC	15	200		[67]
$(CoFe(0.5nm/Pt)_5$	14.3	4,9	1.5	750 nm	20 ns	~ 70	230	-e	[61]
Pt/Co/AlOx	10	1	0.6	500 nm	500x5 ns	~ 10	100	e	[258]
$Co_{63}Cr_{11}Pt_{26}$	10	5	0.048	400 nm	8.2 μs	50	280	-e	[64]
$SrRuO_3$	0.1	100	0.4	$\sim 1\mu$m	100 ms	10	500		[66]
$Tb_{30}Fe_{58}Co_{12}$	0.46-0.59	920	~ 0.01	$\sim \mu$m	100 μs	100-220	8000	-e	[65]
Pt/Co(0.3nm)/Pt	0.83-1.8		10^{-7}-10^{-4}	30 μm	quasi DC		190-490	e	[57]

Table 2: Summary of DW depinning experiment at zero external field. Direction "'-e"' stands for a current induced DW displacement in the direction of the electron flow, and "e" in the direction of the current.

Critical current. We list in Table 2 the critical current densities J_c at zero external magnetic field. . J_c is defined as the smallest current density for which a DW motion is observed. It thus depends on the detection technique, in particular on the smallest DW displacement that can be detected as well as on the length of the current pulse as the DW must have time to propagate over this smallest distance. To illustrate this bias, we list the minimum DW velocity v_{min} generally obtained by dividing the DW displacement by the length of the pulse.The efficiency $\epsilon^* = J_c/H_p$ where H_p is the pinning field is also listed to compare results with different pinning.

Despite large scattering in the data, one can identify different groups of material. A first group composed of multilayers with ultrathin magnetic films with similar order of magnitude for the efficiency ($\sim 5 \times 10^{-14}$ T.m^2/A). Due to variation in the pinning in the different film, this leads to J_c ranging between 3 and 15×10^{11} A/m^2. Another group is composed of $SrRuO_3$ and TbFeCo with much higher efficiency and much lower critical current density in the 10^{10} A/m^2 range. Although different materials are considered, the data in the first group of materials suggest an approximate scaling of the current density with H_p. Several authors studied in more details the dependence of J_c on H_p in the same material. Ravelosona *et al.* [69] and Li *et al.* [275] reported in 0.2-1 μm wide

Pt/Co wire and 8 μm wide TbFeCo nanowire an approximately linear scaling of J_c with the pinning field which is consistent with a depinning controlled by the nonadiabatic torque. However, a different scaling was reported in narrow (70-240 nm wide) $(Co/Ni)_{4,5}$ wire [62, 136, 276] where the critical current was found to be independent of pinning nor on the external field. Fukami *et al.* [136] and Tanigawa *et al.* [62] also studied the dependence of J_c on the wire width w in similar samples. They observe that for w ranging between 70 and 200 nm, the critical current density decreases as w decreases. These observations are more consistent with a depinning process driven by the adiabatic torque expected for narrow wires and not by the nonadiabatic torque (see section 3.2.3).

Domain wall propagation. Several authors studied the dependence of the DW velocity with current density [57, 63, 258, 277, 278]. As observed for field-induced domain wall motion, upon increasing J, one successively observes a slow creep regime where DW motion is controlled by wall pinning and thermal activation and a flow regime with high DW velocity and a linear variation of the DW velocity. In between, an intermediate regime with a higher slope v(J) is observed, which may be identified as a thermally activated depinning regime.

Flow regime The flow regime was observed by Koyama *et al.* [63, 278] in $[Co/Ni]_{4,5}$ nanowires for high current density above 8×10^{11} A.m^2 and Moore and Miron *et al.* [258, 277] in Pt/Co/AlOx nanowires for $J > 2 \times 10^{12}$ A/m^2. In (Co/Ni) nanowires, the velocity is found to increase by about 40 m.s^{-1}/10^{12} A.m^{-2} and a maximum velocity of 60 m/s was reported for $J = 1.3 \times 10^{12}$ A/m^2. In Pt/Co/AlOx nanowires, the velocity is found to increase by 120 m.s^{-1}/10^{12} A.m^{-2} and a maximum velocity of 400 m/s is obtained for $J = 3.5 \times 10^{12}$ A/m^2. Importantly, by comparing this slope to the one measured from the $v(H)$ curve, the authors deduce an equivalence field/current identical to the one obtained from the quasi-static measurements. This clearly indicates that the nonadiabatic torque is the driving force for the DW motion in this regime and that the DW motion is in a steady flow regime. The authors

also propose that the strong transverse in-plane Rashba field identified in this structure [269] may play an important role in the DW motion by stabilizing the DW structure and preventing the occurrence of the Walker breakdown (the angle ψ is frozen). As a consequence, the DW stays in a high mobility regime with $v = u\beta/\alpha$ up to very high current density.

Domain wall creep Moore *et al.* [258] and Lee *et al.* [57] studied the DW creep respectively in Pt/Co(0.6 nm)/AlOx and Pt/Co(0.3 nm)/Pt at very low current density. They show that the $v(J)$ curve can be fitted with a creep law with $\ln(v) \propto J^{-\eta}$ with $\eta = 1/4$. This exponent is the same as the one obtained in the field driven case which suggests that current acts as an effective field on the DW as is expected from the effect of the nonadiabatic torque [155]. However, as underlined by Lee *et al.*, other exponents (1/3, 1/2, -1/2) give also reasonable fits so that there is a high uncertainty on the value of η.

Direction of DW propagation Most authors observe that the DW moves in the direction of the electron flow (see table 2, column "direction"). However, Moore *et al.* [258] and Lee *et al.* [57] observed respectively in Pt/Co(0.6 nm)/Al_2O_3 and Pt/Co(0.3 nm)/Pt a DW motion in the direction opposite to the electron flow. In this studies, the nonadiabatic torque was identified to be the main driving force on the domain wall motion and thus this may be explained by a negative current spin polarization or a negative β value in this material. Negative β values were recently predicted by Garate *et al.* [102] in high spin orbit coupling. This result also indicates the strong dependence of nonadiabatic effects and polarization on the exact structure of the material, as for example, Kim *et al.* [61] observed a DW motion in a direction opposite to the electron flow in a similar structure $[CoFe(0.5nm/Pt]_5$.

4.3.5. Current induced domain wall motion in diluted semi-conductor

We briefly summarize in this section the results obtain by Ohno's group and Ferré's group in the diluted magnetic semionductor (Ga,Mn)As. This semiconductor is an alloy of Mn and GaAs that exhibits carrier-induced ferromagnetism

with a Curie temperature typically around 100 K. The considered composition is characterized by a perpendicular magnetic anisotropy resulting in a Bloch DW structure with $\Delta \sim 5$ nm. In this material, the DW motion was demonstrated for very low current density ($\sim 10^5$ A/m^2) which can be accounted for to the low saturation magnetization as well as the high current spin polarization. In addition, the DW moves in the direction of the current which can be explained by the antiferromagnetic p-d exchange coupling between the hole carriers and localized Mn spins. Yamanouchi *et al.* [194] and Adam *et al.* [76] studied the DW velocity as a function of J. They observe a curve $v(J)$ qualitatively similar to what is found in out-of-plane magnetized ferromagnetic metals with a creep regime at very low current density and a flow regime with a velocity proportional to J at higher current density (see Fig. 17).

Yamanouchi *et al.* [75] studied the current and magnetic field H induced DW velocity at very low current density in the creep regime over more than 5 orders of magnitude in J. They show that v follows a creep law with $\ln(v)$ proportional to $J^{-\eta_J}$ with $\eta_J = 0.33 \pm 0.06$, whereas $\ln(v)$ is proportional to $H^{-\eta_H}$ with $\eta_H = 1.2 \pm 0.1$. As a consequence, current and field acts differently on the DW in the creep regime which seems to exclude the nonadiabatic to be the driven force on the DW. The authors show that that these exponents can be explained by a simple model which consider the sole effect of the adiabatic torque on the DW line.

In the flow regime, Yamanouchi *et al.* [194] found that the slope of $v(J)$ can be explained by the sole effect of the adiabatic torque and thus may correspond to a precessional regime above the Walker breakdown, although they don't exclude a contribution from the nonadiabatic torque. To clarify the nature of the flow regime, Adam *et al.* [76] considered a domain defined by two DWs and add a small external magnetic field H. From the expansion velocity of the domain with H during the current injection, they identify the DW propagation to occur in the steady regime and not in the precession regime. The DW propagation is thus driven by the nonadiabatic torque and they estimate $0.17 < \beta < 0.36$. This value is of the order of the Gilbert damping $\alpha_{DW} = 0.25 \pm 0.05$ deduced from

the dependence of the DW velocity with H. Note that a much lower value of α is obtain from FMR experiment ($\alpha_{FMR} = 0.01$). These results seems in agreement with recent theory which predict high values of β (0.2-1) in (Ga,Mn)As, due to the strong intrinsic spin-orbit coupling in this material [101, 102, 104].

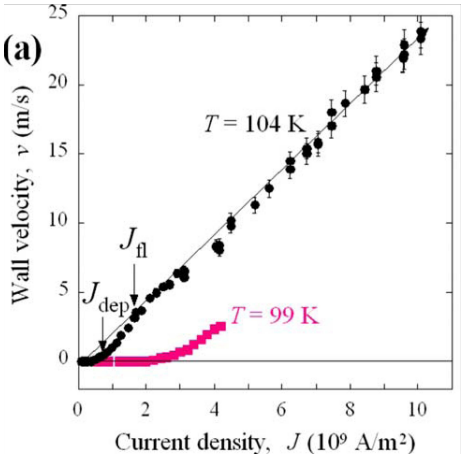

Figure 17: DW Velocity as a function of the current density in ($Ga_{0.93}Mn_{0.07}As$ (50 nm) for different sample temperatures. One can identify three regimes. At low current density ($J \ll J_{dep}$), the creep regime with very slow DW motion. At high current density ($J > J_{fl}$, the flow regime with $v \propto J$. For $J_{dep} < J < J_{fl}$, the intermediate depinning regime. From Ref. [76]

5. Conclusions

In conclusion we have reviewed the physics of domain wall motion induced by spin transfer when spin-polarized currents flow across a domain wall. We first discuss the domain wall spin structures most commonly found in thin wires (also called strips). For in-plane magnetized soft materials, the complex domain wall types occurring and the dependence of the spin structure on the wire geometry are presented and the more conventional domain wall types in out-of-plane magnetized materials are discussed.

We then continue with the theory of the underlying spin torque effect that occurs when spin-polarized conduction electrons interact with the magnetization in a conducting magnetic material. The spatial variation on the magnetization leads to a change of the conduction electron spin direction, which leads to a

transfer of angular momentum (spin transfer) and depending on the mechanism an adiabatic or a non-adiabatic torque is exerted on the magnetization. The details of the influence of these two torques on the domain wall displacement and spin structure changes are discussed first for the zero K case and then at finite temperatures where also creep motion of domain walls occurs. Experimentally in soft in-plane magnetized nanowires, such currents allow for domain wall displacement due to the spin transfer torque effect and in this case all walls (for instance head-to-head and tail-to-tail walls) move in the direction of the electron flow. The exact details of the wall motion depend on the interplay of the acting torques (adiabatic and non-adiabatic spin torque terms) with the intrinsic and shape anisotropies. For sufficiently high current densities, the torques lead to a deformation and even a transformation of the domain wall spin structures (Walker breakdown), which can significantly influence the wall propagation and its velocity. In soft in-plane magnetized wires this leads to transformations between different domain wall types, such as transverse and vortex domain walls. To determine the acting torques quantitatively and in particular measure the non-adiabaticity parameter, various schemes have been put forward, which are being discussed with respect to the results obtained and their robustness.

For out-of-plane magnetized wires with narrow Bloch DWs, recent experiments have shown that the current acts on the DW dynamics similarly to a strong external field which clearly suggests a strong nonadiabatic effect in such materials. Due to the strong pinning in these materials, most experiments were carried out in the thermally activated regime and probed actually the deformation of the pinning barrier by current. It was found that the current-induced spin torque effects nonetheless can be described as an effective field and this equivalence was found to hold also in the viscous flow propagation regime where very high DW velocity were obtained (up to 400 m/s) [279]. From this current-field equivalence, values of the non-adiabaticity are found that are much larger than for in-plane magnetized wires. The origin of this enhancement has currently not been clearly identified but may be related to the high-spin orbit coupling in these materials.

While there are still a number of open questions, as discussed in the previous sections, the demonstration of the manipulation of DWs with current is not only of high interest from a scientific point of view but they are also at the heart of a multitude of devices recently proposed for data storage applications. The most famous example is the race track memory, proposed by S.S.P Parkin [2, 238] where a number of domain walls are shifted synchronously along a vertically integrated wire by current pulses, with each domain wall carrying one bit (see Fig. 18(a)). This device potentially combines the high density and low cost of the hard disk approach with the reliability of solid state memory, due to the absence of mechanically moving parts. A Magnetic Random Access Memory (MRAM) architecture has also been proposed where the magnetic bit is written through propagation of a DW in a narrow track (Fig. 18(b)) [136, 276, 280–282]. Despite a more complex three terminal architecture compared with standard MRAM, a low writing current is obtained even for relatively high current density due to the small cross-section area of the track. Current smaller than 100 μA were thus reported in (Co/Ni) multilayer, which is similar to the critical current obtained in spin torque MRAM with perpendicular anisotropy [283]. In addition, this design bypasses the reliability issue in spin torque MRAM due to damage of the thin insulating barrier of the magnetic tunnel junction used in the magnetic cell.

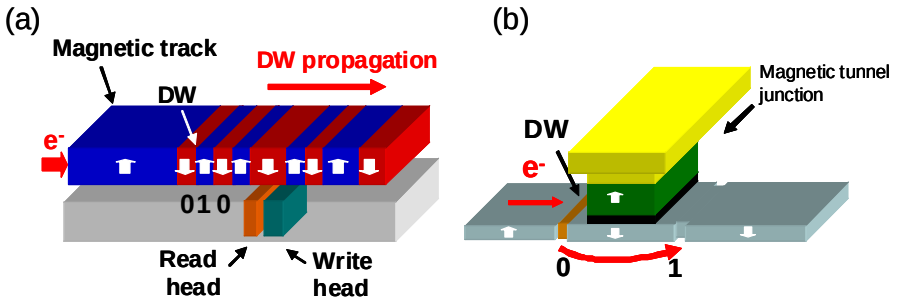

Figure 18: (a) Principle of the race track memory. (b) Cells of a MRAM based on CIDM.

The basic requirements for such devices are a nm-width DWs, and thus out-

of-plane magnetized high anisotropy materials, and a DW velocity on the order of 100 m/s for competitive areal density and operating speed. Sufficiently low current density ($\sim 10^{11}$ A/m^2) is also needed for low write current and to avoid a too high temperature rise when injecting current that could lead to information losses. However, although very low critical current densities (down to the 5×10^{10} A/m^2, see Table 2) were obtained, fast domain wall motion were only observed so far at very high current density ($> 10^{12}$ A/m^2). A first challenge is thus to decrease the current density while maintaining fast motion. This may be achieved by decreasing the intrinsic pinning in the materials but also by engineering new materials with higher spin transfer efficiency and lower damping, for example by playing on the spin-orbit coupling. The use of transverse magnetic field to pin the dynamical DW structure [279, 284–286] and prevent the occurrence of the Walker breakdown with lower mobility seems also promising. Furthermore, this provides an interesting way of controlling the DW structure with the current polarity which may be exploited in devices [279, 286]. Another promising route that was recently proposed is the injection of a spin polarized current perpendicularly to the nanowire plane [189, 287–289] where high DW velocities have been predicted at very low perpendicular current (up to 80 m/s down for 10 μA) [288]. This was confirmed experimentally by Boone *et al.* [189] who measured DW velocity up to 800 m/s at very low critical current density (9×10^{10} A/m^2) in permalloy nanowires excited by spin-polarized current applied perpendicular to the nanowire.

Another issue is the high intrinsic pinning in out-of-plane magnetized materials that can lead to unreliable displacements [258] and furthermore complicates the exact control of the DW position in the track using artificial pinning sites. Another challenge is thus to decrease the intrinsic pinning of the materials and to engineer efficient pinning sites to control the DW position on the nm scale and with a high pinning energy. A possible way may be found in the use of softer compositions based on amorphous materials [59, 290] or epitaxial out-of-plane magnetized material [291].

Although such promising devices motivated a large effort of research in this

field these last years and despite CIDM was proposed more than 30 years ago [83], the understanding of this effect still remains to a large extent incomplete. A key questions deals with the exact nature of the current induced torques and in particular the origin of the amplitude of the nonadiabatic torque. As already stressed, recent experiments seems to indicate higher non-adiabatic effect in out-of-plane materials, but it is currently hard to conclude on its exact value and its origin as the measured β show very large variation depending on the materials and the type of experiments. This may be related with to the fact that the nonadiabatic torque often competes with parasitic effects such as the Oersted field, the Joule heating and the uncontrolled material pinning so that its contribution is hard to extract. Furthermore, even for the same experiments, very different conclusions can be obtained depending on the analysis and the models used to extract β (see for example section 4.3.5). A key point that has mostly not been taken into account is a possible spatial dependence of β. So far β has been assumed to be a materials dependent parameter but a dependence of β for instance on the magnetization gradients as suggested by some experiments and some theoretical calculations would open up an additional path to optimizing the wall propagation. These considerations thus call for further experiments and theoretical studies for a more precise determination of β and in particular its physical origins.

Besides uncertainty in the measurements, many questions still remain open, in particular on:

- *Direction of the DW displacement.* Why does the DW move opposite or in the same direction of the electron flow depending on the material?

- *Relation between β and the Gilbert damping.* Several theories predict β to be of the order of α but no experiments have clearly concluded about this point in out-of-plane magnetized materials and a systematic comparison of β and α in different materials is still lacking. Furthermore, different values of α have been measured for moving DWs or from FMR measurement which needs to be taken into account as α is potentially spin structure-

dependent. Several theories [292, 293] also predicted significant deviation from the Gilbert damping and in particular anisotropic damping, which has not been considered so far.

- *Relation between β and spin relaxation.* The higher β in out-of-plane magnetized could be associated with the high spin-orbit coupling in these materials. More systematic measurements of β with varying spin-orbit coupling are needed to obtain conclusive evidence for this.

- *Relation of β and the DW resistivity.* Several theories predicted a direct link between β [85, 101, 272, 273] and the DW resistivity but there is no clear experimental proof of such a link.

- *Link between current-induced domain wall motion and the spin-motive force* Rather than spin-polarized current leading to domain wall motion, the inverse effect where moving domain walls lead to the generation of a voltage can also occur. Recent experiments measured the voltage due to a fast moving DW above the Walker breakdown in a NiFe nanowire [294]. Duine *et al.* predicted that high β leads to a significant voltage when a DW is moving below the Walker [295].

Answering these fundamental questions would clearly provide important steps towards the understanding of adiabatic and nonadiabatic effect occuring in DW motion. One of the possible approaches to answering these and many of the open questions is to try out various materials, where the electrical transport varies compared to the usually used 3d metals and where effects such as spin-orbit coupling are better controlled and understood. So this review would like to encourage the community to take advantage of the large diversity of available materials, which might hold the key to many of the open questions as well as to the ideal material to make a device based on current-induced domain wall motion a reality.

The authors acknowledge support by the DFG (KL1811 and SFB 767), the E.U. (Human Resources and Mobility Programme and SPINSWITCH MRTN-

CT-2006-035327), the European Research Council through a Starting Independent Researcher Grant (ERC-2007-StG 208162), the Swiss National Science Foundation and the Samsung Advanced Institute of Technology. GM would like to thank A. Thiaville and J.-Y. Chauleau for fruitful discussions.

References

[1] I. R. McFadyen and E. E. Fullerton and M. J. Carey, MRS Bull. 31 (2006) 379.

[2] S. S. P. Parkin, U.S. patent 6,834,005 and patent application 10/984,055, 2004.

[3] S. S. P. Parkin *et al.*, Science 320 (2008) 190.

[4] R. Cowburn, D. Petit, D. Read, O. Petracic, Patent WO 2007/132174A1, 2007.

[5] D. Ilgaz *et al.*, Appl. Phys. Lett. 93 (2008) 132503.

[6] A. Hubert, R. Schäfer, Magnetic Domains - The Analysis of Magnetic Microstructures, Springer, Berlin Heidelberg New York, 1998.

[7] M. Kläui and C. A. F. Vaz, Magnetization configurations and reversal in small magnetic elements, in: H. Kronmüller, S. S. P. Parkin (Eds.), Handbook of Magnetism and Advanced Magnetic Materials, Volume 2, John Wiley and Sons, Chichester, 2007.

[8] J. A. Katine, F. J. Albert, R. A. Buhrman, E. B. Myers, D. C. Ralph, Current-driven magnetization reversal and spin-wave excitations in co/cu/co pillars, Phys. Rev. Lett. 84 (2000) 3149–3152.

[9] S. I. Kiselev, J. C. Sankey, I. N. Krivorotov, N. C. Emley, R. J. Schoelkopf, R. A. Buhrman, D. C. Ralph, Microwave oscillations of a nanomagnet driven by a spin-polarized current., Nature 425 (2003) 380 – 383.

[10] G. Tatara, H. Kohno, J. Shibata, Microscopic approach to current-driven domain wall dynamics, Phys. Rep. 468 (2008) 213–301.

[11] L. D. Landau, E. Lifshitz, On the theory of the dispersion of magnetic permeability in ferromagnetic bodies, Phys. Z. Sowjetunion 8 (1935) 153–169.

[12] L. Néel, Comptes Rendus hebdomadaires des Séances de l'Académie des Sciences 249 (1955) 533.

[13] F. Bloch, Zur theorie des austauschproblems und der remanenzerscheinung der ferromagnetika, Z. Phys. A 74 (1932) 295–335.

[14] J. Rothman, M. Kläui, L. Lopez-Diaz, C. A. F. Vaz, A. Bleloch, J. A. C. Bland, Z. Cui, R. Speaks, Observation of a bi-domain state and nucleation free switching in mesoscopic ring magnets, Phys. Rev. Lett. 86 (2001) 1098–1101.

[15] S. P. Li, D. Peyrade, M. Natali, A. Lebib, Y. Chen, U. Ebels, L. D. Buda, K. Ounadjela, Flux closure structures in cobalt rings, Phys. Rev. Lett. 86 (2001) 1102–1105.

[16] M. Kläui, C. A. F. Vaz, L. Lopez-Diaz, J. A. C. Bland, Vortex formation in narrow ferromagnetic rings, J. Phys.: Cond. Mat. 15 (2003) R985–R1023.

[17] M. Kläui, J. Phys.: Condens. Matter 20 (2008) 313001.

[18] J. I. Martin *et al.*, J. Magn. Magn. Mater. 256 (2002) 449.

[19] D. Backes *et al.*, Microelectron. Eng. 83 (2006) 1726.

[20] L. J. Heyderman, C. David, M. Kläui, C. A. F. Vaz, J. A. C. Bland, Nanoscale ferromagnetic rings fabricated by electron-beam lithography, J. Appl. Phys. 93 (2003) 10011–10013.

[21] L. J. Heyderman, M. Kläui, B. Nöhammer, C. A. F. Vaz, J. A. C. Bland, C. David, Fabrication of nanoscale magnetic ring structures and devices, Microelectron. Eng. 73-74 (2004) 780–784.

[22] Novel techniques for characterizing and preparing samples, in: H. Kronmüller, S. S. P. Parkin (Eds.), Handbook of Magnetism and Advanced Magnetic Materials, Volume 3, John Wiley and Sons, Chichester, 2007.

[23] H. Kronmüller, M. Fähnle, Micromagnetism and the Microstructure of Ferromagnetic Solids, Cambridge University Press, Cambridge, 2003.

[24] J. Miltat, M. J. Donahue, Numerical micromagnetics: Finite difference methods, in: H. Kronmüller, S. S. P. Parkin (Eds.), Handbook of Magnetism and Advanced Magnetic Materials, Volume 2, John Wiley and Sons, Chichester, 2007.

[25] T. Schrefl *et al.*, Numerical methods in micromagnetics (finite element method), in: H. Kronmüller, S. S. P. Parkin (Eds.), Handbook of Magnetism and Advanced Magnetic Materials, Volume 2, John Wiley and Sons, Chichester, 2007.

[26] A. Thiaville, Y. Nakatani, Domain-wall dynamics in nanowires and nanostrips, in: B. Hillebrands, K. Ounadjela (Eds.), Spin dynamics in confined magnetic structures III, Springer, Berlin Heidelberg New York, 2006.

[27] R. D. McMichael, M. J. Donahue, Head to head domain wall structures in thin magnetic strips, IEEE Trans. Magn. 33 (1997) 4167–4169.

[28] A. Wachowiak, J. Wiebe, M. Bode, O. Pietzsch, M. Morgenstern, R. Wiesendanger, Direct observation of internal spin structure of magnetic vortex cores, Science 298 (2002) 577.

[29] F. Junginger *et al.*, Appl. Phys. Lett. 92 (2008) 112502.

[30] E. Feldtkeller *et al.*, Phys. Kondens. Mater. 4 (1965) 8.

[31] Y. Nakatani, A. Thiaville, J. Miltat, Head-to-head domain walls in soft nano-strips: a refined phase diagram, J. Magn. Magn. Mater. 290-291 (2005) 750–753.

[32] D. Backes *et al.*, Appl. Phys. Lett. 91 (2007) 112502.

[33] N. Kazantseva, R. Wieser, U. Nowak, Transition to linear domain walls in nanoconstrictions, Phys. Rev. Lett. 94 (2005) 037206.

[34] L. N. Bulaevskii and V. L. Ginzburg, Sov. Phys. JETP 18 (1964) 530.

[35] M. Kläui, C. A. F. Vaz, J. A. C. Bland, L. J. Heyderman, F. Nolting, A. Pavlovska, E. Bauer, S. Cherifi, S. Heun, A. Locatelli, Head-to-head domain-wall phase diagram in mesoscopic ring magnets, Appl. Phys. Lett. 85 (2004) 5637–5639.

[36] M. Laufenberg, D. Backes, W. Bührer, D. Bedau, M. Kläui, U. Rüdiger, C. A. F. Vaz, J. A. C. Bland, L. J. Heyderman, F. Nolting, S. Cherifi, A. Locatelli, R. Belkhou, S. Heun, E. Bauer, Observation of thermally activated domain wall transformations, Appl. Phys. Lett. 88 (2006) 052507.

[37] Y. G. Yoo, M. Kläui, C. A. F. Vaz, L. J. Heyderman, J. A. C. Bland, Switching field phase diagram of co nanoring magnets, Appl. Phys. Lett. 82 (2003) 2470–2472.

[38] M. Laufenberg, D. Bedau, H. Ehrke, M. Kläui, U. Rüdiger, D. Backes, L. J. Heyderman, F. Nolting, C. A. F. Vaz, J. A. C. Bland, T. Kasama, R. E. Dunin-Borkowski, S. Cherifi, A. Locatelli, S. Heun, Quantitative determination of domain wall coupling energetics, Appl. Phys. Lett. 88 (2006) 212510.

[39] T. J. Bromwich *et al.*, J. Appl. Phys. 99 (2006) 08H304.

[40] M. Kläui, C. A. F. Vaz, W. Wernsdorfer, E. Bauer, S. Cherifi, S. Heun, A. Locatelli, G. Faini, E. Cambril, L. J. Heyderman, J. A. C. Bland, Domain wall behaviour at constrictions in ferromagnetic ring structures, Physica B 343 (2004) 343–349.

[41] The oommf package is available at http://math.nist.gov/oommf., 2000.

[42] L. Heyne *et al.*, J. Appl. Phys. 103 (2008) 07D928.

[43] G. Meier *et al.*, Phys. Rev. Lett. 98 (2007) 187202.

[44] B. van Waeyenberge *et al.*, Nature 444 (2006) 461.

[45] K. W. Chou *et al.*, Appl. Phys. Lett. 90 (2007) 202505.

[46] C. A. F. Vaz, M. Kläui, L. J. Heyderman, C. David, F. Nolting, J. A. C. Bland, Multiplicity of magnetic domain states in circular elements probed by photoemission electron microscopy, Phys. Rev. B 72 (2005) 224426.

[47] M. Kläui, U. Rüdiger, C. A. F. Vaz, J. A. C. Bland, S. Cherifi, A. Locatelli, S. Heun, A. Pavlovska, E. Bauer, L. J. Heyderman, Magnetic states in wide annular structures, J. Appl. Phys. 99 (2006) 08G308.

[48] M. Kläui, M. Laufenberg, L. Heyne, D. Backes, , U. Rüdiger, C. A. F. Vaz, J. A. C. Bland, L. J. Heyderman, S. Cherifi, A. Locatelli, T. O. Mentes, L. Aballe, Current-induced vortex nucleation and annihilation in vortex domain walls, Appl. Phys. Lett. 88 (2006) 232507.

[49] E. Hempe, M. Klui, T. Kasama, D. Backes, F. Junginger, S. Krzyk, L. J. Heyderman, R. Dunin-Borkowski, U. Rdiger, Domain walls, domain wall transformations and structural changes in permalloy nanowires when subjected to current pulses, physica status solidi (a) 204 (2007) 3922–3928.

[50] M. H. Park, Y. K. Hong, B. C. Choi, M. J. Donahue, H. Han, S. H. Gee, Vortex head-to-head domain walls and their formation in onion-state ring elements, Phys. Rev. B 73 (2006) 094424.

[51] D. McGrouther *et al.*, Appl. Phys. Lett. 91 (2007) 22506.

[52] Y. S. Dedkov, M. Fonin, C. König, U. Rüdiger, G. Güntherodt, S. Senz, D. Hesse, Room-temperature observation of high-spin polarization of epitaxial cro2(100) island films at the fermi energy, Appl. Phys. Lett. 80 (2002) 4181–4183.

[53] M. Fonin *et al.*, J. Appl. Phys. (under review).

[54] M. Ziese *et al.*, Phys. Rev. B 02 (2002) 134408.

[55] O. Boulle, J. Kimling, P. Warnicke, M. Kläui, U. Rüdiger, G. Malinowski, H. J. M. Swagten, B. Koopmans, C. Ulysse, G. Faini, Nonadiabatic spin

transfer torque in high anisotropy magnetic nanowires with narrow domain walls, Phys. Rev. Lett. 101 (2008) 216601.

[56] L. S. E. Alvarez, K. Wang, S. Lepadatu, S. Landi, S. J. Bending, C. H. Marrows, Spin-Transfer-Torque-Assisted Domain-Wall creep in a Co/Pt multilayer wire, Phys. Rev. Lett. 104 (2010) 137205.

[57] J. Lee, K. Kim, J. R., K. Moon, S. Yun, G. Gim, K. Lee, K. Shin, H. Lee, S. Choe, Roles of adiabatic and nonadiabatic spin transfer torques on magnetic domain wall motion, arXiv:1006.1216v1 (2009).

[58] M. Cormier, A. Mougin, J. Ferré, A. Thiaville, N. Charpentier, F. Piéchon, R. Weil, V. Baltz, B. Rodmacq, Effect of electrical current pulses on domain walls in Pt/Co/Pt nanotracks with out-of-plane anisotropy: Spin transfer torque versus joule heating, Phys. Rev. B 81 (2010) 024407.

[59] O. Boulle, L. Heyne, J. Rhensius, M. Kläui, U. Rüdiger, L. Joly, L. L. Guyader, F. Nolting, L. J. Heyderman, G. Malinowski, H. J. M. Swagten, B. Koopmans, C. Ulysse, G. Faini, J. Appl. Phys. 105 (2009) 07C106.

[60] I. M. Miron, P.-J. Zermatten, G. Gaudin, S. Auffret, B. Rodmacq, A. Schuhl, Domain wall spin torquemeter., Phys. Rev. Lett. 102 (2009) 137202.

[61] K.-J. Kim, J.-C. Lee, Y. J. Cho, C.-W. Lee, K.-H. Shin, S. Seo, K.-J. Lee, H.-W. Lee, S.-B. Choe, Current-induced domain-wall motion in $[cofe/pt]_5$ nanowire with perpendicular magnetic anisotropy, IEEE Trans. Mag. 45 (2009) 3773 –3775.

[62] H. Tanigawa, T. Koyama, G. Yamada, D. Chiba, S. Kasai, S. Fukami, T. Suzuki, N. Ohshima, N. Ishiwata, Y. Nakatani, T. Ono, Domain wall motion induced by electric current in a perpendicularly magnetized Co/Ni Nano-Wire, Appl. Phys. Express 2 (2009) 053002.

[63] T. Koyama, G. Yamada, H. Tanigawa, S. Kasai, N. Ohshima, S. Fukami, N. Ishiwata, Y. Nakatani, T. Ono, Control of domain wall position by

electrical current in structured Co/Ni wire with perpendicular magnetic anisotropy, Appl. Phys. Express 1 (2008) 101303.

[64] H. Tanigawa, K. Kondou, T. Koyama, K. Nakano, S. Kasai, N. Ohshima, S. Fukami, N. Ishiwata, T. Ono, Current-Driven domain wall motion in CoCrPt wires with perpendicular magnetic anisotropy, Appl. Phys. Express 1 (2008) 011301.

[65] S. Li, H. Nakamura, T. Kanazawa, X. Liu, A. Morisako, Current-induced domain wall motion in tbfeco nanowires with perpendicular magnetic anisotropy, in: 11th Joint MMM-Intermag Conference, EW-01.

[66] M. Feigenson, J. W. Reiner, L. Klein, Efficient current-induced domain-wall displacement in srruo3., Phys. Rev. Lett. 98 (2007) 247204.

[67] C. Burrowes, A. P. Mihai, D. Ravelosona, J. Kim, C. Chappert, L. Vila, A. Marty, Y. Samson, F. Garcia-Sanchez, L. D. Buda-Prejbeanu, I. Tudosa, E. E. Fullerton, J. Attane, Non-adiabatic spin-torques in narrow magnetic domain walls, Nat. Phys. 6 (2010) 17–21.

[68] D. Ravelosona, D. Lacour, J. A. Katine, B. D. Terris, C. Chappert, Nanometer scale observation of high efficiency thermally assisted current-driven domain wall depinning, Phys. Rev. Lett. 95 (2005) 117203.

[69] D. Ravelosona, S. Mangin, J. A. Katine, E. E. Fullerton, B. D. Terris, Threshold currents to move domain walls in films with perpendicular anisotropy, Appl. Phys. Lett. 90 (2007) 072508.

[70] C. Burrowes, D. Ravelosona, C. Chappert, S. Mangin, E. E. Fullerton, J. A. Katine, B. D. Terris, Role of pinning in current driven domain wall motion in wires with perpendicular anisotropy, Appl. Phys. Lett. 93 (2008) 172513.

[71] A. Hubert, R. Schäfer, Magnetic domains: the analysis of magnetic microstructures, Springer-Verlag Berlin Heidelberg New York, 1998.

[72] V. L. Sobolev, Internal structure of a domain wall in ultrathin magnetic film, J. Magn. Magn. Mat. 177-181 (1998) 195–196.

[73] M. Yamanouchi, D. Chiba, F. Matsukura, H. Ohno, Current-induced domain-wall switching in a ferromagnetic semiconductor structure, Nature 428 (2004) 539.

[74] M. Yamanouchi, D. Chiba, F. Matsukura, T. Dietl, H. Ohno, Velocity of domain-wall motion induced by electrical current in the ferromagnetic semiconductor (ga,mn)as, Phys. Rev. Lett. 96 (2006) 096601.

[75] M. Yamanouchi, J. Ieda, F. Matsukura, S. E. Barnes, S. Maekawa, H. Ohno, Universality Classes for Domain Wall Motion in the Ferromagnetic Semiconductor (Ga,Mn)As, domain wall thermal effect, Science 317 (2007) 1726 – 1729.

[76] J. Adam, N. Vernier, J. Ferré, A. Thiaville, V. Jeudy, A. Lemaître, L. Thevenard, G. Faini, Nonadiabatic spin-transfer torque in (Ga,Mn)As with perpendicular anisotropy, Phys. Rev. B 80 (2009) 193204.

[77] J. Slonczewski, M. A.P, Magnetic domain walls in bubble materials, Academic Press, 1979.

[78] S. W. Jung, W. Kim, T. D. Lee, K. J. Lee, H. W. Lee, Current-induced domain wall motion in a nanowire with perpendicular magnetic anisotropy, Appl. Phys. Lett. 92 (2008) 202508–3.

[79] A. Mougin, M. Cormier, J. P. Adam, P. J. Metaxas, J. Ferre, Domain wall mobility, stability and walker breakdown in magnetic nanowires, Europhys. Lett. 78 (2007) 57007.

[80] D. G. Porter, M. J. Donahue, Velocity of transverse domain wall motion along thin, narrow strips, J. Appl. Phys. 95 (2004) 6729.

[81] A. Bellec, S. Rohart, M. Labrune, J. Miltat, A. Thiaville, Domain wall structure in magnetic bilayers with perpendicular anisotropy, Europhys. Lett. 91 (2010) 17009.

[82] J. M. B. Ndjaka, A. Thiaville, J. Miltat, Transverse wall dynamics in a spin valve nanostrip, J. Appl. Phys. 105 (2009) 023905.

[83] L. Berger, Low-field magnetoresistance and domain drag in ferromagnets, J. Appl. Phys. 49 (1978) 2156.

[84] L. Berger, Exchange interaction between ferromagnetic domain wall and electric current in very thin metallic films, J. Appl. Phys. 55 (1984) 1954.

[85] G. Tatara, H. Kohno, Theory of current-driven domain wall motion: Spin transfer versus momentum transfer, Phys. Rev. Lett. 92 (2004) 086601.

[86] J. Xiao, A. Zangwill, M. D. Stiles, Spin-transfer torque for continuously variable magnetization, Phys. Rev. B 73 (2006) 54428.

[87] X. Waintal, M. Viret, Current-induced distortion of a magnetic domain wall, Europhys. Lett. 65 (2004) 427 – 433.

[88] Y. Ban, G. Tatara, Spin-transfer torque in disordered weak ferromagnets, Phys. Rev. B 80 (2009) 184406.

[89] A. Vanhaverbeke, M. Viret, Simple model of current-induced spin torque in domain walls, Phys. Rev. B 75 (2007) 024411.

[90] G. Tatara, H. Kohno, J. Shibata, Microscopic approach to current-driven domain wall dynamics, Phys. Rep. 468 (2008) 213–301.

[91] A. Yamaguchi, T. Ono, S. Nasu, K. Miyake, K. Mibu, T. Shinjo, Real-Space observation of Current-Driven domain wall motion in submicron magnetic wires, Phys. Rev. Lett. 92 (2004) 077205.

[92] J. Zhang, P. M. Levy, S. Zhang, V. Antropov, Identification of transverse spin currents in noncollinear magnetic structures, Phys. Rev. Lett. 93 (2004) 256602.

[93] A. Thiaville, Y. Nakatani, J. Miltat, Y. Suzuki, Micromagnetic understanding of current-driven domain wall motion in patterned nanowires, Europhys. Lett. 69 (2005) 990–996.

[94] G. Tatara, T. Takayama, H. Kohno, J. Shibata, Y. Nakatani, H. Fukuyama, Threshold Current of Domain Wall Motion under Extrinsic Pinning,-Term and Non-Adiabaticity, J. Phys. Soc. Jpn. 75 (2006) 064708.

[95] Y. Tserkovnyak, H. J. Skadsem, A. Brataas, G. E. W. Bauer, Current-induced magnetization dynamics in disordered itinerant ferromagnets, Phys. Rev. B 74 (2006) 144405.

[96] Y. Tserkovnyak, A. Brataas, G. E. W. Bauer, Theory of current-driven magnetization dynamics in inhomogeneous ferromagnets, J. Magn. Magn. Mater. 320 (2008) 1282–1292.

[97] G. Tatara, P. Entel, Calculation of current-induced torque from spin continuity equation, Phys. Rev. B 78 (2008) 064429.

[98] S. E. Barnes, S. Maekawa, Current-Spin coupling for ferromagnetic domain walls in fine wires, Phys. Rev. Lett. 95 (2005) 107204.

[99] H. Kohno, G. Tatara, J. Shibata, Microscopic calculation of spin torques in disordered ferromagnets, J. Phys. Soc. Jap 75 (2006) 113706.

[100] R. A. Duine, A. S. Núñez, J. Sinova, A. H. MacDonald, Functional keldysh theory of spin torques, Phys. Rev. B 75 (2007) 214420.

[101] A. K. Nguyen, H. J. Skadsem, A. Brataas, Giant current-driven domain wall mobility in (Ga,Mn)As, Phys. Rev. Lett. 98 (2007) 146602.

[102] I. Garate, K. Gilmore, M. D. Stiles, A. H. MacDonald, Nonadiabatic spin-transfer torque in real materials, Phys. Rev. B 79 (2009) 104416.

[103] K. Obata, G. Tatara, Current-induced domain wall motion in rashba spin-orbit system, Phys. Rev. B 77 (2008) 214429.

[104] K. M. D. Hals, A. K. Nguyen, A. Brataas, Intrinsic coupling between current and domain wall motion in (Ga,Mn)As, Phys. Rev. Lett. 102 (2009) 256601.

[105] X. Waintal, M. Viret, Current-induced distortion of a magnetic domain wall, Europhys. Lett. 65 (2004) 7.

[106] J. ichiro Ohe, B. Kramer, Dynamics of a domain wall and spin-wave excitations driven by a mesoscopic current., Phys. Rev. Lett. 96 (2006) 027204.

[107] M. Thorwart, R. Egger, Current-induced nonadiabatic spin torques and domain-wall motion with spin relaxation in a ferromagnetic metallic wire, Phys. Rev. B 76 (2007) 214418.

[108] G. Tatara, H. Kohno, J. Shibata, Theory of domain wall dynamics under current, J. Phys. Soc. Jpn. 77 (2008) 031003.

[109] L. D. Landau, E. M. Lifshitz, Theory of the dispersion of magnetic permeability in ferromagnetic bodies, Phys. Z. Sowietunion 8 (1935) 153.

[110] T. L. Gilbert, A lagrangian formulation of the gyromagnetic equation of the magnetic field, Phys. Rev. 100 (1955) 1243.

[111] A. P. Malozemoff, J. C. Slonczewski, Magnetic domain walls in bubble materials, Academic Press, New York, NY, 1979.

[112] A. A. Thiele, On the momentum of ferromagnetic domains, J. Appl. Phys. 47 (1976) 2759.

[113] J. C. Slonczewski, Force, momentum and topology of a moving magnetic domain, J. Magn. Magn. Mater. 12 (1976) 108–122.

[114] A. Thiaville, Y. Nakatani, F. Piéchon, J. Miltat, T. Ono, Transient domain wall displacement under spin-polarized current pulses, Eur. Phys. Jour. B 60 (2007) 13 pages.

[115] A. Thiaville, Y. Nakatani, Domain wall dynamics in nanowires and nanostrips, Springer, Berlin / Heidelberg, 2006.

[116] A. Thiaville, Y. Nakatani, Micromagnetics of Domain-Wall dynamics in soft nanostrips, in: Nanomagnetism and Spintronics, Elsevier, Amsterdam, 2009, pp. 231–276.

[117] L. Thomas, M. Hayashi, X. Jiang, R. Moriya, C. Rettner, S. S. P. Parkin, Oscillatory dependence of current-driven magnetic domain wall motion on current pulse length, Nature 443 (2006) 197–200.

[118] P. Bruno, Geometrically constrained magnetic wall, Phys. Rev. Lett. 83 (1999) 2425 – 2428.

[119] A. Thiaville, Domain wall motion by spin-polarized current: a micromagnetic study, J. Appl. Phys. 95 (2004) 7049.

[120] N. L. Schryer, L. R. Walker, The motion of 180° domain walls in uniform dc magnetic fields, J. Appl. Phys. 45 (1974) 5406–5421.

[121] G. Tatara, H. Kohno, J. Shibata, Theory of domain wall dynamics under current, J. Phys. Soc. Jap 77 (2008) 031003.

[122] J.-Y. Chauleau, R. Weil, A. Thiaville, J. Miltat, Magnetic domain walls displacement : automotion vs. spin-transfer torque, arXiv:1007.5233v1 (2010).

[123] J. He, Z. Li, S. Zhang, Effects of current on vortex and transverse domain walls, J. Appl. Phys. 99 (2006) 08G509.

[124] P. Warnicke, Y. Nakatani, S. Kasai, T. Ono, Long-range vortex domain wall displacement induced by an alternating current: Micromagnetic simulations, Phys. Rev. B 78 (2008) 012413.

[125] S. M. Seo, K. J. Lee, W. Kim, T. D. Lee, Effect of shape anisotropy on threshold current density for current-induced domain wall motion, Appl. Phys. Lett. 90 (2007) 252508.

[126] Y. Nakatani, A. Thiaville, J. Miltat, Faster magnetic walls in rough wires, Nat. Mater. 2 (2003) 521–523.

[127] J. He, Z. Li, S. Zhang, Current-driven domain-wall depinning, J. Appl. Phys. 98 (2005) 016108.

[128] E. Martinez, L. Lopez-Diaz, O. Alejos, L. Torres, M. Carpentieri, Domain-wall dynamics driven by short pulses along thin ferromagnetic strips: Micromagnetic simulations and analytical description, Phys. Rev. B 79 (2009) 094430.

[129] T. Ono, Y. Nakatani, Magnetic domain wall oscillator, Appl. Phys. Express 1 (2008) 061301.

[130] J. He, S. Zhang, Localized steady-state domain wall oscillators, Appl. Phys. Lett. 90 (2007) 142508.

[131] A. Bisig, L. Heyne, O. Boulle, M. Kläui, Tunable steady-state domain wall oscillator with perpendicular magnetic anisotropy, Appl. Phys. Lett. 95 (2009) 162504.

[132] H. Min, R. D. McMichael, M. J. Donahue, J. Miltat, M. D. Stiles, Effects of disorder and internal dynamics on vortex wall propagation, Phys. Rev. Lett. 104 (2010) 217201.

[133] S. Fukami, T. Suzuki, N. Ohshima, K. Nagahara, N. Ishiwata, Intrinsic threshold current density of domain wall motion in nanostrips with perpendicular magnetic anisotropy for use in low-write-current mrams, IEEE Trans. Mag. 44 (2008) 2539 –2542.

[134] T. Suzuki, S. Fukami, N. Ohshima, K. Nagahara, N. Ishiwata, Analysis of current-driven domain wall motion from pinning sites in nanostrips with perpendicular magnetic anisotropy, J. Appl. Phys. 103 (2008) 113913.

[135] S. Fukami, T. Suzuki, N. Ohshima, K. Nagahara, N. Ishiwata., Micromagnetic analysis of current driven domain wall motion in nanostrips with perpendicular magnetic anisotropy, J. Appl. Phys. 103 (2008) 07E718.

[136] S. Fukami, Y. Nakatani, T. Suzuki, K. Nagahara, N. Ohshima, N. Ishiwata, Relation between critical current of domain wall motion and wire dimension in perpendicularly magnetized Co/Ni nanowires, Appl. Phys. Lett. 95 (2009) 232504.

[137] E. Martinez, L. Lopez-Diaz, O. Alejos, L. Torres, Thermally activated domain wall depinning in thin strips with high perpendicular magnetocrystalline anisotropy, domain wall thermal effect, J. Appl. Phys. 106 (2009) 043914–5.

[138] F. Garcia-Sanchez, H. Szambolics, A. P. Mihai, L. Vila, A. Marty, J. Attan?, J. Toussaint, L. D. Buda-Prejbeanu, Effect of crystalline defects on domain wall motion under field and current in nanowires with perpendicular magnetization, domain wall thermal effect, Phys. Rev. B 81 (2010) 134408.

[139] H. Szambolics, J. C. Toussaint, A. Marty, I. M. Miron, L. D. Buda-Prejbeanu, Domain wall motion in ferromagnetic systems with perpendicular magnetization, J. Magn. Magn. Mat. 321 (2009) 1912 – 1918.

[140] H. Szambolics, Nouvelles formulations éléments finis pour le micromagn?tisme et Déplacement de parois par courant polarisé en spin, Ph.D. thesis, Institut Polytechnique de Grenoble, 2009.

[141] M. Yan, A. Kákay, S. Gliga, R. Hertel, Beating the walker limit with massless domain walls in cylindrical nanowires, Phys. Rev. Lett. 104 (2010) 057201.

[142] L. Heyne, J. Rhensius, Y. Cho, D. Bedau, S. Krzyk, C. Dette, H. S. Körner, J. Fischer, M. Laufenberg, D. Backes, L. J. Heyderman, L. Joly, F. Nolting, G. Tatara, H. Kohno, S. Seo, U. Rüdiger, M. Kläui, Geometry-dependent scaling of critical current densities for current-induced domain wall motion and transformations, Phys. Rev. B 80 (2009) 184405.

[143] G. Malinowski, A. Lörincz, S. Krzyk, P. Möhrke, D. Bedau, O. Boulle, J. Rhensius, L. J. Heyderman, Y. J. Cho, S. Seo, M. Kläui, Current-induced domain wall motion in ni 80 fe 20 nanowires with low depinning fields, J. of Phys. D: Appl. Phys. 43 (2010) 045003.

[144] T. Ono, Y. Yoshida, Y. Jiang, M. Esashi, Noise-Enhanced sensing of light and magnetic force based on a nonlinear silicon microresonator, Appl. Phys. Express 1 (2008) 123001.

[145] A. Bisig, J. Rhensius, M. Kammerer, M. Curcic, H. Stoll, G. Schütz, B. V. Waeyenberge, K. W. Chou, T. Tyliszczak, L. J. Heyderman, S. Krzyk, A. von Bieren, M. Kläui, Direct imaging of current induced magnetic vortex gyration in an asymmetric potential well, Appl. Phys. Lett. 96 (2010) 152506.

[146] S. Mizukami, E. P. Sajitha, D. Watanabe, F. Wu, T. Miyazaki, H. Naganuma, M. Oogane, Y. Ando, Gilbert damping in perpendicularly magnetized Pt/Co/Pt films investigated by all-optical pump-probe technique, Appl. Phys. Lett. 96 (2010) 152502.

[147] A. Yamaguchi, S. Nasu, H. Tanigawa, T. Ono, K. Miyake, K. Mibu, T. Shinjo, Effect of joule heating in current-driven domain wall motion, Appl. Phys. Lett. 86 (2005) 012511.

[148] M. Laufenberg, W. Bührer, D. Bedau, P.-E. Melchy, M. Kläui, L. Vila, G. Faini, C. A. F. Vaz, J. A. C. Bland, U. Rüdiger, Temperature dependence of the spin torque effect in current-induced domain wall motion, Phys. Rev. Lett. 97 (2006) 046602.

[149] C. Schieback, D. Hinzke, M. Kläui, U. Nowak, P. Nielaba, Temperature dependence of the current-induced domain wall motion from a modified Landau-Lifshitz-Bloch equation, Phys. Rev. B 80 (2009) 214403–8.

[150] G. Tatara, E. Saitoh, M. Ichimura, H. Kohno, Domain-wall displacement

triggered by an ac current below threshold, Appl. Phys. Lett. 86 (2005) 232504.

[151] E. Martinez, L. Lopez-Diaz, O. Alejos, L. Torres, C. Tristan, Thermal effects on domain wall depinning from a single notch, Phys. Rev. Lett. 98 (2007) 267202.

[152] E. Martinez, L. Lopez-Diaz, O. Alejos, L. Torres, C. Tristan, Erratum: Thermal effects on domain wall depinning from a single notch [phys. rev. lett. 98, 267202 (2007)], Phys. Rev. Lett. 99 (2007) 099901.

[153] E. Martinez, L. Lopez-Diaz, L. Torres, C. Tristan, O. Alejos, Thermal effects in domain wall motion: Micromagnetic simulations and analytical model, Phys. Rev. B 75 (2007) 174409.

[154] R. A. Duine, C. M. Smith, Creep of current-driven domain-wall lines: Effects of intrinsic versus extrinsic pinning, Phys. Rev. B 77 (2008) 094434.

[155] M. E. Lucassen, H. J. van Driel, C. M. Smith, R. A. Duine, Current-driven and field-driven domain walls at nonzero temperature, Phys. Rev. B 79 (2009) 224411.

[156] R. A. Duine, A. S. Núñez, A. H. MacDonald, Thermally assisted current-driven domain-wall motion, Phys. Rev. Lett. 98 (2007) 056605.

[157] F. Garcia-Sanchez, H. Szambolics, A. P. Mihai, L. Vila, A. Marty, J.-P. Attané, J.-C. Toussaint, L. D. Buda-Prejbeanu, Effect of crystalline defects on domain wall motion under field and current in nanowires with perpendicular magnetization, Phys. Rev. B 81 (2010) 134408.

[158] J.-V. Kim, C. Burrowes, Influence of magnetic viscosity on domain wall dynamics under spin-polarized currents, Phys. Rev. B 80 (2009) 214424.

[159] Y. Le Maho, J.-V. Kim, G. Tatara, Spin-wave contributions to current-induced domain wall dynamics, Phys. Rev. B 79 (2009) 174404.

[160] W. F. Brown, Thermal fluctuations of a Single-Domain particle, Phys. Rev. 130 (1963) 1677.

[161] M. E. Lucassen, R. A. Duine, Fluctuations of current-driven domain walls in the nonadiabatic regime, Phys. Rev. B 80 (2009) 144421.

[162] D. A. Garanin, Fokker-planck and landau-lifshitz-bloch equations for classical ferromagnets, Phys. Rev. B 55 (1997) 3050–3057.

[163] S. Lemerle, J. Ferré, C. Chappert, V. Mathet, T. Giamarchi, P. Le Doussal, Domain wall creep in an ising ultrathin magnetic film, Phys. Rev. Lett. 80 (1998) 849–852.

[164] F. Cayssol, D. Ravelosona, C. Chappert, J. F. ', J. P. Jamet, Domain wall creep in magnetic wires, Phys. Rev. Lett. 92 (2004) 107202.

[165] M. Kläui, Head-to-head domain walls in magnetic nanostructures, J. Phys. Cond. Matt. 20 (2008) 313001.

[166] H. Kronmüller, S. S. P. P. (Eds.), Handbook of Magnetism and Advanced Magnetic Materials, Wiley (Chichester), 2008.

[167] J. Smit, Magnetoresistance of ferromagnetic metals and alloys at low temperatures, Physica 17 (1951) 612–627.

[168] I. A. Campbell, A. Fert, O. Jaoul, The spontaneous resistivity anisotropy in ni-based alloys, Journal of Physics C: Solid State Physics 3 (1970) S95.

[169] T. R. McGuire, R. I. Potter, Anisotropic magnetoresistance in ferromagnetic 3d alloys, IEEE Trans. Mag. 11 (1975) 1018.

[170] C. H. Marrows, Spin-polarised currents and magnetic domain walls, Advances in Physics 54 (2005) 585–713.

[171] M. Kläui, C. A. F. Vaz, J. A. C. Bland, W. Wernsdorfer, G. Faini, E. Cambril, L. J. Heyderman, Domain wall motion induced by spin polarized currents in ferromagnetic ring structures, Appl. Phys. Lett. 83 (2003) 105–107.

[172] M. Kläui, C. A. F. Vaz, J. Rothman, J. A. C. Bland, W. Wernsdorfer, G. Faini, E. Cambril, Domain wall pinning in narrow ferromagnetic ring structures probed by magnetoresistance measurements, Phys. Rev. Lett. 90 (2003) 097202.

[173] M. Hayashi, L. Thomas, Y. B. Bazaliy, C. Rettner, R. Moriya, X. Jiang, S. S. P. Parkin, Influence of current on field-driven domainwall motion in permalloy nanowires from time resolved measurements of anisotropic magnetoresistance, Phys. Rev. Lett. 96 (2006) 197207.

[174] M. Hayashi, L. Thomas, Y. B. Bazaliy, C. Rettner, R. Moriya, X. Jiang, S. S. P. Parkin, Influence of current on field-driven domain wall motion in permalloy nanowires from time resolved measurements of anisotropic magnetoresistance, Phys. Rev. Lett. 96 (2006) 197207.

[175] M. Hayashi, L. Thomas, C. Rettner, R. Moriya, S. S. P. Parkin, Direct observation of the coherent precession of magnetic domain walls propagating along permalloy nanowires, Nature Phys. 3 (2007) 21–25.

[176] M. N. Baibich, J. M. Broto, A. Fert, F. N. Van Dau, F. Petroff, P. Etienne, G. Creuzet, A. Friederich, J. Chazelas, Giant magnetoresistance of (001)fe/(001)cr magnetic superlattices, Phys. Rev. Lett. 61 (1988) 2472–2475.

[177] G. Binasch, P. Grünberg, F. Saurenbach, W. Zinn, Enhanced magnetoresistance in layered magnetic structures with antiferromagnetic interlayer exchange, Phys. Rev. B 39 (1989) 4828.

[178] B. Dieny, V. S. Speriosu, S. S. P. Parkin, B. A. Gurney, D. R. Wilhoit, D. Mauri, Giant magnetoresistive in soft ferromagnetic multilayers, Phys. Rev. B 43 (1991) 1297–1300.

[179] T. Ono, H. Miyajima, K. Shigeto, T. Shinjo, Magnetization reversal in submicron magnetic wire studied by using giant magnetoresistance effect, Appl. Phys. Lett. 72 (1998) 1116–1117.

[180] T. Ono, H. Miyajima, K. Shigeto, K. Mibu, N. Hosoito, T. Shinjo, Propagation of a Magnetic Domain Wall in a Submicrometer Magnetic Wire, Science 284 (1999) 468–470.

[181] T. Ono, H. Miyajima, K. Shigeto, K. Mibu, N. Hosoito, T. Shinjo, Propagation of the magnetic domain wall in submicron magnetic wire investigated by using giant magnetoresistance effect, J. Appl. Phys. 85 (1999) 6181–6183.

[182] J. Grollier, Lacour, V. Cros, A. Hamzic, A. Vaurès, A. Fert, D. Adam, G. Faini, Switching the magnetic configuration of a spin valve by current-induced domain wall motion, J. Appl. Phys. 92 (2002) 4825–4827.

[183] J. Grollier, P. Boulenc, V. Cros, A. Hamzić, A. Vaurès, A. Fert, G. Faini, Switching a spin valve back and forth by current-induced domain wall motion, Appl. Phys. Lett. 83 (2003) 509–511.

[184] C. K. Lim, T. Devolder, C. Chappert, J. Grollier, V. Cros, A. Vaurès, A. Fert, G. Faini, Domain wall displacement induced by subnanosecond pulsed current, Appl. Phys. Lett. 84 (2004) 2820–2822.

[185] S. Laribi, V. Cros, M. Muñoz, J. Grollier, A. Hamzić, C. Deranlot, A. Fert, E. Martínez, L. López-Díaz, L. Vila, G. Faini, S. Zoll, R. Fournel, Reversible and irreversible current induced domain wall motion in cofeb based spin valves stripes, Appl. Phys. Lett. 90 (2007) 232505.

[186] L. Thomas, M. Hayashi, X. Jiang, R., C. Rettner, S. S. P. Parkin, Perturbation of spin-valve nanowire reference layers during domain wall motion induced by nanosecond-long current pulses, Appl. Phys. Lett. 92 (2008) 112504.

[187] S. Pizzini, V. Uhlíř, J. Vogel, N. Rougemaille, S. Laribi, V. Cros, E. Jiménez, J. Camarero, C. Tieg, E. Bonet, M. Bonfim, R. Mattana, C. Deranlot, F. Petroff, C. Ulysse, G. Faini, A. Fert, High domain wall

velocity at zero magnetic field induced by low current densities in spin valve nanostripes, Appl. Phys. Express 2 (2009) 023003.

[188] A. J. Zambano, W. P. P. Jr, Detecting domain-wall trapping and motion at a constriction in narrow ferromagnetic wires using perpendicular-current giant magnetoresistance, Appl. Phys. Lett. 85 (2004) 1562 – 1564.

[189] C. T. Boone, J. A. Katine, M. Carey, J. R. Childress, X. Cheng, I. N. Krivorotov, Rapid domain wall motion in permalloy nanowires excited by a spin-polarized current applied perpendicular to the nanowire, Phys. Rev. Lett. 104 (2010) 097203.

[190] D. Morecroft, I. A. Colin, F. J. Castaño, J. A. C. Bland, C. A. Ross, Current-induced magnetization reversal in $nife/cu/co/au$ notched mesoscopic bars, Phys. Rev. B 76 (2007) 054449.

[191] V. Uhlr, S. Pizzini, N. Rougemaille, V. Cros, E. Jimenez, L. Ranno, O. Fruchart, M. Urbanek, G. Gaudin, J. Camarero, C. Tieg, F. Sirotti, J. Vogel, Direct observation of oersted-field-induced magnetization dynamics in magnetic nanowires, arXiv:1002.1302v2 (2010).

[192] J. Wunderlich, D. Ravelosona, C. Chappert, F. Cayssol, V. Mathet, A. Thiaville, Influence of Geometry on Domain Wall Propagation in a Mesoscopic Wire, IEEE Trans. Mag. 37 (2001) 2104–2107.

[193] J. P. Attané, D. Ravelosona, A. Marty, Y. Samson, C. Chappert, Thermally activated depinning of a narrow domain wall from a single defect, Phys. Rev. Lett. 96 (2006) 147204.

[194] M. Yamanouchi, D. Chiba, F. Matsukura, T. Dietl, H. Ohno, Velocity of domain-wall motion induced by electrical current in the ferromagnetic semiconductor (ga,mn)as., Phys. Rev. Lett. 96 (2006) 096601.

[195] H. Tanigawa, K. Kondou, T. Koyama, K. Nakano, S. Kasai, N. Ohshima, S. Fukami, N. Ishiwata, T. Ono, Current-driven domain wall motion in

cocrpt wires with perpendicular magnetic anisotropy, Appl. Phys. Express 1 (2008) 011301.

[196] T. Koyama, G. Yamada, H. Tanigawa, S. Kasai, N. Ohshima, S. Fukami, N. Ishiwata, Y. Nakatani, T. Ono, Control of domain wall position by electrical current in structured co/ni wire with perpendicular magnetic anisotropy, Appl. Phys. Express 1 (2008) 101303.

[197] T. Schrefl, J. Fidler, K. Kirk, J. Chapman, Domain structures and switching mechanisms in patterned magnetic elements, J. Magn. Magn. Mater. 175 (1997) 193 – 204. Proceedings of the First Toyota Workshop on Magnetism and Magnetic Materials for High Density Information Storage.

[198] H. Hopster, H. P. Oepen, Magnetic microscopy of nanostructures, Springer-Verlag, Berlin Heidelberg New York, 2005.

[199] C. Brownlie, S. McVitie, J. N. Chapman, C. D. W. Wilkinson, Lorentz microscopy studies of domain wall trap structures, J. Appl. Phys. 100 (2006) 033902.

[200] M. Kläui, H. Ehrke, U. Rüdiger, T. Kasama, R. E. Dunin-Borkowski, D. Backes, L. J. Heyderman, C. A. F. Vaz, J. A. C. Bland, G. Faini, E. Cambril, W. Wernsdorfer, Direct observation of domain-wall pinning at nanoscale constrictions, Appl. Phys. Lett. 87 (2005) 102509.

[201] D. McGrouther, S. McVitie, J. N. Chapman, A. Gentils, Controlled domain wall injection into ferromagnetic nanowires from an optimized pad geometry, Appl. Phys. Lett. 91 (2007) 022506.

[202] Y. Togawa, T. Kimura, K. Harada, T. Akashi, T. Matsuda, A. Tonomura, Y. Otani, Domain nucleation and annihilation in uniformly magnetized state under current pulses in narrow ferromagnetic wires, Japanese Journal of Applied Physics 45 (2006) L1322 – L1324.

[203] Y. Togawa, T. Kimura, K. Harada, T. Matsuda, A. Tonomura, Y. Otani, T. Akashi, Current-excited magnetization reversal under in-plane mag-

netic field in a nanoscaled ferromagnetic wire, Appl. Phys. Lett. 92 (2008) 012505.

[204] P.-O. Jubert, R. Allenspach, A. Bischof, Magnetic domain walls in constrained geometries, Phys. Rev. B 69 (2004) 220410.

[205] P.-O. Jubert, M. Kläui, A. Bischof, U. Rüdiger, R. Allenspach, Velocity of vortex walls moved by current, J. Appl. Phys. 99 (2006) 08G523.

[206] M. Kläui, P.-O. Jubert, R. Allenspach, A. Bischof, J. A. C. Bland, G. Faini, U. Rüdiger, C. A. F. Vaz, L. Vila, C. Vouille, Direct observation of domain-wall configurations transformed by spin currents, Phys. Rev. Lett. 95 (2005) 026601.

[207] G. Schütz, W. Wagner, W. Wilhelm, P. Kienle, R. Zeller, R. Frahm, G. Materlik, Absorption of circularly polarized x rays in iron, Phys. Rev. Lett. 58 (1987) 737–740.

[208] J. Stöhr, Y. Wu, B. D. Hermsmeier, M. G. Samant, G. R. Harp, S. Koranda, D. Dunham, B. P. Tonner, Element-specific magnetic microscopy with circularly polarized x-rays, Science 259 (1993) 658.

[209] J. Stöhr, S. Anders, X-ray spectromicroscopy of complex materials and surfaces, IBM J. Res. Develop. 44 (2000) 535–551.

[210] P. Fischer, Curr. Opin. Solid State Mater. Sci. 7 (2003) 173.

[211] A. L. D. Kilcoyne, T. Tyliszczak, W. F. Steele, S. Fakra, P. Hitchcock, K. Franck, E. Anderson, B. Harteneck, J. Synchrotron Radiat. 10 (2003) 125.

[212] D. Attwood, Soft X-Rays and Extreme Ultraviolet Radiation: Principles and Applications, Cambridge Univ. Press, 1999.

[213] S. Eisebitt, J. Lüning, W. F. Schlotter, M. Lörgen, O. Hellwig, W. Eberhardt, J. Stöhr, Lensless imaging of magnetic nanostructures by x-ray spectro-holography, Nature 432 (2004) 885–888.

[214] J. Raabe, C. Quitmann, C. H. Back, F. Nolting, S. Johnson, C. Buehler, Quantitative analysis of magnetic excitations in landau flux-closure structures using synchrotron-radiation microscopy, Phys. Rev. Lett. 94 (2005) 217204.

[215] H. Stoll, A. Puzic, B. van Waeyenberge, P. Fischer, J. Raabe, M. Buess, T. Haug, R. Höllinger, C. Back, D. Weiss, G. Denbeaux, High-resolution imaging of fast magnetization dynamics in magnetic nanostructures, Appl. Phys. Lett. 84 (2004) 3328 – 3330.

[216] M. Mansuripur, The physical principles of magneto-optical recording, Cambridge University Press, 1998.

[217] C. Chappert, H. Bernas, J. Ferré;, V. Kottler, J.-P. Jamet, Y. Chen, E. Cambril, T. Devolder, F. Rousseaux, V. Mathet, H. Launois, Planar Patterned Magnetic Media Obtained by Ion Irradiation, Science 280 (1998) 1919–1922.

[218] D. A. Allwood, G. Xiong, M. D. Cooke, C. C. Faulkner, D. Atkinson, N. Vernier, R. P. Cowburn, Submicrometer Ferromagnetic NOT Gate and Shift Register, Science 296 (2002) 2003–2006.

[219] D. A. Allwood, N. Vernier, G. Xiong, M. D. Cooke, D. Atkinson, C. C. Faulkner, R. P. Cowburn, Shifted hysteresis loops from magnetic nanowires, Appl. Phys. Lett. 81 (2002) 4005–4007.

[220] D. Atkinson, D. A. Allwood, G. Xiong, M. D. Cooke, C. C. Faulkner, R. P. Cowburn, Magnetic domain-wall dynamics in a submicrometre ferromagnetic structure, Nature Mater. 2 (2003) 85–87.

[221] D. A. Allwood, G. Xiong, R. P. Cowburn, Domain wall diodes in ferromagnetic planar nanowires, Appl. Phys. Lett. 85 (2004) 2848–2850.

[222] N. Vernier, D. A. Allwood, D. Atkinson, M. D. Cooke, R. P. Cowburn, Domain wall propagation in magnetic nanowires by spin-polarized current injection, EPL (Europhys. Lett.) 65 (2004) 526.

[223] G. S. D. Beach, C. Nistor, C. Knutson, M. Tsoi, J. L. Erskine, Dynamics of field-driven domain-wall propagation in ferromagnetic nanowires, Nature Mater. 4 (2005) 741–744.

[224] G. S. D. Beach, C. Knutson, C. Nistor, M. Tsoi, J. L. Erskine, Nonlinear domain-wall velocity enhancement by spin-polarized electric current, Phys. Rev. Lett. 97 (2006) 057203.

[225] J. Yang, C. Nistor, G. S. D. Beach, J. L. Erskine, Magnetic domain-wall velocity oscillations in permalloy nanowires, Phys. Rev. B 77 (2008) 014413.

[226] P. . Möhrke, T. A. Moore, M. Kläui, J. Boneberg, D. Backes, S. Krzyk, L. J. Heyderman, P. Leiderer, U. Rüdiger, Single shot kerr magnetometer for observing real-time domain wall motion in permalloy nanowires, J. Phys. D: Appl. Phys. 41 (2008) 164009.

[227] M. Yamanouchi, D. Chiba, F. Matsukura, H. Ohno, Current-induced domain-wall switching in a ferromagnetic semiconductor structure, Nature 428 (2004) 539–542.

[228] T. Devolder, C. Chappert, Y. Chen, E. Cambril, H. Bernas, J. P. Jamet, J. Ferré, Sub-50 nm planar magnetic nanostructures fabricated by ion irradiation, Appl. Phys. Lett. 74 (1999) 3383–3385.

[229] C. Nistor, G. S. D. Beach, J. L. Erskine, Versatile magneto-optic kerr effect polarimeter for studies of domain-wall dynamics in magnetic nanostructures, Rev. Sci. Instrum. 77 (2006) 103901.

[230] L. Heyne, J. Rhensius, A. Bisig, S. Krzyk, P. Punke, M. Kla?ui, L. J. Heyderman, L. L. Guyader, F. Nolting, Direct observation of high velocity current induced domain wall motion, Appl. Phys. Lett. 96 (2010) 032504.

[231] G. Meier, M. Bolte, R. Eiselt, B. Krüger, D. H. Kim, P. Fischer, Direct imaging of stochastic domain-wall motion driven by nanosecond current pulses, Phys. Rev. Lett. 98 (2007) 187202.

[232] L. Bocklage, B. Krüger, T. Matsuyama, M. Bolte, U. Merkt, D. Pfannkuche, G. Meier, Dependence of magnetic Domain-Wall motion on a fast changing current, Phys. Rev. Lett. 103 (2009) 197204.

[233] L. Heyne, M. Kläui, D. Backes, T. A. Moore, S. Krzyk, U. Rüdiger, L. J. Heyderman, A. F. Rodríguez, F. Nolting, T. O. Mentes, M. A. Nino, A. Locatelli, K. Kirsch, R. Mattheis, Relationship between nonadiabaticity and damping in permalloy studied by current induced spin structure transformations., Phys. Rev. Lett. 100 (2008) 066603.

[234] M. Hayashi, L. Thomas, C. Rettner, R. Moriya, Y. B. Bazaliy, S. S. P. Parkin, Current driven domain wall velocities exceeding the spin angular momentum transfer rate in permalloy nanowires, Phys. Rev. Lett. 98 (2007) 037204.

[235] M. Laufenberg, W. Bührer, D. Bedau, P.-E. Melchy, M. Kläui, U. Rüdiger, L. Vila, G. Faini, C. A. F. Vaz, J. A. C. Bland, Temperature dependence of the spin torque effect in current-induced domain wall motion, Phys. Rev. Lett. 97 (2006) 046602.

[236] M. Eltschka, M. Wötzel, J. Rhensius, S. Krzyk, U. Nowak, M. Kläui, T. Kasama, R. E. Dunin-Borkowski, L. J. Heyderman, H. J. van Driel, R. A. Duine, Nonadiabatic spin torque investigated using thermally activated magnetic domain wall dynamics, Phys. Rev. Lett. 105 (2010) 056601.

[237] M. Hayashi, L. Thomas, Y. B. Bazaliy, C. Rettner, R. Moriya, X. Jiang, S. S. P. Parkin, Influence of current on field-driven domain wall motion in permalloy nanowires from time resolved measurements of anisotropic magnetoresistance., Phys. Rev. Lett. 96 (2006) 197207.

[238] S. S. P. Parkin, M. Hayashi, L. Thomas, Magnetic Domain-Wall Racetrack Memory, Science 320 (2008) 190 – 194.

[239] H. Ohno, T. Dietl, Spin-transfer physics and the model of ferromagnetism in (Ga,Mn)As, J. Magn. Magn. Mat. 320 (2008) 1293–1299.

[240] F. Matsukura, D. Chiba, H. Ohno, SPINTRONICS, volume 82, Elsevier, pp. 207–240.

[241] D. Chiba, M. Yamanouchi, F. Matsukura, H. Ohno, Current-induced domain wall motion in ferromagnetic semiconductor structures, Magnetics Japan 4 (2009) 390.

[242] J. Ferre, Spin Dynamics in Confined Magnetic Structures I, volume 83, Springer-Verlag, Berlin, Heidelberg, p. 127.B.

[243] J. I. Hong, S. Sankar, A. E. Berkowitz, W. F. E. Jr., J. Magn. Magn. Mater. 285 (2005) 359.

[244] T. Thomson, G. Hu, B. D. Terris, Intrinsic distribution of magnetic anisotropy in thin films probed by patterned nanostructures, Phys. Rev. Lett. 96 (2006) 257204.

[245] F. Cayssol, Etude de la dynamique d'une paroi de domaine magnétique dans des pistes submicroniques, Ph.D. thesis, Université Paris 7, 2003.

[246] P. J. Metaxas, J. P. Jamet, A. Mougin, M. Cormier, J. Ferre, V. Baltz, B. Rodmacq, B. Dieny, R. L. Stamps, Creep and flow regimes of magnetic domain-wall motion in ultrathin pt/co/pt films with perpendicular anisotropy, Phys. Rev. Lett. 99 (2007) 217208.

[247] K. Kim, J. Lee, S. Ahn, K. Lee, C. Lee, Y. J. Cho, S. Seo, K. Shin, S. Choe, H. Lee, Interdimensional universality of dynamic interfaces, Nature 458 (2009) 740–742.

[248] M. Yamanouchi, D. Chiba, F. Matsukura, H. Ohno, Current-induced domain-wall switching in a ferromagnetic semiconductor structure, Nature 428 (2004) 539–542.

[249] H. W. Schumacher, D. Ravelosona, F. Cayssol, J. Wunderlich, C. Chappert, R. J. Haug, V. Mathet, A. Thiaville, Control of the magnetic domain wall propagation in Pt/Co/Pt ultra thin lms using direct mechanical AFM lithography, J. Magn. Magn. Mat. 240 (2002) 53–56.

[250] A. Aziz, S. J. Bending, H. G. Roberts, S. Crampin, P. J. Heard, C. H. Marrows, Angular dependence of domain wall resistivity in artificial magnetic domain structures., Phys. Rev. Lett. 97 (2006) 206602.

[251] T. Aign, Phys. Rev. Lett. 81 (1998) 2000.

[252] L. Néel, Théorie du trainage magnétique des ferromagnétiques en grains fins avec applications aux terres cuites, Ann. Geophys. 5 (1949) 99.

[253] P. Gaunt, Magnetic viscosity and thermal activation energy, J. Appl. Phys. 59 (1986) 4129.

[254] P. Gaunt, Ferromagnetic domain wall pinning by a random array of inhomogeneities, Philosophical Magazine Part B 48 (1983) 261–276.

[255] C.-Y. You, I. M. Sung, B.-K. Joe, Analytic expression for the temperature of the current-heated nanowire for the current-induced domain wall motion, Appl. Phys. Lett. 89 (2006) 222513.

[256] C. Y. You, S. S. Ha, Temperature increment in a current-heated nanowire for current-induced domain wall motion with finite thickness insulator layer, Appl. Phys. Lett. 91 (2007) 022507.

[257] M. Hayashi, L. Thomas, C. Rettner, X. Jiang, S. S. P. Parkin, Temporal evolution of exchange bias in spin-valve nanowires on the nanosecond time scale, Europhys. Lett. 78 (2007) 67006.

[258] T. A. Moore, I. M. Miron, G. Gaudin, G. Serret, S. Auffret, B. Rodmacq, A. Schuhl, S. Pizzini, J. Vogel, M. Bonfim, High domain wall velocities induced by current in ultrathin pt/co/alox wires with perpendicular magnetic anisotropy, Appl. Phys. Lett. 93 (2008) 262504.

[259] C. Chappert, H. Bernas, J. Ferre, V. Kottler, J. P. Jamet, Y. Chen, E. Cambril, T. Devolder, F. Rousseaux, V. Mathet, et al., Planar patterned magnetic media obtained by ion irradiation, Science 280 (1998) 1919.

[260] T. Devolder, Light ion irradiation of Co/Pt systems: Structural origin of the decrease in magnetic anisotropy, Phys. Rev. B 62 (2000) 5794 – 5802.

[261] T. Devolder, J. Ferré, C. Chappert, H. Bernas, J.-P. Jamet, V. Mathet, Magnetic properties of he^{+} irradiated pt/co/pt ultrathin films, Phys. Rev. B 64 (2001) 064415.

[262] S. Hankemeier, K. Sachse, Y. Stark, R. Frömter, H. P. Oepen, Ultrahigh current densities in permalloy nanowires on diamond, Appl. Phys. Lett. 92 (2008) 242503.

[263] J. Heinen, O. Boulle, K. Rousseau, G. Malinowski, M. Kla?ui, H. J. M. Swagten, B. Koopmans, C. Ulysse, G. Faini, Current-induced domain wall motion in Co/Pt nanowires: Separating spin torque and oersted-field effects, Appl. Phys. Lett. 96 (2010) 202510.

[264] D. Partin, M. Karnezos, L. deMenezes, L. Berger, Non-uniform current distribution in the neighborhood of a ferromagnetic domain wall in cobalt at 4.2 k, J. Appl. Phys. 45 (1974) 1842.

[265] M. Viret, A. Vanhaverbeke, F. Ott, J.-F. Jacquinot, Current induced pressure on a tilted magnetic domain wall, Phys. Rev. B 72 (2005) 140403.

[266] A. Thiaville, Y. Nakatani, J. Miltat, Y. Suzuki, Micromagnetic understanding of current-driven domain wall motion in patterned nanowires, Europhys. Lett. 69 (2005) 990.

[267] M. Feigenson, J. W. Reiner, L. Klein, Current-induced magnetic instability in srruo3, J. Appl. Phys. 103 (2008) 07e741.

[268] D. Ravelosona, D. Lacour, J. A. Katine, B. D. Terris, Current-driven narrow domain wall depinning in perpendicular spin valves, IEEE Trans. Mag. 41 (2005) 2618 – 2620.

[269] I. M. Miron, G. Gaudin, S. Auffret, B. Rodmacq, A. Schuhl, S. Pizzini, J. Vogel, P. Gambardella, Current-driven spin torque induced by the rashba effect in a ferromagnetic metal layer, Nat. Mater. 9 (2010) 230–234.

[270] D. Petit, A.-V. Jausovec, D. Read, R. P. Cowburn, J. Appl. Phys. 103 (2008) 114307.

[271] J. Foros, A. Brataas, Y. Tserkovnyak, G. E. W. Bauer, Current-induced noise and damping in nonuniform ferromagnets, Phys. Rev. B 78 (2008) 140402.

[272] L. Berger, Relation between damping, current-induced torques, and wall resistance for domain walls in magnetic nanowires, Phys. Rev. B 75 (2007) 174401.

[273] Y. Tserkovnyak, C. H. Wong, Theory of spin magnetohydrodynamics, Phys. Rev. B 79 (2009) 014402.

[274] L. Klein, Y. Kats, A. F. Marshall, J. W. Reiner, T. H. Geballe, M. R. Beasley, A. Kapitulnik, Domain wall resistivity in SrRuO3, Phys. Rev. Lett. 84 (2000) 6090.

[275] S. Li, H. Nakamura, T. Kanazawa, X. Liu, A. Morisako, Current-Induced domain wall motion in TbFeCo wires with perpendicular magnetic anisotropy, IEEE Trans. Mag. 46 (2010) 1695–1698.

[276] T. Suzuki, S. Fukami, K. Nagahara, N. Ohshima, N. Ishiwata, Evaluation of scalability for Current-Driven domain wall motion in a Co/Ni multilayer strip for memory applications, IEEE Trans. Mag. 45 (2009) 3776–3779.

[277] M. Miron, Etude de l'interaction entre un courrant polarisé en spin et une paroi de domaine magnétique dans des matériaux à aimantation perpendiculaire, Ph.D. thesis, Université Joseph Fourier, 2009.

[278] T. Koyama, H. Tanigawa, G. Yamada, N. Ohshima, S. Fukami, N. Ishiwata, D. Chiba, S. Kasai, R. Nakatani, O. T, in: International Conference on Magnetism, Karlsruhe, TuB -4.2-08.

[279] I. M. Miron, T. Moore, H. Szambolics, G. Gaudin, L. D. Buda-Prejbeanu, S. Auffret, B. Rodmacq, S. Pizzini, J. Vogel, M. Bonfim, A. Schuhl, Fast current-induced domain wall motion controlled by the rashba effect, Nature Physics, submitted, 2010.

[280] V. Cros, J. Grollier, M. M. Sancher, A. Fert, F. N. V. Dau, Brevet International (2005) WO 2006/064022.

[281] S. Fukami, T. Suzuki, K. Nagahara, N. Ohshima, Y. Ozaki, S. Saito, R. Nebashi, N. Sakimura, H. Honjo, K. Mori, C. Igarashi, S. Miura, N. Ishiwata, T. Sugibayashi, Low-current perpendicular domain wall motion cell for scalable high-speed mram, VLSI Technology, 2009 Symposium on, p. 230.

[282] M. Kläui, R. Allenspach, P.-O. Jubert, U.S Patent (2007) US 7,242,604 B2.

[283] S. Ikeda, K. Miura, H. Yamamoto, K. Mizunuma, H. D. Gan, M. Endo, S. Kanai, J. Hayakawa, F. Matsukura, H. Ohno, A perpendicular-anisotropy CoFeBMgO magnetic tunnel junction, Nat. Mater. 9 (2010) 721–724.

[284] J.-Y. Lee, K.-S. Lee, S.-K. Kim, Remarkable enhancement of domain-wall velocity in magnetic nanostripes, Appl. Phys. Lett. 91 (2007) 122513.

[285] J. Lu, X. R. Wang, Motion of transverse domain walls in thin magnetic nanostripes under transverse magnetic fields, J. Appl. Phys. 107 (2010) 083915.

[286] A. Vanhaverbeke, A. Bischof, R. Allenspach, Control of domain wall polarity by current pulses., Phys. Rev. Lett. 101 (2008) 107202.

[287] A. Rebei, O. Mryasov, Dynamics of a trapped domain wall in a spin-valve nanostructure with current perpendicular to the plane, Phys. Rev. B 74 (2006) 014412.

[288] A. V. Khvalkovskiy, K. A. Zvezdin, Y. V. Gorbunov, V. Cros, J. Grollier, A. Fert, A. K. Zvezdin, High domain wall velocities due to spin currents perpendicular to the plane., Phys. Rev. Lett. 102 (2009) 067206.

[289] C. T. Boone, I. N. Krivorotov, Magnetic domain wall pumping by spin transfer torque, Phys. Rev. Lett. 104 (2010) 167205.

[290] R. Lavrijsen, G. Malinowski, J. H. Franken, J. T. Kohlhepp, H. J. M. Swagten, B. Koopmans, M. Czapkiewicz, T. Stobiecki, Reduced domain wall pinning in ultrathin Pt/Co[sub 100?x]B[sub x]/Pt with perpendicular magnetic anisotropy, Appl. Phys. Lett. 96 (2010) 022501.

[291] M. Gottwald, S. Girod, S. Andrieu, S. Mangin, Tuneable perpendicular magnetic anisotropy in single crystal [Co/Ni](111) superlattices, IOP Conference Series: Materials Science and Engineering 12 (2010) 012018.

[292] S. Zhang, S. S. Zhang, Generalization of the Landau-Lifshitz-Gilbert equation for conducting ferromagnets, Phys. Rev. Lett. 102 (2009) 086601.

[293] K. Gilmore, M. D. Stiles, J. Seib, D. Steiauf, M. Fhnle, Anisotropic damping of the magnetization dynamics in ni, co, and fe, Physical Review B 81 (2010) 174414.

[294] S. A. Yang, G. S. D. Beach, C. Knutson, D. Xiao, Q. Niu, M. Tsoi, J. L. Erskine, Universal electromotive force induced by domain wall motion., Phys. Rev. Lett. 102 (2009) 067201.

[295] R. A. Duine, Effects of nonadiabaticity on the voltage generated by a moving domain wall, Phys. Rev. B 79 (2009) 014407.